MEMS BASED MICROBIAL FUEL CELL WITH MICROLITER VOLUME
FOR MICROSCALE POWER GENERATION

A THESIS SUBMITTED TO
THE GRADUATE SCHOOL OF NATURAL AND APPLIED SCIENCES
OF
MIDDLE EAST TECHNICAL UNIVERSITY

BY

BEGÜM ŞEN DOĞAN

IN PARTIAL FULFILLMENT OF THE REQUIREMENTS
FOR
THE DEGREE OF DOCTOR OF PHILOSOPHY
IN
MICRO AND NANOTECHNOLOGY

SEPTEMBER 2020

Approval of the thesis:

MEMS BASED MICROBIAL FUEL CELL WITH MICROLITER VOLUME FOR MICROSCALE POWER GENERATION

submitted by **BEGÜM ŞEN DOĞAN** in partial fulfillment of the requirements for the degree of **Doctor of Philosophy** in **Micro and Nanotechnology, Middle East Technical University** by,

Prof. Dr. Halil Kalıpçılar
Dean, Graduate School of **Natural and Applied Sciences**   _____

Prof. Dr. Almıla Güvenç Yazıcıoğlu
Head of the Department, **Micro and Nanotechnology**   _____

Prof. Dr. Haluk Külah
Supervisor, **Electrical and Electronics Engineering, METU**   _____

Assoc. Prof. Dr. Ebru Özgür
Co-Supervisor, **Mikro Biyosistemler A.Ş.**   _____

Examining Committee Members:

Prof. Dr. Burcu Akata Kurç
Micro and Nanotechnology, METU   _____

Prof. Dr. Haluk Külah
Electrical and Electronics Eng, METU   _____

Prof. Dr. Uğur Tamer
Analytical Chemistry, Gazi University   _____

Assoc. Prof. Dr. Yılser Devrim
Energy Eng., Atılım University   _____

Assoc. Prof. Ender Yıldırım
Mechanical Eng., METU   _____

Date: 24.09.2020

I hereby declare that all information in this document has been obtained and presented in accordance with academic rules and ethical conduct. I also declare that, as required by these rules and conduct, I have fully cited and referenced all material and results that are not original to this work.

Name, Last name: Begüm Şen Doğan

Signature:

ABSTRACT

MEMS BASED MICROBIAL FUEL CELL WITH MICROLITER VOLUME FOR MICROSCALE POWER GENERATION

Şen Doğan, Begüm
Doctor of Philosophy, Micro and Nanotechnology
Supervisor: Prof. Dr. Haluk Külah
Co-Supervisor: Assoc. Prof. Dr. Ebru Özgür

September 2020, 145 pages

Fuel cells can be a part of the solution to energy problem in the world. They can supply power in both macro and micro scales. Especially, MEMS based microscale microbial fuel cells (μMFC) may hold the answer to manufacture easy, cheap, fast, and mobile power sources and sensors. μMFCs are electrochemical devices converting chemical energy into electrical energy utilizing microorganisms as biocatalyst, instead of precious metal catalysts used in conventional fuel cells. They can be integrated to power, for example, lab-on-a-chip systems, or they can be used as stand-alone biosensors for sensing applications.

This study focused on the development of a compact microbial fuel cell with microliter volume fabricated using silicon MEMS technology. The aim was to have high power density and low start-up time to be integrated as a power source for small devices.

Several μMFC systems were operated under different conditions throughout the study. Effects of external load, anolyte type, operating conditions, and chemical modification of gold anode surfaces were compared in terms of start-up time and

power densities using *Shewanella oneidensis* MR-1. Performances were evaluated using polarization curves, Electrochemical Impedance Spectroscopy, and Scanning Electron Microcopy. The results showed that μMFCs modified with cysteamine self-assembled monolayers resulted in more than a 50% reduction in start-up times due to better bacterial attachment on the anode surface. The volumetric power density ($330\,\mu W/cm^3$) was found to be similar in cysteamine-modified and bare gold μMFCs and was comparable to results reported in similar studies in the literature.

Keywords: Microbial Fuel Cell, Biofilm, Surface Modification, Thiol, MEMS

ÖZ

MİKRO ÖLÇEKLİ GÜÇ ÜRETİMİ İÇİN MEMS TABANLI MİKROLİTRE HACİMLİ MİKROBİYAL YAKIT PİLİ

Şen Doğan, Begüm
Doktora, Mikro ve Nanoteknoloji
Tez Yöneticisi: Prof. Dr. Haluk Külah
Ortak Tez Yöneticisi: Doç. Dr. Ebru Özgüre

Eylül 2020, 145 sayfa

Yakıt pilleri, dünyadaki enerjine probleminin çözümünün bir parçası olabilirler. Hem makro hem de mikro düzeyde güç üretebilirler. Özellikle, MEMS tabanlı mikro ölçekli mikrobiyal yakıt pilleri (μMYP), kolay, ucuz, hızlı ve taşınabilir güç kaynaklarının ve sensörlerin üretimi için bir cevap olabilir. μMYP'ler, konvansiyonel yakıt pillerinde kullanılan metal katalizörlerin aksine mikroorganizmaların katalizör olarak kullanıldığı, kimyasal enerjiyi elektriksel enerjiye dönüştüren elektrokimyasal cihazlardır. Örneğin, çip-üstü-laboratuvar sistemlerine güç sağlamak üzere entegre edilebilecekleri gibi kendi başlarına bir biyosensör olarak kullanılabilirler.

Bu çalışma, silisyum MEMS teknolojisi ile üretilmiş, mikrolitre hacimli, kompakt bir mikrobiyal yakıt pilinin geliştirilmesi üzerine odaklanmıştır. Küçük cihazlar için güç kaynağı olarak entegre edilmek üzere yüksek güç yoğunluğuna ve düşük başlatma süresine sahip olacak şekilde tasarlanması amaçlanmıştır.

Çalışma boyunca birçok μMYP farklı koşullarda çalıştırılmıştır. Dış yükün, anolit tipinin, çalışma koşullarının ve altın anot yüzeylerinin kimyasal modifikasyonunun başlatma süresi ve güç yoğunluğu üzerine etkileri *Shewanella oneidensis* MR-1

kullanılarak karşılaştırılmıştır. Performans parametreleri polarizasyon eğrileri, Elektrokimyasal Empedans Spektroskopisi ve Taramalı Elektron mikroskopu kullanılarak karşılaştırılmıştır. Sonuçlar, kendiliğinden oluşan sisteamin tek katmanıyla işlem görmüş µMYP'lerinin anot yüzeyinde daha iyi bakteriyel tutunma sağladığı için başlatma süresini %50'den fazla kısalttığını göstermiştir. Sisteaminle işlenmiş ve işlenmemiş altın yüzeyler kullanılan µMYP'lerde, hacimsel güç yoğunluğu (330 µW/cm^3) benzer olarak bulunmuştur ve bu değerler literatürdeki benzer çalışma sonuçlarıyla aynı ölçektedir.

Anahtar Kelimeler: Mikrobiyal Yakıt Pili, Biyofilm, Yüzey Modifikasyonu, Tiyol, MEMS

To Doğanay and All My Other Family,

ACKNOWLEDGMENTS

TABLE OF CONTENTS

LIST OF TABLES

LIST OF FIGURES

FIGURES

LIST OF ABBREVIATIONS

ABBREVIATIONS

3-MPA	3-mercaptopropionic acid
4-ATP	4-aminothiophenol
11-MUA	11-mercaptoundecanoic acid
AFM	Atomic force microscopy
BHF	Buffered hydrofluoric acid
BOD	Biological Oxygen Demand
CFU	Colony forming unit
CYS	Cysteamine
DET	Direct Electron Transfer
DI	Deionized
DRIE	Deep reactive ion etching
EIS	Electrochemical impedance spectroscopy
EPS	Extracellular polymeric substance
ID	Inner diameter
MEMS	Microelectromechanical system
MET	Mediated Electron Transfer
MFC	Microbial fuel cell
OCV	Open circuit voltage
OD	Outer diameter
PBS	Phosphate buffered saline
PDMS	Polydimethylsiloxane
PECVD	Plasma enhanced chemical vapor deposition
PEEK	Polyether ether ketone
PEM	Proton exchange membrane
PR	Photoresist
RIE	Reactive ion etching

SAM	Self-assembled monolayer
SEM	Scanning electron microscopy
TMAH	Tetramethylammonium hydroxide
TSA	Tryptic soy agar
TSB	Tryptic soy broth

LIST OF SYMBOLS

SYMBOLS

P	Power (W)
I	Current (A)
R	Resistance (Ω)
V	Voltage (V)

GREEK LETTERS

μ	Microscale

CHAPTER 1

INTRODUCTION

Awareness of depletion of fossil fuel resources and growing consciousness about the environmental consequences of their use open roads to finding new, renewable, and sustainable energy sources to protect the future of Earth [1]. In this scope, electrochemical power sources which convert chemical or light energy directly into electrical energy, are under the focus of many research groups as a sustainable power supply [2]–[4].

Fuel cell is a power source that is derived from an electrochemical reaction which is highly efficient and operates on mostly easily available fuel sources [5]. Researchers have focused on developing different types of fuel cells with various applications. Namely, hydrogen fuel cells, alcohol-based fuel cells, solid oxide fuel cells and biological fuel cells are the main types. However, most of these fuel cells have not yet been commercialized.

Hydrogen fuel cells require complex hydrogen storage solutions and alcohol-based fuel cells, suffer from slow electrochemical reaction kinetics and fuel crossover from anode to cathode [6]. Furthermore, the conventional hydrogen and solid oxide fuel cells require complex fuel reforming [7]–[9]. An additional disadvantage of hydrogen fuel cell is usage of platinum as a catalyst which is expensive, and it has limited availability.

Another fuel cell type which is also extensively being researched is biological fuel cell. Biological fuel cells are alternative power generating devices based on electrocatalysis of several substrates by microorganisms (microbial fuel cells, MFC) or enzymes (enzymatic fuel cells) [10].

As the beginning milestone of the electrochemical power sources, in 1800, Alessandro Volta has invented the first electrochemical cell which is called Voltaic Cell. 39 years later, in 1839, William Grove demonstrated the first hydrogen fuel cell which was called Gas Cell at the time [11].

In 1911, Potter has constructed the first microbial fuel cell through feeding yeast with glucose. An open circuit voltage (OCV) of 0.32 V was reported from 5 g of *Saccharomyces cerevisiae* mixed with a 0.55-M glucose culture medium [12]. However, the researches on microbial fuel cells were not attractive in those days due to lack of application areas for that much small power. In 1931, Cohen assembled a microbial fuel cell with voltage output of 35 V at 0.2 mA [13].

In 1960's, NASA focused on fuel cell development to use in space vessels, as the energy demand in space could not be delivered by traditional batteries [14], [15].

In 1964, the first enzyme-based glucose / O_2 biological fuel cell operating at neutral pH was developed by Yahiro *et al.* [16].

In 1980's, an increase in current output was achieved by the addition of electron mediators to the anodic culture medium [17]–[20].

Between 1991 and 1993, Derek Lovley studied microbial metal oxide reduction, showed the importance of metal-reducing bacteria like *Geobacter sulfurreducens* can perform extracellular electron transfer, for microbial fuel cells [21]. This was an important breakthrough for biological fuel cell development.

At the end of the 1990's, Wilkinson suggested to use microbial fuel cells for the powering of self–sustaining robots [22]–[24].

In 2001, Prof. Byung Hong Kim showed that bacteria in wastewater or wastewater sludge can use electrodes as an electron acceptor without adding artificial mediators [25]–[27]. This discovery was very important for biological fuel cells to be used both as a power generator and a water treatment medium.

From the beginning of the second millennia, researches on both conventional and biological fuel cells accelerated. There were new trials to develop more efficient cells by changing configuration, dimensions, and other parameters. In 2002, Kjeang *et al.* developed the first microfluidic fuel cell [28]. In 2003, Chiao *et al.* constructed the first micromachined microbial fuel cell [29]. In 2004, first microfluidic biological fuel cell is demonstrated by Moore *et al.* [30].

The latest milestone to mention was the development of first µL scale microbial fuel cell by Chiao *et al.* in 2006 [31]. This breakthrough opened new application areas for especially biological fuel cells such as stand-alone biosensors and power source for implantable devices.

CHAPTER 2

MICROBIAL FUEL CELLS

2.1 Fundamentals of Biological Fuel Cells

Biological fuel cells (BFCs) convert chemical energy into electricity based on oxidation and reduction reactions in electrochemical cell assemblies. In BFCs, at least one reaction is catalyzed by a biological catalyst, namely enzymes or bacteria, instead of expensive and scarce catalysts used in standard fuel cells. Self-replication and reaction specificity of bacteria and enzymes are also outstanding advantages over catalysts like platinum [32]–[34].

There are three types of biological fuel cell: microbial, enzymatic, and photosynthetic fuel cells.

Microbial Fuel Cells

Microbial fuel cells (MFCs) are small bioreactors that convert the energy in the chemical bonds of organic compounds into electrical energy through catalytic activity of bacteria under anaerobic conditions. Microbe term is also used instead of bacteria but due the pejorative implication as pathogenic, it is not preferred by most of the researchers.

The mechanism of power generation in MFCs is shown in Figure 2.1. Electron generated by bacterial metabolism is transmitted electronically through the electron transport chain (ETC) on the bacterial membrane to the anode as the final electron acceptor and transferred to the cathode by an external metal wire. The protons formed by the metabolism pass to cathode through the proton exchange membrane, which has selective permeability. The electrons in the cathode combine with the

protons to reduce oxygen and the electrochemical reaction is completed. Electric current is obtained when the electrons pass through a load-carrying external cable in the cathode. Since bacteria can transfer their electrons to the metal surface only in an oxygen-free environment, an anaerobic environment must be provided in the anode. To provide this requirement, anode and cathode compartments must be separated by proton exchange membrane, and anode should be sealed with an oxygen impermeable gasket. It has been shown that the dissolved oxygen in the liquid does not change the obtained power because the bacteria rapidly consume it [35].
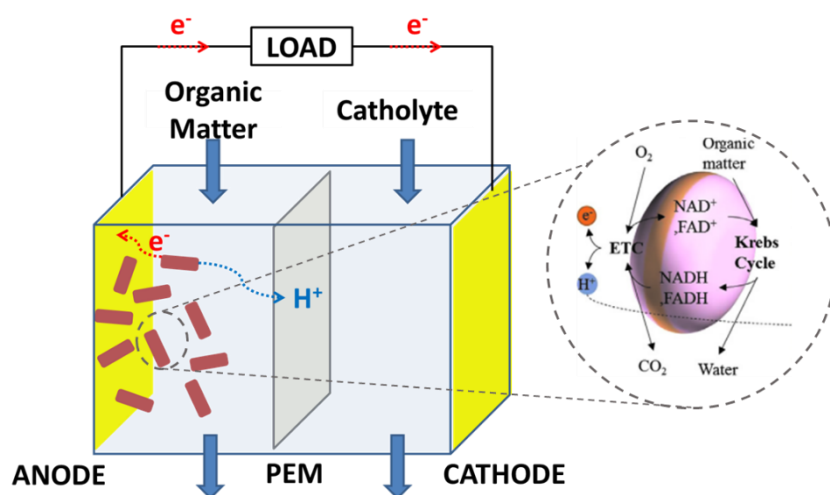
Figure 2.1. Microbial fuel cell mechanism (adapted from [36]), Krebs Cycle: cycle for cellular respiration; PEM: Proton Exchange Membrane; NADH, NAD$^+$, FADH, FAD$^+$: coenzymes for electron transport, ETC: Electron transport chain.

MFCs generate electrical power through the metabolic products of microbial respiration requiring a continual supply of carbon source [37], [38]. Bacteria oxidize organic matter in the anodic chamber, completing respiration by transferring electrons to the anode. During this process, chemical energy is captured throughout the electron transport chain. The coenzymes, nicotinamide adenine dinucleotide (NAD$^+$/NADH) and flavin adenine dinucleotide (FAD$^+$/FADH$_2$), are repeatedly oxidized and reduced through the enzymes in Krebs cycle and ETC to generate a H$^+$

6

gradient across the bacterial membrane, which is used to synthesize adenosine triphosphate (ATP), the biological energy unit. Electrons generated during the process are transferred through the ETC in the cell membrane to the anode as final electron acceptor [36], [39] (Figure 2.2). In case of bioanode, the anode needs to provide a suitable environment for bacteria to attach and deposit electrons, while the cathode must facilitate the occurrence of electron accepting reactions. These reactions have been observed in a wide range of temperature: low temperatures (<15°C) room temperatures (15–35°C) and high temperatures (50–60°C) [40]–[43].
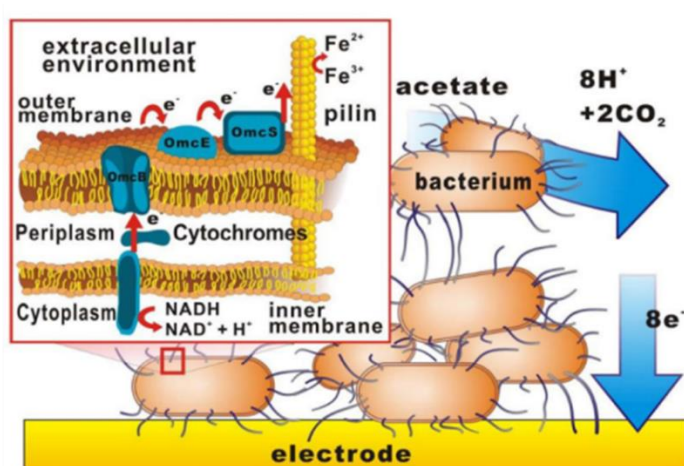
Figure 2.2. Electron transfer mechanism on bacterial membrane [44], Acetate: an organic matter; Cytochrome: protein for electron transport; Pilin: wire-like appendage; Periplasm: matrix between inner and outer membranes; cytoplasm: fluid inside the cell; OmcB, OmcE, OmcS: different cytochromes.

Studies have shown that some bacteria prefer metal oxides as the ultimate electron acceptor, and these bacteria are called exoelectrogens. Exoelectrogenic bacteria (e.g., *Geobacter* and *Shewanella sp.*) have been used frequently in recent years for the development of MFCs. There are other types of bacteria used but they need for electron carrier molecules, called mediators, to transport electrons between the bacterial membrane and the anode surface. In MFCs, isolated bacteria as well as mixed bacterial cultures can be used.

Different substrates such as carbohydrates, volatile fatty acids, alcohols, amino acids, proteins, and inorganic components can be used in MFCs [45]. When complex mediums are used as substrates like Tryptic Soy Broth, it is difficult to quantify the number of electrons involved. However, as an example, when glucose ($C_6H_{12}O_6$) is used as fuel in a microbial fuel cell with oxygen as the reductant, the reactions occurring in the anode and cathode compartments are given below:

Anode $C_6H_{12}O_6 + 6H_2O \rightarrow 6CO_2 + 24e^- + 24H^+$ (1)

Cathode $6O_2 + 24e^- + 24H^+ \rightarrow 12H_2O$ (2)

Overall $C_6H_{12}O_6 + 6O_2 \rightarrow 6CO_2 + 6H_2O$ (3)
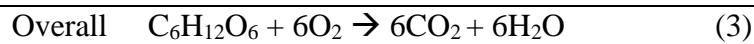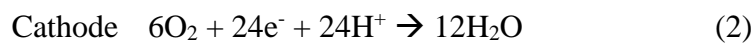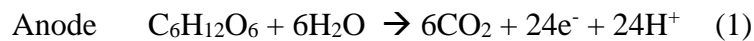
The type substrate is chosen considering the requirements of the bacteria to be used in the anode chamber. *Shewanella oneidensis* is facultative anaerobic bacteria frequently used in MFC studies. It is preferred in MFCs, under anaerobic conditions, because it can use a wide variety of solid metal-oxide surfaces as the final electron acceptor. It is suggested that *S. oneidensis* does this by cytochrome-type lipoproteins in the cell membrane, a constituent of ETC [46]. The inhibition of cytochrome synthesis by genetic modifications has been observed to impede the anaerobic growth of the resulting bacterium. Some other studies have suggested that *S. oneidensis* forms electrons in metal oxide surfaces by forming electrically conductive nanowires on their cell surface in the absence of oxygen [47]. The general conclusion is that the bacterium uses both methods together.

Enzymatic Fuel Cells

Enzymatic fuel cells, shown in Figure 2.3, convert chemical energy into electricity using isolated enzymes that metabolize chemicals while generating current under mild temperature and neutral pH value [48]–[51].
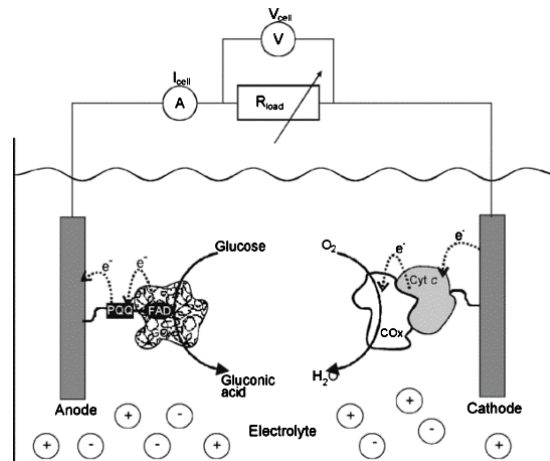
Figure 2.3. A single chamber enzymatic fuel cell running on glucose and O_2 [52].

Glucose is the most used fuel for enzymatic fuel cells [53]–[56]. Fructose [57], [58], ethanol [59], [60], methanol [61] and lactose [20], [62] are some other fuels used. Some of different enzymes used are alcohol dehydrogenase, glucose dehydrogenase [31], diaphorase [32] and bilirubin oxidase [64].

There have been several studies to use enzymatic fuel cells as implanted *in vivo* microscale power sources. There are studies showing enzymatic fuel cells implanted into animals and plants such as snails, grapes [65] and insects [66].

Since enzymes are substrate selective, it eliminates the need of proton exchange membranes (PEMs) and fuel crossover does not occur. Due to the improved mass transport rates by eliminating PEMs, enzymatic fuel cells can generate higher power densities than microbial fuel cells. Moreover, no acclimation is necessary when enzymes are used as catalysts [30]. However, enzymes require isolation and purification prior to operation and replenishing during the operation of the fuel cell and MFCs does not require specific enzyme isolation, purification, and immobilization on the electrode surface [67]. Furthermore, bacteria have the advantage of long lifetime over enzymes but they are more prone to oxygen intrusion inside the chamber [68].

9

Photosynthetic Microbial Fuel Cells

Photosynthetic fuels cells, also called biological solar cells, are based on the microbial photosynthesis process. During photosynthesis, the photosynthetic bacteria capture solar energy and converts carbon dioxide and water into oxygen and carbohydrates. Electrons released during photosynthetic reactions flow through the external circuit and recombine with protons in cathode chamber. Photosynthetic fuel cells can continuously generate electricity from solar energy without additional organic matter by increasing the electrochemical potential inside the cell to split and recreate water, producing oxygen, protons, and electrons [69]. However, their internal resistance is higher than that of other biological fuel cells and restricts their power generation performance [36]. The first microscale photosynthetic fuel cell was demonstrated in 2006 by generating an areal power density of 40 pW/cm^2 [31].

2.1.1   Electron Transfer, Exoelectrogenic Bacteria and Biofilms

Bacteria or algae can be used as the exoelectrogenic microorganisms for biological fuel cells. They are also called as electricigens, electrode respiring bacteria or electroactive bacteria. Exoelectrogenic microorganisms have ability to transfer electrons extracellularly. The mechanism used in this process is called Extracellular Electron Transfer (EET) [70], [71]. EET is a natural process and it occurs when electroactive bacteria perform anaerobic respiration.

Not all bacteria types are exoelectrogenic, but non-exoelectrogenic bacteria may still favor the synergistic exoelectrogenic biofilm consortium by performing other functions such as providing organic nutrients. Electron transfer between bacteria and electrodes rely on two mechanisms, namely direct electron transfer (DET) and mediated electron transfer (MET) [72].

Direct Electron Transfer

Direct extracellular electron transfer mechanism does not require artificial means. Chemical reactions can occur where the electron transfer occurs directly between

10

enzymes and electrodes when the active sites of extracellular enzymes are sufficiently close to the electrode surface. However, some microbial cells contain electrically conductive pili extending for tens of micrometers and serving as electrical conduits for long range direct electron transfer [73], [74].

Mediated Electron Transfer

Most microorganisms cannot give away sufficient number of electrons outside of cells so they need mediators, also called electron shuttles to facilitate the transport of electrons. This process is called as Mediated Electron Transfer (MET) where direct contact between the bacterial cell membrane and the electrode surface is not required. Mediators can be added externally to bacterial solutions and they can be redox-active chemical species such as ferricyanide [72], methylene blue [9] or neutral red [75] Aside from externally added mediators, some bacteria can excrete their own mediators [73]. Depending on MET, *Saccharomyces cerevisiae* cannot produce high power density, because the diffusion rates of the mediators significantly limit the rate of EET by diffusion [31], [42], [76]. However, utilization of mediators can harm environment and raise the operation costs, hence, it may not be practical to use mediator in large scale operations. Also, mediators must be chemically regenerated and at higher concentrations, most redox mediators are toxic to bacteria [68], [77].

Shewanella oneidensis

The performance of the MFCs is mainly based on the type of biocatalyst. *Shewanella*, *Pseudomonas* and *Geobacter* species have been widely used as biocatalysts in microbial fuel cells [78]–[80]. Some microbial fuel cells use pure culture but there are also some examples of mixed-culture fuel cells that obtain results better or similar to pure-culture using MFCs [42], [81], [82]. *Geobacter* form a conductive biofilm matrix for fast EET, resulting in high power densities [83], [84]. Even though *Geobacter sulfurreducens* show higher power densities in MFCs, *Shewanella oneidensis* may be more applicable for some MFC applications where oxygen toleration is necessary [85]. *Shewanella oneidensis* MR-1, first isolated from

sediments of Oneida Lake, New York [86], [87] is known for its ability to respire insoluble metal oxides enabling the electron transfer to an anode without addition of an external mediator [88]. This non-pathogenic facultative anaerobic γ-proteobacterium is closely related to *Escherichia coli* and shows a good genetic tractability [89], [90].

Biofilm Formation

In MFCs, power generation can be catalyzed by both planktonic bacteria helped with extracellular electron carrier molecule secretion and biofilms formed by bacteria on conductive surfaces [91], [92]. *Shewanella oneidensis* is capable of both DET by forming biofilm and MET by planktonic cells secreting flavin electron carrier molecule. It is shown that *Shewanella oneidensis* biofilm can reach a tower structure up to 45 μm dispersed throughout the biofilm [93]. Biofilm formation (Figure 2.4) is vital to provide stable and continuous power generation in MFCs because most of the planktonic cells move away from the electrode during the supply of nutrients.
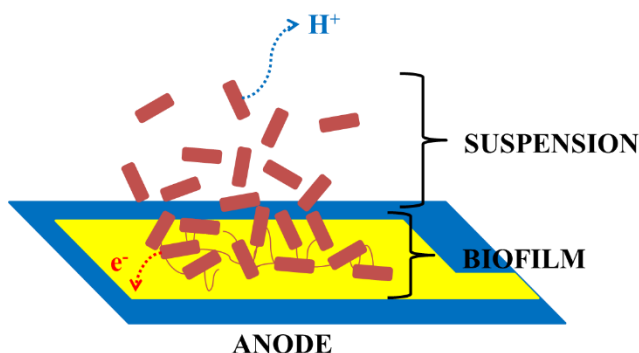
Figure 2.4. Schematic of biofilm on anode surface.

The time required for bacteria to form biofilms on electrode surface varies depending on various factors such as hydrodynamic conditions, bacterial metabolism, nutrient content, and surface characteristics. To obtain a high-quality, fast forming biofilm, the rate and content of the nutrient supply should be optimized. For some bacteria, it lasts for a few hours, but for some bacteria it can last up to several weeks to form

biofilm layers. Biofilm formation time for *S. oneidensi*s is reported as 1-7 days in literature [94], [95]. The start-up time of MFCs is an essential performance parameter, and it shows the duration of the fuel cell to reach a stable power generation value. It is highly dependent on the biofilm formation duration.

2.1.2   Micro-scale Microbial Fuel Cell Architecture and Materials

The fundamental criteria designing microbial fuel cells are the cell configuration and the material to manufacture the fuel cell. Generally, the fuel cells consist of electrolytes, anode, cathode, PEM, electrical contacts, sealing gaskets and liquid handling ports to chambers [5]. Electrode spacing between the anode and the cathode and electrode materials have crucial importance.

For micro-scale MFCs, silicon is the most common substrate material for microfabrication due to the availability of creating different metal layers. Other materials are glass, fused silica, various polymers, alumina, bulk aluminum [96] and bulk metallic glass [97]. The first µMFC was manufactured by using silicon wafers [31], [98]. Depending on the material preferred, photolithography or soft lithography techniques are used to manufacture the microscale biological fuel cell. There are also µMFC fabricated using biocompatible and cheaper polymer materials [99]–[101].

Low-cost, flexible thin materials like paper is one of the popular materials for biosensors with the ability to move fluids through capillary action. Simple electrical connections between single MFC units helps to build feasible systems with a drop of inoculum [36]. Carbon-based anodes are favorable for bacterial attachment but conventional carbon-based materials are incompatible with microfabrication methods. Carbon-MEMS (C-MEMS) allow direct two- and three-dimensional microscale manufacturing of carbon electrodes [102].

Different µMFC configurations (Figure 2.5) designed are double chamber, single chamber, microfluidic, stacks and arrays with differing operational and performance advantages exploiting the micro-scaling.

Double Chamber

Double chamber configuration is the most preferred design since block the oxygen diffusion into the anode chamber. They also have the advantage of suitability to both batch and continuous mode operation. Anode and cathode compartments are separated by an ion exchange membrane [103], [104]. Thickness of PEM increases the internal resistance of double chamber microscale MFCs and this exhibits as a performance limiting factor.

Single Chamber

Single chamber fuel cells have only one compartment that contains both the anode and the cathode. They have the advantage of simpler designs and easiness to scale-up. A single chamber MFC with air-cathode may increase the performance by decreasing the distance travelled by protons between anode and cathode [105], [106]. Compared to the double chamber MFCs, single chamber fuel cells have smaller internal resistance but microbial contamination and back diffusion of oxygen from cathode to anode without a PEM inhibits the performance [107].

Microfluidic (Laminar Flow)

A microfluidic μMFC is built with a single microfluidic channel having all the fluid ports, reaction sites and electrode structures. They generally operate with two parallel laminar flows inside the channel without a physical barrier separating the anode and the cathode [77], [78]. Mixing of the two streams (anolyte and catholyte) occurs by diffusion only and is restricted to an interfacial width at the center of the channel. Considering that microscale MFCs can be built by simple fabrication processes without a PEM to separate two chambers, microfluidic MFCs might offer a superior potential as an on-chip power source [29]. However, their performance is not comparable to other reported MFCs to diffusion and crossover of anolyte and catholyte [110]. Further studies on operational conditions and electrolyte types may improve these drawbacks.

14
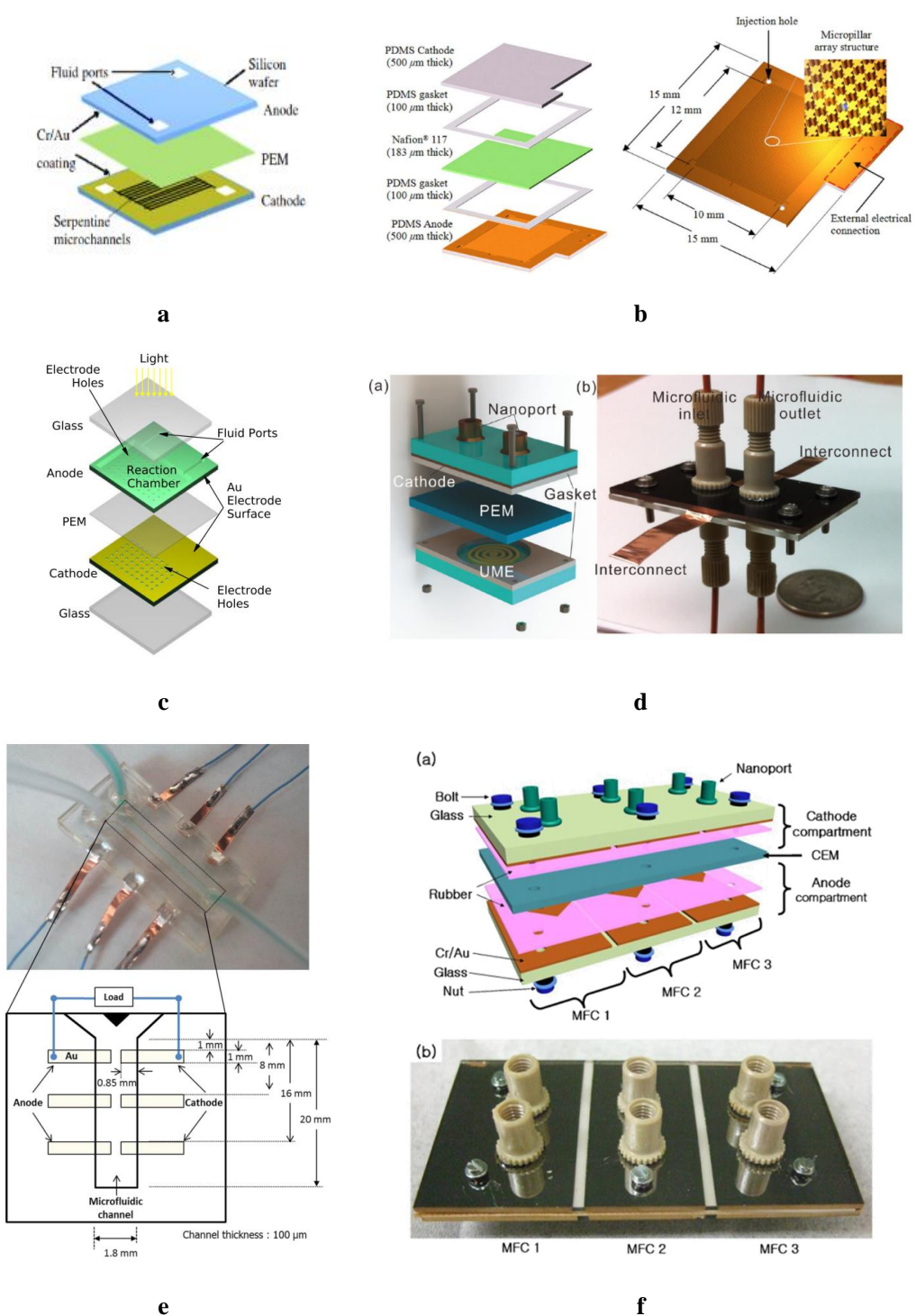
Figure 2.5. a: Exploded view of a double chamber µMFC [31]; b: Schematic image of a PDMS µMFC [76]; c: Schematic of a photosynthetic MFC [31]; d: Schematic and image of a glass µMFC [31]; e: Schematic and image of a laminar flow µMFC [110]; f: Schematic and image of a µMFC stack [111].

Stacks and Arrays

The total output voltage and power density of single µMFC units are not sufficient for practical applications yet. Hence, adaptation of stacked MFCs in series or parallel are currently under study to increase the performance. Furthermore, microfabrication enables the development of MFC arrays for high-throughput analyses to be built on a small footprint, enabling parallel operation of all the single µMFC units in the array with minimum chemical consumption. Numerous µMFC arrays that enable high-throughput parallel screening and analysis of microbial activities have been developed by different research groups [101], [112], [113].

Choi *et al.* built microliter sized MFCs in series by integrating three MFCs into a sandwich of two glass slides, incorporating two chambers of 50 µL volumetric capacity that were separated by a PEM. However, the individual MFCs voltages varied and one of them had reversed polarity with the low external resistor [111]. Voltage reversal has been one of the main challenges of macroscale MFC arrays too [114]–[116]. It has been reported that an insufficient supply of nutrients is the main cause of voltage reversal and can occur during a sudden change of fuel demand such as during start-up or switching of the load [117]. Thus, further study to solve voltage reversal is required to use stacks or arrays of MFCs for high power output [129].

2.1.3 Advantages of Micro-scaling in MFCs

Micro-scale MFCs (µMFC) are a recently developed class of microbial fuel cells to profit the characteristics of smaller dimensions [118]. The advantage of µMFCs stems from the reducing dimensions which brings the increasing surface to volume ratio.

In MFCs mass transfer rate and the reaction kinetics can limit the overall reaction rate of heterogeneous reactions [68]. When the overall reaction rate is controlled by mass transfer, micro-scaling of MFCs provide possible higher surface mass flux

[119] and mass transfer resistance can be reduced. Furthermore, in large surface area MFCs, higher electron transfer efficiency is possible due to the increase in the ratio of bacteria attached to surface to bacteria suspended in liquid. Larger surface area can be obtained by roughening the surface or creating microstructures on the surface. With the help of MEMS microfabrication technology, microbial fuel cells having microliter volume and large surface area can be developed.

Especially for laminar flow MFCs, since viscous and surface forces dominate the fluid flow in micro-scale [120], adopting micro-scaling to build µMFCs is also important for creating a controlled micro-environment where the reactions and the flow can be investigated in detail. This advantage is used by Hou *et al.* to investigate the bacteria with high electrogenic activity in an MFC array [113].

Proton diffusion length shortens with the decreasing dimensions. Thus, electrolyte resistance reduces in µMFCs. However, it is crucial to note emphasize that going smaller than biofilm dimensions (10-100 µm in height generally) will affect the performance negatively due to the inhibition of the biofilm structure.

In micro scale applications, costly reagents necessary in the fuel cell are consumed in a minimal amount. Also, handling of the hazardous materials, if any, will be at minimum.

Miniaturization of fuel cells increases the portability, so the application areas widens. Implantable power sources are the result of going into microscale.

Besides the advantages of µMFCs, there is still a disadvantage to be eliminated in microscale fuel cells. Their power generation densities are smaller than their macroscale counterparts due to the higher internal resistances. This is proposed to be due to poor contact between bacteria and electrode. Increasing the surface to volume ratio further and adopting electrode materials favored by bacteria may help to decrease the internal resistance. Also, solutions with higher electrolyte conductivity and thinner proton exchange membranes can be preferred.

2.2   Evaluation of Performance for Microbial Fuel Cells

The overall performance of an μMFC is evaluated in terms of different parameters, but main indicator is open circuit voltage (OCV) and power and current densities. These are usually estimated by analyzing polarization curve or linear sweep voltammetry (LSV). OCV is the voltage of an MFC under a no–load conditions [73]. Maximum theoretical OCV of a single MFC is 1.14 V (-0.32 V for NADH, +0.82 V for oxidant redox potentials) but until now 0.8 V was achieved [117]. A typical micro-sized MFC produces an OCV of about 400-600 mV [68], [121].

Current and power densities are given in terms of electrode area. If the bioanode is used, the anode area is taken for the density calculations. The theoretical maximum power generation from an MFC is limited. The power densities of the early μMFCs range between 0.019 and 0.4 $\mu W/cm^2$ [59], [31], [99]. Metabolic by-products, electron storage inside bacteria and capacitance effect in the biofilm-anode interface can also decrease MFC performance [36], [122], [123].

Theoretically, microbial fuel cells can attain a maximum cell voltage of 1.14 V under open circuit conditions. However, it is lower in practice due to several losses occurring the fuel cell namely activation, ohmic and concentration losses (Figure 2.6). The internal resistance of the fuel cell stems from these losses and they limit the power generation. To increase the performance of the μMFC, the internal resistance should be decreased by increasing anode surface area, by improving anode-bacteria interactions or by increasing the operating temperature [124]. Activation losses can be decreased by increasing nutrient concentration or operation temperature. Ohmic losses can be decreased by utilizing high conductivity electrodes and electrolytes and by decreasing the distance between anode and cathode. Concentration losses can be minimized by improvement mass transport with the help of effective flow circulation inside the chambers.
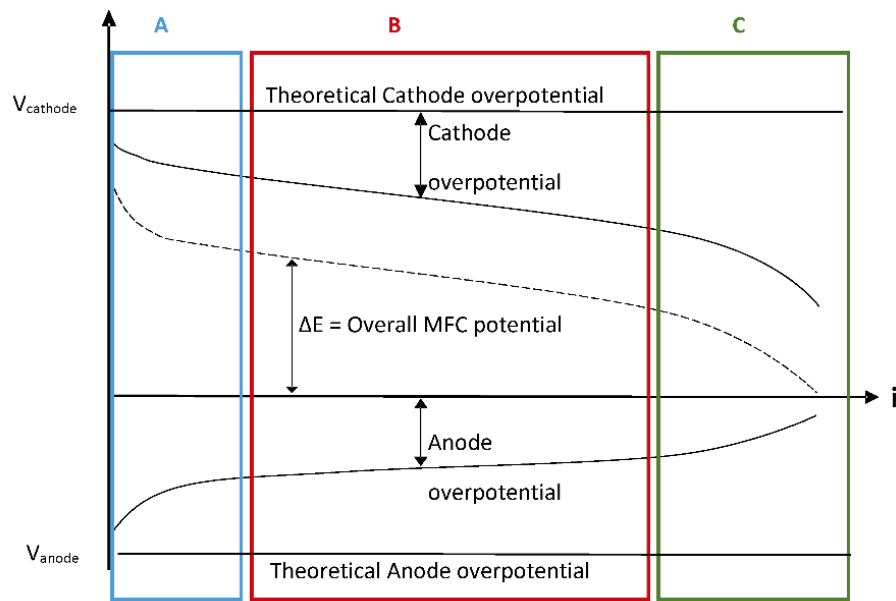
Figure 2.6. The polarization curve for a typical MFC. A: activation losses, B: ohmic losses, C: concentration losses [124].

Not all the energy harvested from an organic matter is converted to electricity in MFCs. Some of it is used by the biofilm for its survival. Some energy is wasted due to overpotentials, namely activation overpotential, concentration (or mass transfer) overpotential near an electrode, and ohmic loss due to internal resistance of the system. The wasted energy is released as unrecoverable low-grade heat [73]. Coulombic efficiency is a parameter showing the extent of electron conversion from the substrate to electricity [17], [72], [125]. It is the ratio of total coulombs calculated by integrating the current over the time for organic matter consumption to the theoretical number of coulombs that can be harvested from the complete oxidation of organic matter. Most studies do not provide Coulombic efficiency [36]. Columbic efficiencies of μMFCs is generally less than 20% which is lower than that of macro-scale MFCs [84], [126].

The start-up time also is an essential parameter to evaluate the MFC performance and it depends on the duration of biofilm formation to establish the initial bacteria-anode electron transfer. Conventional macroscale MFCs show very long start-up

times ranging from 4 to 103 days in literature [77] but μMFCs exhibit a much shorter start-up phase, 2-3 days, compared to their macroscopic MFCs [42].

2.2.1   Linear Voltammetry and Polarization Curves

In MFC studies, voltammetry experiments are used extensively to evaluate performance by obtaining polarization curves. Polarization is the change of electrode potential from its equilibrium state due to a flow of current. Polarization curves show the voltage versus current.

Potential drop across a fixed external resistor (R_{ext}) is measured and the current is calculated from Ohm's law accordingly. Thus, power is usually calculated as:

$$I = V/R_{ext} \qquad (1)$$
$$P = V^2/R_{ext} \qquad (2)$$

Power overshoot can result in inaccurate performance evaluation by polarization curves for MFCs. It is mostly due to the fast scan rates causing less time available for stabilization during polarization study. Winfield *et al.* observed also that one of the reasons for the power overshoot seen in power curves from MFCs might be due to immature biofilm on the anode electrode. They showed that anode modification might help in increasing capacitance and developing mature biofilm [127]. Thus, it is necessary to allow sufficient time during polarization studies before changing the load on the system.

2.2.2   Electrochemical Impedance Spectroscopy

Characterization of the fuel cells with electrochemical analysis can help to see performance limiting parts of the system. Especially, Electrochemical Impedance Spectroscopy (EIS) is a reliable and fast tool to identify the parameters of fuel cells including the internal resistance of the overall system. EIS is widely used in the

characterization of surface coatings, batteries, fuel cells, and corrosion phenomena. There are also numerous studies investigating MFC performance using EIS technique [128]–[131].

EIS can give information about the surface modification quality and biofilm formation on anode surface. The main advantage of EIS is its capacity to resolve in the frequency domain the individual contributions of the various factors that determine the overall PEM fuel cell power losses namely kinetic, ohmic and mass transport losses. However, a reference electrode is necessary for individual analysis inside the chambers. By implementing miniature reference electrodes inside anode and cathode chambers, it is possible to determine overall internal resistance, anode chamber resistance and cathode chamber resistance separately.

Electrochemical impedance can be measured by applying an AC signal with varying frequencies to an electrochemical cell and measuring the current through the cell using a potentiostat/galvanostat and a frequency response analyzer (FRA). The impedance Z_ω, ratio between the potential and current, of the system is a complex quantity with a magnitude and a phase shift which depends on the frequency of the signal.

Three conditions must be fulfilled to ensure the reliability of the EIS measurement data. Linearity requires that the applied AC amplitude must be small enough so that the response of the cell can be assumed to be linear but still large enough to measure a response. Stability requires that the overall state of the system must not change drastically during the acquisition of the data by selecting an adequate frequency range and measurement conditions. Causality requires that measured AC response of the system must be directly correlated to the applied AC stimulus by shielding the fuel cell from outside perturbations.

The electrochemical cell in an impedance experiment can consist of two, three, or four electrodes. The most basic form of the cell has two electrodes.

Using the measured data Nyquist plot and Bode diagrams can be drawn. The plot of the real part of impedance against the imaginary part is the Nyquist plot which gives

a quick overview of the data to make some qualitative interpretations by analyzing the shape of the curve.

After EIS measurements, data can be analyzed by Thevenin theorem: the fuel cell should be modeled with an equivalent circuit using constant phase element, Warburg impedance and passive electrical elements such as resistors, capacitors, inductors used in electrical circuits. These elements have physical meaning depending on the process to be analyzed and they can be combined in series and/or parallel to obtain complex equivalent circuits.

Figure 2.7 shows a basic model called simplified Randle's circuit including two resistors and one capacitor. It includes the electrolyte resistance, double-layer capacitance and polarization resistance.

Figure 2.7. Simplified Randle's model as an equivalent circuit. RΩ: electrolyte resistance, Rp: polarization resistance, C/CPE: Capacitance/Constant phase element.

Figure 2.8 exemplifies a Nyquist plot of an µMFC modeled with a simplified Randle's circuit which is formed by resistor and a capacitor in parallel and they are in series with another resistor. The polarization resistance is calculated as 31.8 kΩ in that case.
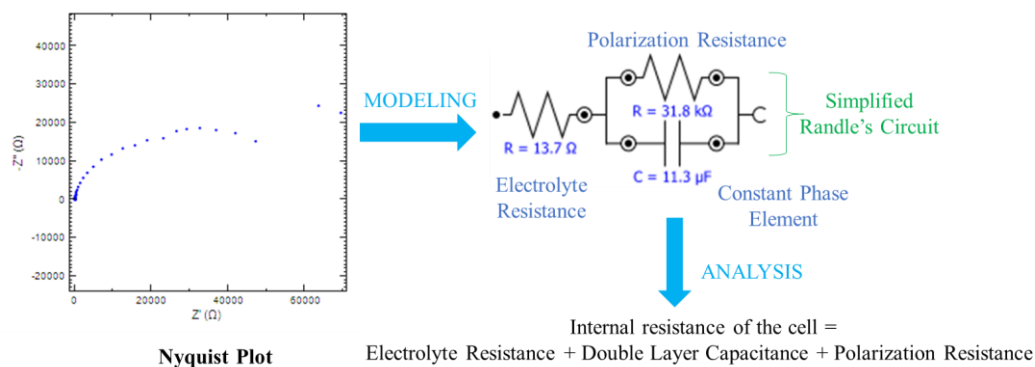
Figure 2.8. A sample EIS analysis of a µMFC.

When mixed kinetic and diffusion control are non-negligible the equivalent circuit should include a solution resistance (R_S), a double layer capacitor C or a CPE, the charge transfer resistance and the Warburg element, Z_W, which contains information on the diffusion coefficient of the species. The equivalent circuit elements most used in analysis of MFC models and their corresponding mathematical expressions related to impedance are shown in Table 2.1.

Table 2.1. Equivalent circuit elements most used in MFC analysis.

Equivalent Element	Expression	Symbol
R, resistance	$Z_R = R$	
C, capacitance	$Z_C = 1/j\omega C$	
L, inductance	$Z_L = j\omega L$	
W, infinite Warburg	$Z_W = 1/Y_0\sqrt{(j\omega)}$	
Q, Constant Phase Element (CPE)	$Z_Q = 1/Y_0(j\omega)^\alpha$	

Figure 2.9 shows an example of equivalent circuit of an interface with Electrical Double Layer.
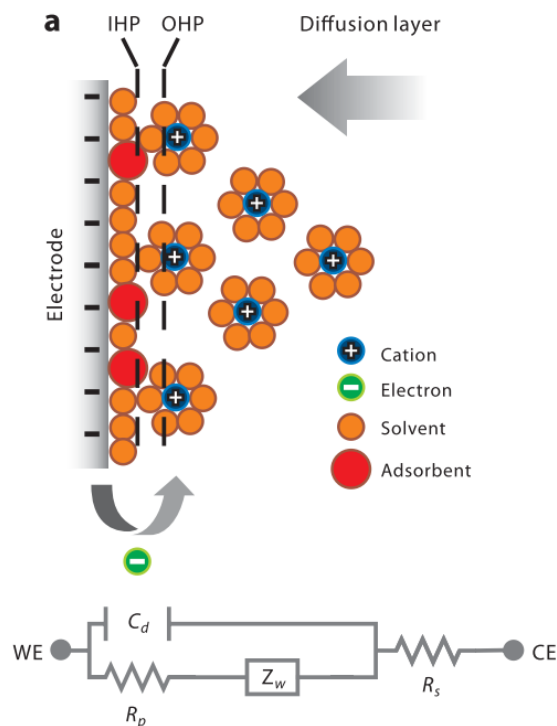
Figure 2.9. Top: an electrified interface in which the electrode is negatively charged and counter cations are aligned along the electrified surface; Bottom: electrical circuit elements corresponding to each interface component for an idealized Randles electrical equivalent circuit for the interface (C_d, double-layer capacitor; CE, counter electrode; IHP, inner Helmholtz plane; OHP, outer Helmholtz plane; R_p, polarization resistance; R_s, solution resistance; WE, working electrode; Z_W, Warburg impedance) [132].

2.3   Strategies for Performance Enhancement of MFCs

Although the power densities and start-up times are not feasible for real-world applications yet, they can be enhanced by adapting different improvement strategies such as addition of artificial electron mediators, enhancement of surface to volume ratio, improving chamber architecture, enhancing electrode-bacteria interactions by

tuning electrode surface characteristics and adopting mixed culture or genetically modified bacteria. These strategies can increase biofilm thickness, speed up the start-up time and most importantly decrease the internal resistance of the MFCs. They can be classified as operational level, biofilm level and single cell level as described by Guo et al [133]. Figure 2.10 is adopted from their study and summarizes strategies at different scales.
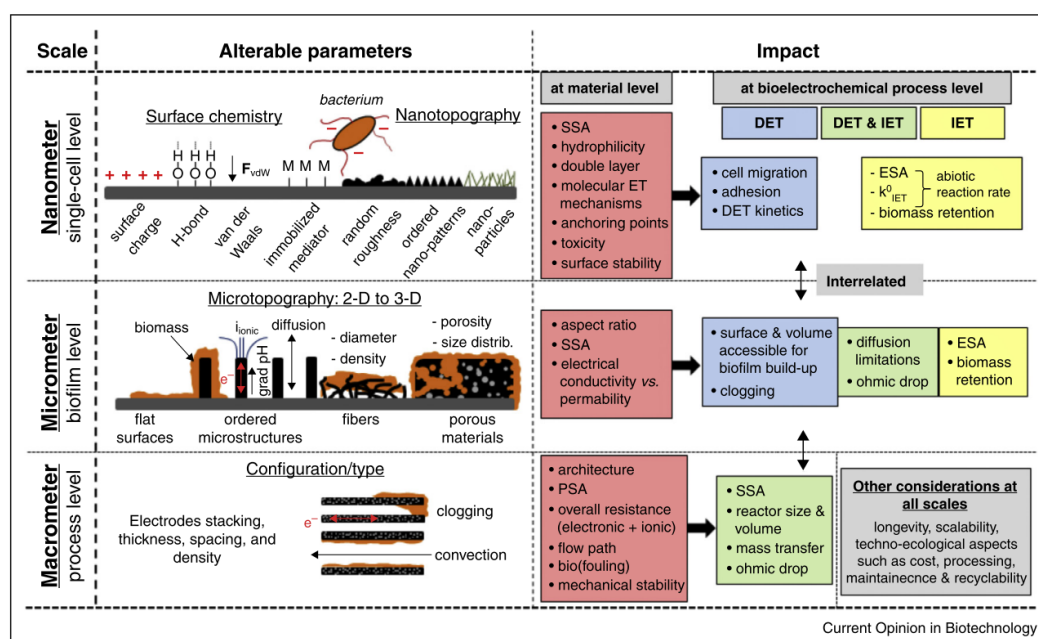
Figure 2.10. Strategies to enhance the performance of bioelectrochemical systems at different physical levels [133].

2.3.1 Architecture

MFC architecture can affect biofilm formation and power output. Qian *et al.* showed that the shallow anode chamber increased the probability of cell attachment and biofilm formation on the anode surface [42]. Arrangement of electrodes and distance between them can be optimized for a better mass transport. Standard proton exchange membranes are thick (20-250 µm) for micro-scale applications, and they

make up an important portion of the internal resistance. Developing MFCs without proton exchange membrane such as microfluidic MFCs [134] and air-cathode MFCs [135] may help to decrease the internal resistance of the system.

2.3.2   Surface Modification

Surface chemistry and surface morphology of the electrode is very crucial for improving the interactions between biofilm and electrode. To improve anode-bacteria interactions, gold electrode surface can be modified by different coatings because many factors influence bacterial adhesion on the surface; hydrophilicity, shape, zeta potential, roughness, surface area, pH and size of the surface [124], [136], [137]. Modification of the electrode surfaces to increase the electron transfer rates not only affect the current densities but also modify the diversity in bacterial community attached to the electrode [138].

Improving the electrode surface characteristics can result in better surface contact for the bacterial biofilm. Biofilms are complex structures adhering to surfaces and consist of colonies of single bacterial species or multiple bacterial species. They can be found with a self-produced polymeric matrix attached to biotic or abiotic surfaces [139]. Their structure varies from Gram-positive to Gram-negative bacteria. The biofilm quality is affected not only by the interactions between the electrode surface and bacteria, but also by the operational parameters of the fuel cell [93], [140]. Although bacterial adhesion to a surface is the first step of biofilm formation, other parameters also exist, such as hydrophobic interactions, electrostatic interactions, the electrode surface roughness, surface charges, and cell surface structures [141]. A study by Friman *et al*. published in 2013 showed that both the plankton bacterial cells and the biofilm contributed to the overall MFC voltage, and the biofilm contribution was three-times higher [142]. Additionally, Slate *et al*. reviewed studies showing the relation between the biofilm quality and power output [143].

Electrodes in fuel cells require a high conductivity, chemical stability, corrosion resistivity, and high mechanical strength. Since the anode is responsible for the growth of bacteria on the surface, it must have a good biocompatibility, as well as excellent electrical properties, to enable efficient electron transfer [19]. Generally, carbon-based materials are preferred in MFC studies due to their low cost. Another reason for their common use is that bacteria attach to carbon surfaces more easily, for instance, compared to bare gold surfaces. On the other hand, carbon-based materials have a major disadvantage, which is their low electrical conductivity, especially compared to gold. Although the cost of gold electrodes constricts their employment in large systems, they are widely used for fundamental research in miniaturized micro-scale MFC systems [144].

Thiols

Gold surfaces can be enhanced by surface modification methods via the addition of different functional groups. Alkanethiols are widely preferred for modifying gold surfaces in the literature due to the strong and well-proven gold–thiol interaction [145]–[147]. Thiols form highly ordered self-assembled monolayers (SAMs) present on the gold surfaces with a functional head group and terminal sulfur group attached by a spacer group with different carbon chain lengths (Figure 2.11). Since thiols with carboxyl or amine functional groups can bind to proteins on the bacterial membrane, the functionalization of gold surfaces with such groups will favor bacterial attachment [148], [149] and this may, in turn, accelerate biofilm formation. However, these self-assembled monolayers may increase the electron transfer resistance, depending on the length of the carbon chain of the molecule to be used [150]. Cysteamine (CYS), an alkanethiol with an amine functional group, is known to favor bacterial attachment [151]. Another thiol is 11-mercaptoundecanoic acid (11-MUA), containing a carboxyl functional group. Some studies have shown that more current was generated by creating an SAM of carboxyl terminated alkanethiols compared to non-functionalized gold electrodes [148], [152]. This was explained by the phenomenon in which carboxylic acid could accommodate cytochromes on the

27

electrode surface through very strong hydrogen bonding with the peptide bonds in the protein backbone.
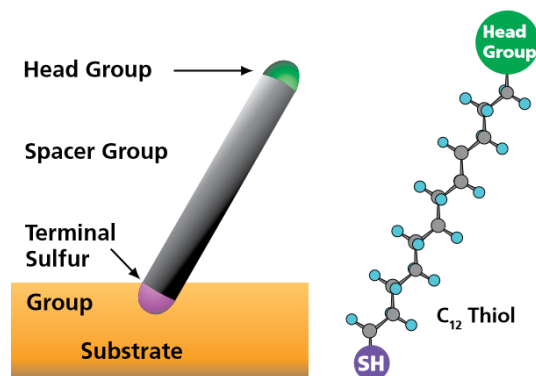
Figure 2.11. Thiol group assembled on a substrate surface [153].

Zeolites

Zeolites are porous, crystalline, porous aluminosilicates with an ability to exchange some of their constituent cations with aqueous solutions. Their characteristics mostly depend on their Si/Al ratio. Zeolites, such as Zeolite Linde Type A [154], Zeolite Y [155] and NaX [156], are recently evaluated in macroscale microbial fuel cell studies to enhance biofilm formation due to their varying surface properties [154], [156]. They are either added to inoculum as carrier of bacteria [157]–[159] or used in the modification of the electrode surface [160], [161]. Although most of the studies demonstrated improvement in power output, a study showed that zeolite coating on carbon cloth pretreated in 10% HNO_3 solution decreased the power density by 20% [162].

2.3.3   Bacteria Inoculum

There are several strategies related to bacteria to improve the MFC performance such as involving genetically engineered exoelectrogenic bacteria, improvement of biofilm formation, and improving acclimatization [40], [113]. The bacteria inoculum

can be acclimatized to promote the growth of bacteria suspended by supplementing vitamins, essential nutrients, by offering anaerobic conditions and by adjusting the inoculum properties like pH [163]. Furthermore, the power output of a MFC can be improved by increasing the membrane permeability of the exoelectrogens in the inoculum by chemical treatment to favor the secretion of electron shuttles [164]. Another technique is transplanting of mature electroactive biofilms from natural environments (wastewater plants, sediments, soil, etc.) or from an already colonized electrode to promote the bacterial growth [165]. A more complex method related to bacteria to enhance MFC performance is gene editing method to study its effects on the performance. [166], [167].

2.3.4 Poised Potential

Recent findings [168]–[171] show that bacteria may use different electron transfer systems when poised potential is applied to anode, significant current enhancement may be achieved by setting the anode potential which may be due to better biofilm [71], [123]. Setting the electrode potential can control the bacterial metabolism and affect the performance of MFCs when the poised potential on the electrode ria match the potential of redox component involved in EET across the bacterial membrane [140].

2.4 Applications of Microbial Fuel Cells

Microbial fuel cell is a promising technology for both bioelectricity generation and wastewater treatment. Researches on organisms, enzymes, electrode materials, electrode and cell configurations are going on in order to generate enhanced power density in microbial fuel cells. Microscale microbial fuel cells are attracting attention in numerous applications such as portable power supplies, and toxicity biosensors [36], [41], [97], [172]. Power densities are not feasible yet for most of these

applications but specific improvement strategies facilitate the development of MFCs to be compatible with different applications.

After investigating the literature about µMFC studies up to now, it is possible to classify the applications developed recently in two main categories: power generation devices and biosensors. Figure 2.11 summarizes the distribution of focused areas based on µMFC in literature.
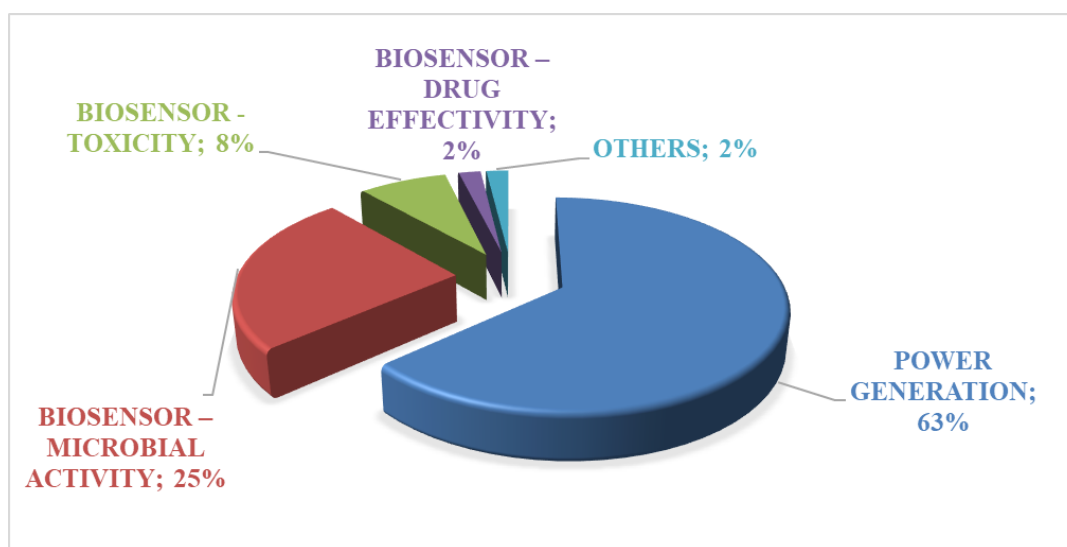
Figure 2.12. Application areas of µMFC in literature.

Power generation is the most preferred aim of µMFCs due to the applications reaching success in their macroscale counterparts. The difficulty of energy conversion in micrometer to nanometer dimensions pushes the researchers look for developing power generators in confined areas. At this point, µMFCs can be the answer to check. The smaller scales and self-sustainability are important parameters to be emphasized to generate power in micro-world.

Although the power densities obtained in µMFCs have not reached the target values for running the micro-scale devices, the results are promising. Trials on improvement of chamber and/or cell geometries, chamber or electrode materials, electrode surface

characteristics, and even modification on microbial genetics are accumulating day to day to obtain high performance μMFCs.

One of the popular topics in micro-scale applications is developing cheap, robust, simple, portable, reusable, or disposable, specific, functional and easy-to-use biosensors. This is also valid for the μMFC technology. In recent years, since μMFCs can favor most of the requirements of biosensors, studies for developing biosensors based on μMFC technique have increased. As in micro-scale biosensors, μMFC based biosensors also have different functionalities to be used as analytical tools: monitoring microbial activities, detecting toxicity levels or type of toxicant, and analyzing the effectivities of chemicals against other substances namely drugs. There are several studies about μMFC based biosensors focused on monitoring microbial activity. The aim is generally to identify or characterize the type of the microbes to be studied.

The linear relationship between the current density generated by the microbial fuel cells and the Biological Oxygen Demand (BOD) concentration supports using MFCs as BOD biosensors through bacterial metabolic activity [173] for monitoring water quality [174]–[176]. Bacteria affected by toxic substances or other organic contaminants have a lowered metabolism and thus a lower substrate consumption rate, decreasing the current generation. However, in this case, due to the volume to be processed, hundreds of μMFC arrays may be necessary for effective results.

2.5   Latest Trends in Literature

MFC technology has started to be researched intensively in the last fifteen years as a new electricity generation method. The main goal of the system is to be able to produce renewable electricity from organic components using bacteria. Electrons released due to consumption of organic components present in various wastes by the bacteria are transferred to the surface of a conductive electrode, and an electric current is obtained when the electrons passes through a load connecting the anode

and cathode. The proton exchange membrane, which separates the anode and cathode chambers, allows the proton transport from anode chamber to cathode chamber. Thus, electrochemical reaction is completed in the cathode chamber.

Exoelectrogenic bacteria, which can transfer the electrons generated by their metabolism to the metal surfaces, are important in MFC studies. Many macroscale studies aimed to characterize microbial fuel cells and increase the efficiency by trying different microorganisms. These studies have also addressed the problems encountered in MFCs. For example, since the total volume ratio of the electrode surface area decreases at large scales, the mass transfer kinetic resistance increases in macroscale. This causes proton and electron transport to slow down, resulting in reduced efficiency. This fact greatly impedes the transition of macro scale MFCs to real applications. Similar findings have led scientists to work on smaller scales and to different applications. As the total volume ratio of the electrode surface area increases in small-sized MFCs, the distance between the electrodes decreases, the mass transfer kinetic resistance decreases and the proton transport can be made easier. The efficiency of such MFC systems depends on the electrode surface area to volume ratio, the distance between electrodes, catalytic activity of electrodes, conductivity of electrolytes and resistance generated by PEM.

The major advantage of adopting microscale microbial fuel cells (μMFCs) arises from their reduced sizes. As the electrode surface area to volume ratio maximizes in micro-scale, mass transfer resistance reduces significantly. There are several μMFC studies reported in literature with μW level power output utilizing different microorganisms. The main problem encountered during these studies is relatively high internal resistances of μMFC systems, which decreases the efficiency. Besides, those studies generally utilized polydimethylsiloxane (PDMS) material which have a high O_2 permeability, reducing the electron transfer efficiency, and the efficiency of the overall system compared to the macro-scale counterparts. Fabrication of MFCs by silicon MEMS technology may handle oxygen intrusion problem.

It's been projected by researchers that the μMFC can be developed as stand-alone power sources, integrated power sources for body implants like peacemaker, or sensors to detect biological oxygen demand, lactate, toxicity, etc. in daily life, medicine, biotechnology or military [95], [98], [113], [177], [178].

2.6   Objective of the Thesis Study

The objective of this study is to develop a compact microbial fuel cell with microliter volume fabricated using silicon MEMS technology by overcoming existing performance limits. Start-up time and power density are the main parameters to compare the outcome of the study. The primary target areas are:

- enhancement of electrode and fuel cell architecture by adjusting their shapes and sizes.
- prevention or minimization of the oxygen diffusion into the anode chamber by an improved assembly.
- improvement of the operation conditions.
- power generation in microwatts level (~100 μW/cm^3).
- enhancement of bacteria attachment by decorating anode surface with functional groups.

CHAPTER 3

DEVICE DESIGN, FABRICATION AND ASSEMBLY

Further enhancements are necessary to integrate µMFCs into real life. Improvement of chamber and/or cell geometries and electrode surface characteristics can have intense effects on the performance. Considering the requirements of an µMFC studies, a new electrode and assembly were designed.

3.1   Design and Microfabrication of Planar Electrodes

In this study a dual chamber µMFC with gold electrodes for anode and cathode was designed. The design required two electrodes as anode and cathode, fluid ports for liquid handling, gaskets to prevent leakage, a proton exchange membrane, and an assembly system.

One of the important parameters during the design was electrode material and its active surface area which are crucial for the performance. Their enhancement may allow to decrease the mass transfer resistance and activation losses to keep internal resistance of the fuel cell small. Electrode material was chosen to be gold which has a very high electrical conductivity. Although gold may not be feasible for large-scale applications of fuel cells due to its cost, it is advantageous for small-scale applications. It is also compatible with MEMS based microfabrication techniques which have the capability to comply with mass production. Thus, electrodes were microfabricated with silicon wafers in batches.

Another parameter was the depth of chambers which defines the distance between the electrodes. In this study, this depth was planned to be formed by two different strategies. First one was the etching of reservoirs on silicon substrates. The other one

was defining the depth with the thickness of gasket layer. These thicknesses were defined to be kept minimum for shorter distance between anode and cathode but it could not be shorter than average biofilm thicknesses (10-100 µm).

Considering these parameters, several electrodes and µMFC assemblies were designed and fabricated.

3.1.1 First Generation Preliminary Electrodes

The study started with the usage of 1st generation µMFC electrodes. They were designed and microfabricated by METU BioMEMS researchers before the start of this study. There were two set of masks: one included electrode active areas having fully covered with gold, and the other one had ultra-micro electrodes (UME). Active area on UME was almost one third of fully covered gold electrodes because there were several gold lines acting as electrodes but between them there were isolated lines. UME is an electrode which has at least one dimension smaller than 25 µm. As the dimension of an UME approaches the diffusion layer thickness, the diffusion of the substrate, hence the mass transfer enhances.

There were a variety of designed electrodes. However, some of them were not feasible to use in this study. Thus, only Serpentine Electrode (SE) and Serpentine Ultra-Micro Electrode (S-UME) were used. These electrodes have serpentine shaped channel to manipulate to flow inside the chambers. Figure 3.1 shows the masks used during the fabrication of these electrodes. The masks were designed with Cadence® software (Virtuoso Layout Editor, Cadence Design Systems Inc., San Jose, CA, USA). Then, they were printed on glass substrates with chromium.
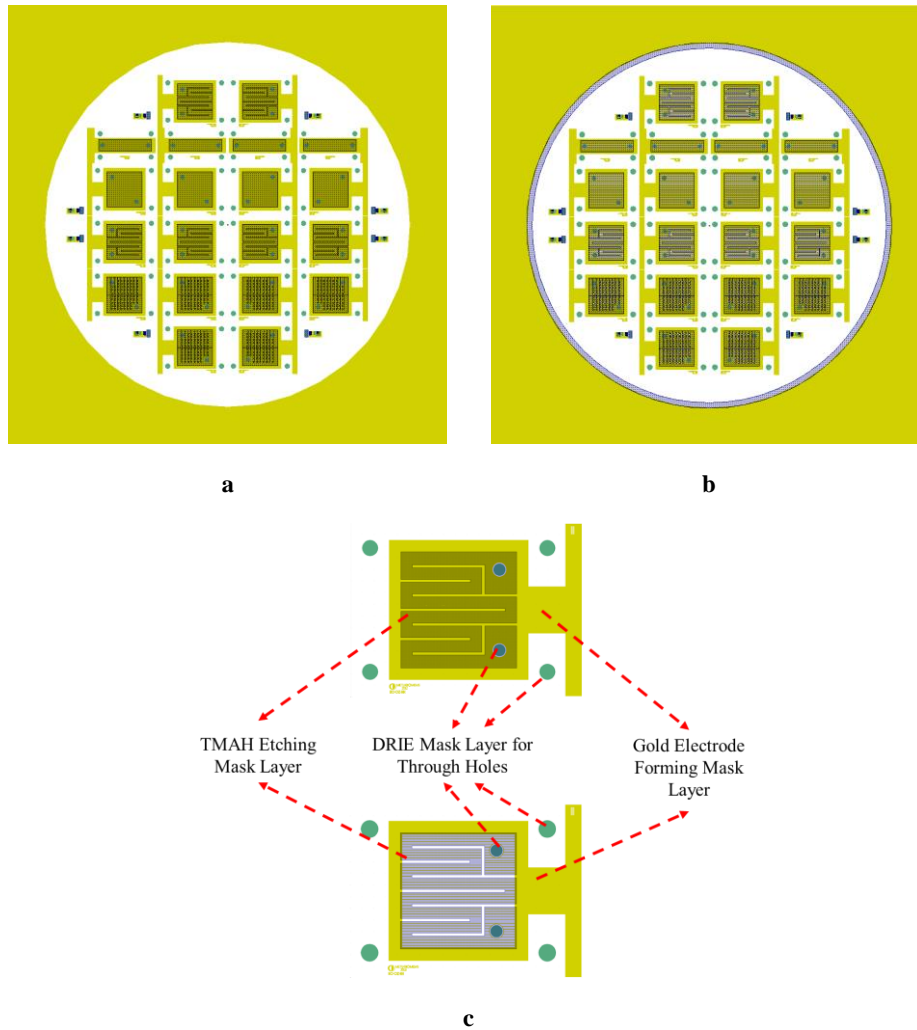
Figure 3.1. Designs of 4" mask for microfabrication of 1st generation electrodes. a: Mask including serpentine electrodes on wafer level; b: Mask including serpentine ultra-micro electrodes on wafer level; c: Die level masks for SE and S-UME electrode designs used in the study.

Using the fabricated masks, microfabrication was performed in cleanroom facilities of METU MEMS by METU BioMEMS researchers before the start of this study. As the first step, 4″ polished silicon wafer was cleaned and a SiO_2 layer was formed on both sides of the wafer to act as a mask during TMAH etching step. Then, the oxide layer was patterned with TMAH Etching Mask and the wafer was etched for ~50 µm with 25% TMAH at 80°C for 2.5 hours. After stripping the SiO_2 with BHF, a fresh

SiO$_2$ was coated on front side of the wafer by plasma-enhanced chemical vapor deposition (PECVD) to provide passivation.

Cr/Au layers (30 nm / 300 nm) were sputtered and patterned respectively by the standard photolithography process by coating photoresist (PR) on the wafer and exposing it with Gold Layer Forming Mask under UV light.

The through-holes were drilled via deep reactive-ion etching (DRIE) after patterning with photolithography using DRIE Mask for Through Holes. Before dicing, a protective photoresist layer was coated on the wafer to protect the electrode surfaces from debris formed during dicing step. After the process on the wafer was finished, it was diced into 20 electrodes as seen in Figure 3.2.
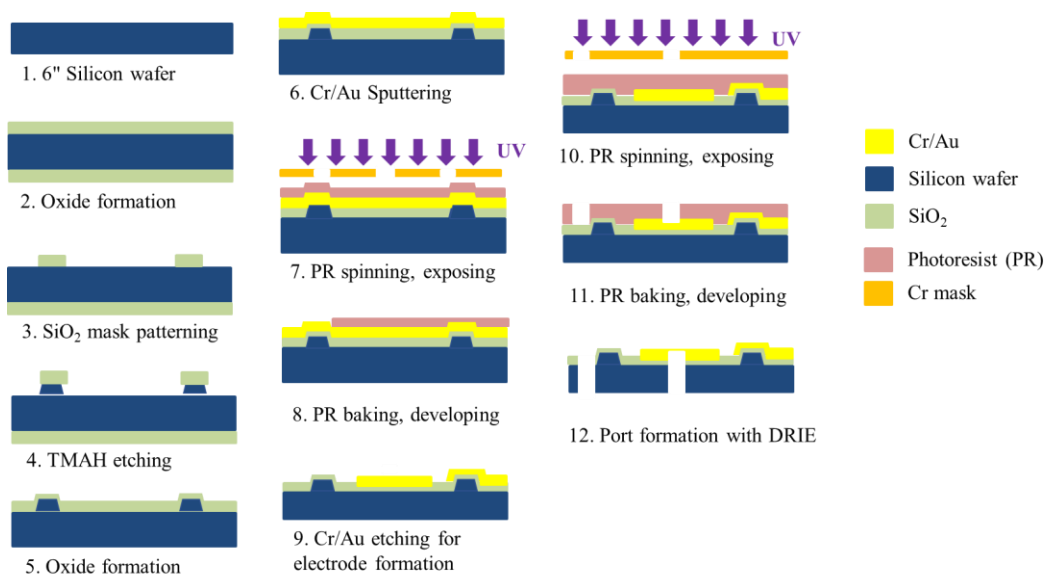
Figure 3.2. Microfabrication steps for 1st generation electrodes (UV: ultraviolet).

Figure 3.3 shows the serpentine channel and other structures etched with TMAH on silicon wafer with the close-up view of serpentine channels under optical microscopy. TMAH etched silicon <111> plane anisotropically with an angle of

38

54.7° with respect to <100> plane. The completed wafer with gold layer and etched through holes is also depicted before the dicing step.

a   b

c   d
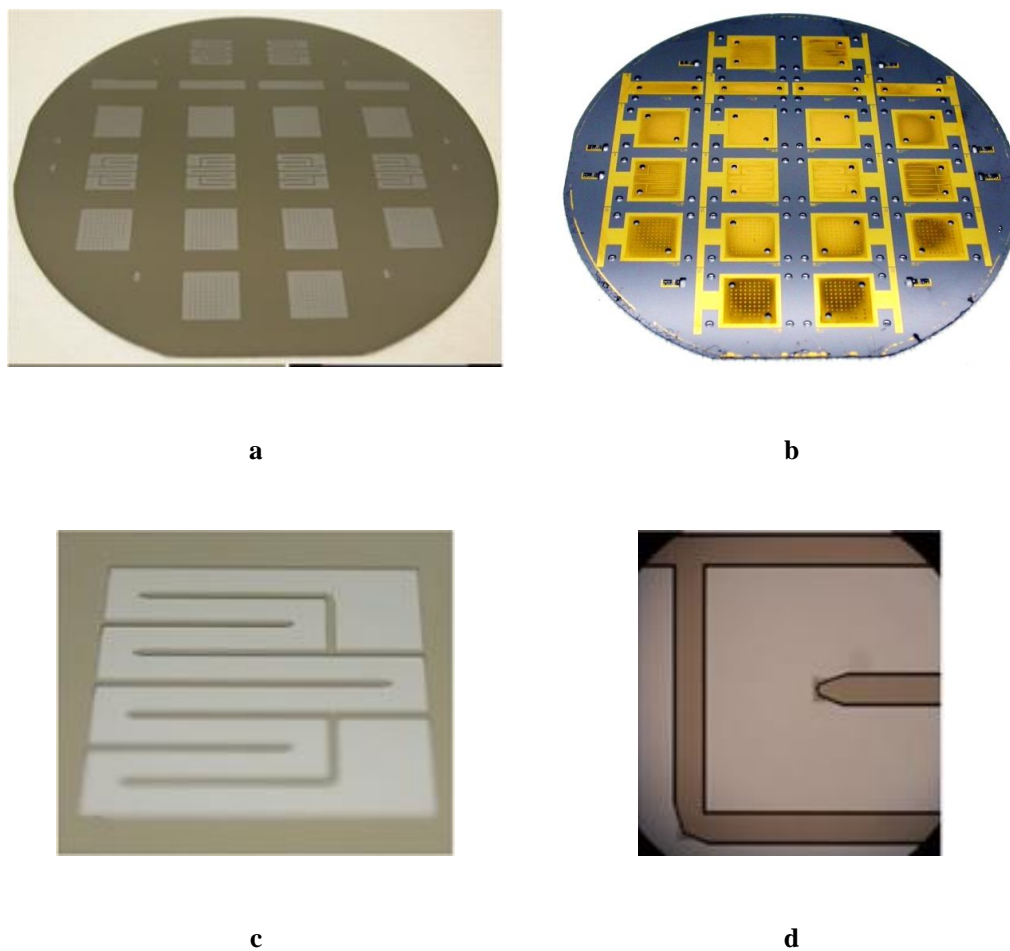
Figure 3.3. Microfabricated 1st generation electrodes. a: TMAH etched silicon wafer; b: Silicon wafer after sputtering of gold layers and before dicing; c: TMAH etched serpentine channels on silicon; d: Close-up of serpentine channel before gold sputtering where blunt corners were observed outer on right-angles due to TMAH etching.

Figure 3.4 shows the SE and S-UME diced. Both has the same structural elements except the active gold layer area. They were planned to be adapted to same μMFC

assembly. However, it is important to emphasize that, both anode and cathode had the same electrode type, either SE or S-UME.
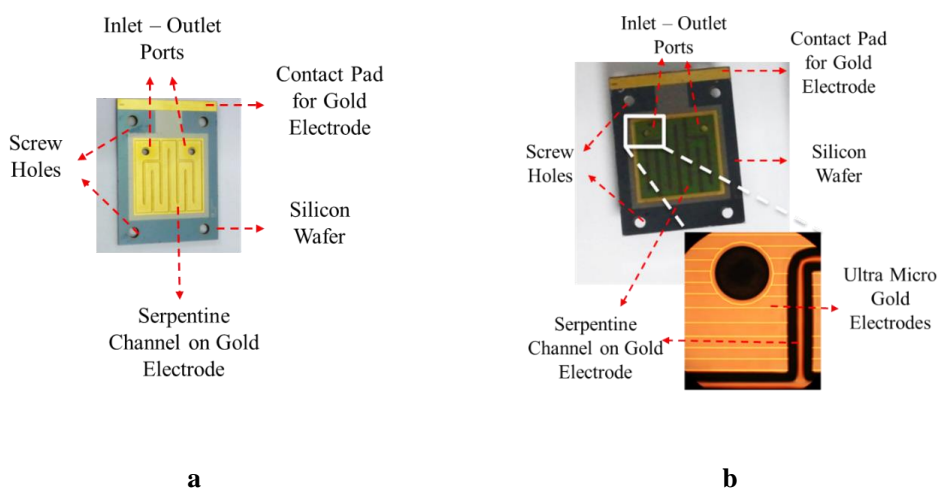
Figure 3.4. Diced 1st generation electrodes. a: Serpentine electrodes; b: Serpentine ultra-micro electrodes.

3.1.2 Second Generation Improved Electrodes

After performing experiments with 1st generation electrodes for electrode geometry comparison and for the investigation of operational conditions, it was decided to improve the electrode designs. First, it was concluded that depth of serpentine channels was not enough to manipulate to flow effectively because gasket thickness was higher. Also, it was planned to perform detailed Electrochemical Impedance Spectroscopy (EIS) analysis of fuel cell components which required the implementation of planar reference electrode (Figure 3.5). Another important factor was the unstable electrical connections in the previous generation where contact pads were small for soldering thick wiring.
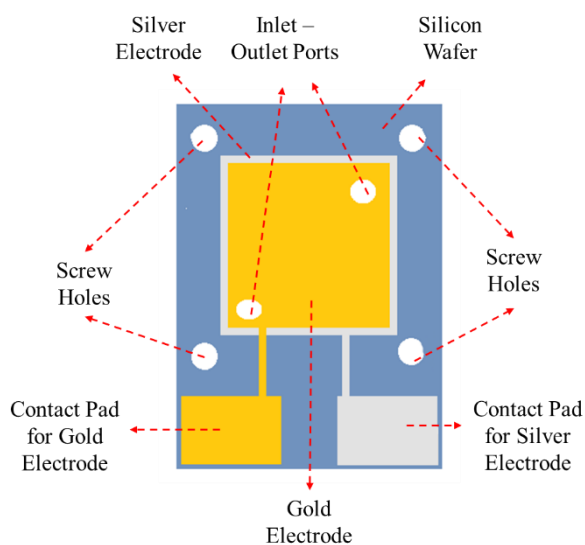
Figure 3.5. 2nd generation electrode design schematic.

Several µMFC electrode designs with different surface structures were analyzed to enhance the flow distribution inside the anode and cathode chambers. Flow of the anolyte and catholyte are important to be distributed homogenously so that mass transfer will be enhanced. Different surface protrusions forming channels were simulated with the help of microfluidic unit of COMSOL Multiphysics software. The flow was simulated to be laminar and flow distribution at 3 µL/min flow rate was studied (Figure 3.6).

Main electrode shape was both square and round because it was proposed that the corners of the square electrodes may not be effectively used even though there are channel forming structures as seen on the Figure 3.6. Designs with better flow characteristics and a plain round design were chosen to be microfabricated.
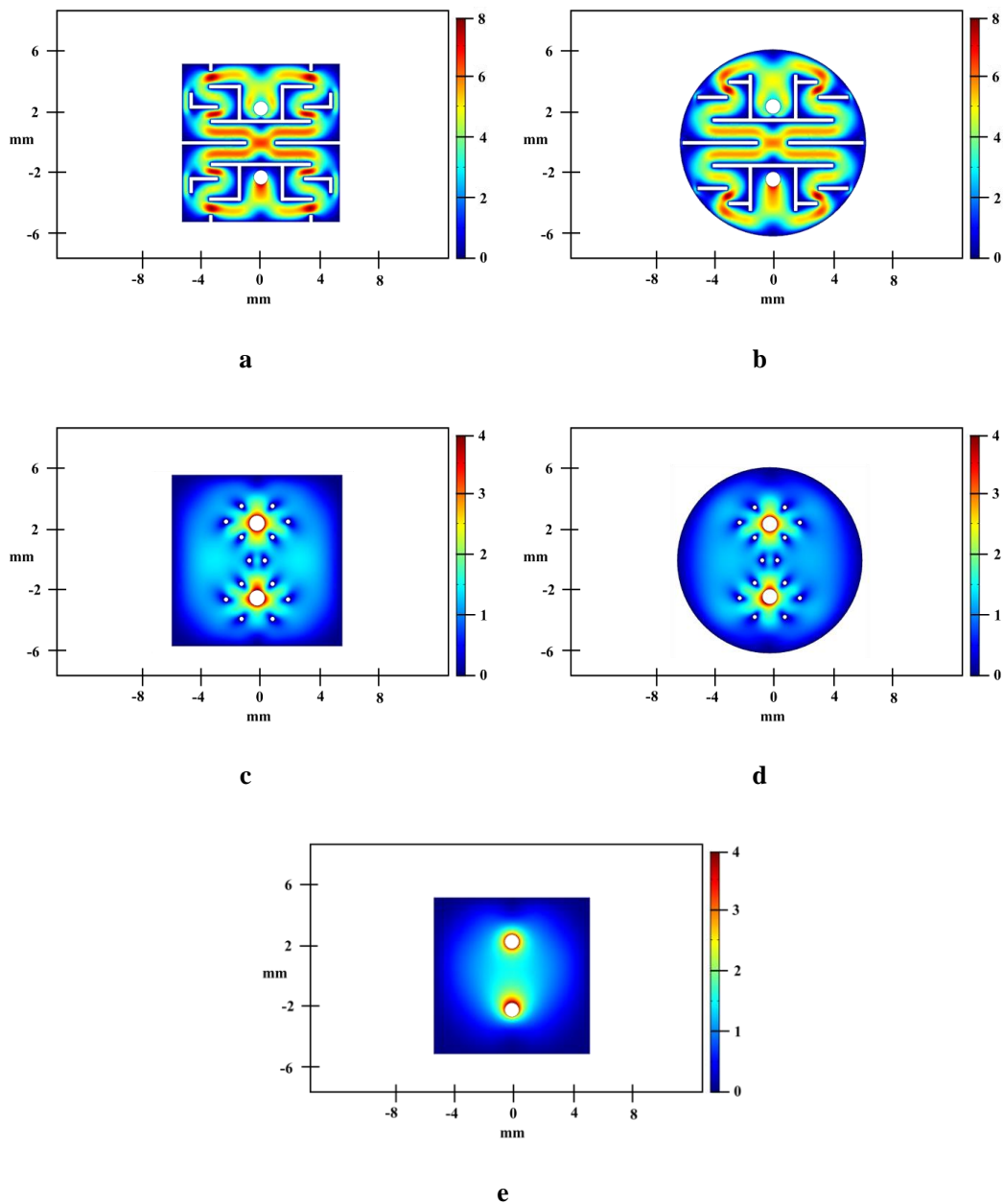
Figure 3.6. μMFC electrode flow simulations inside chambers. a: square electrodes with channels; b: round electrode with channels; c: square electrode with protrusions around ports; d: round electrode with protrusions around ports; e: plain square electrode.

As 1st generation electrodes, new designs were also microfabricated using silicon MEMS technology. Their microfabrication masks were drawn with CADENCE

software. There were four-different chrome-glass masks for TMAH Etching, Gold Layer Forming, Silver Layer Forming and DRIE for through holes (Figures 3.7 and 3.8).
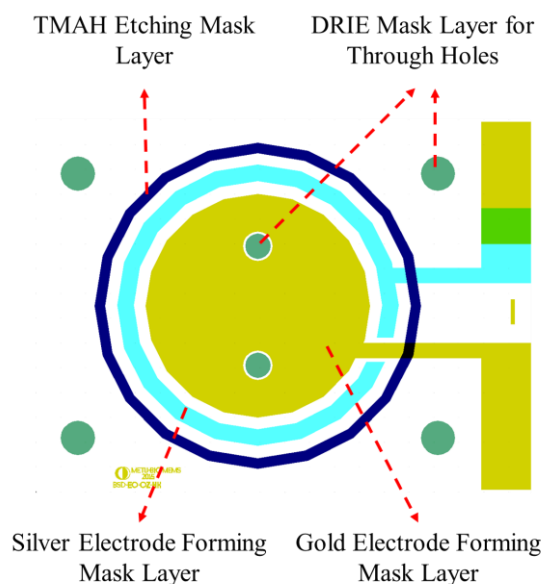
Figure 3.7. Microfabrication layers of different masks for round µMFC electrode.

All the designs had 150 µm high and 400 µm thick walls around the electrode to act like a reservoir for the flow. The 1st generation electrodes had only recessed areas inside the electrodes. In contrast, 2nd generation designs had recessed areas on both sides of the wall. Outer recessed area was to place a 170 µm thick gasket so that when µMFC was assembled both the etched wall and the gasket would minimize liquid leakage.
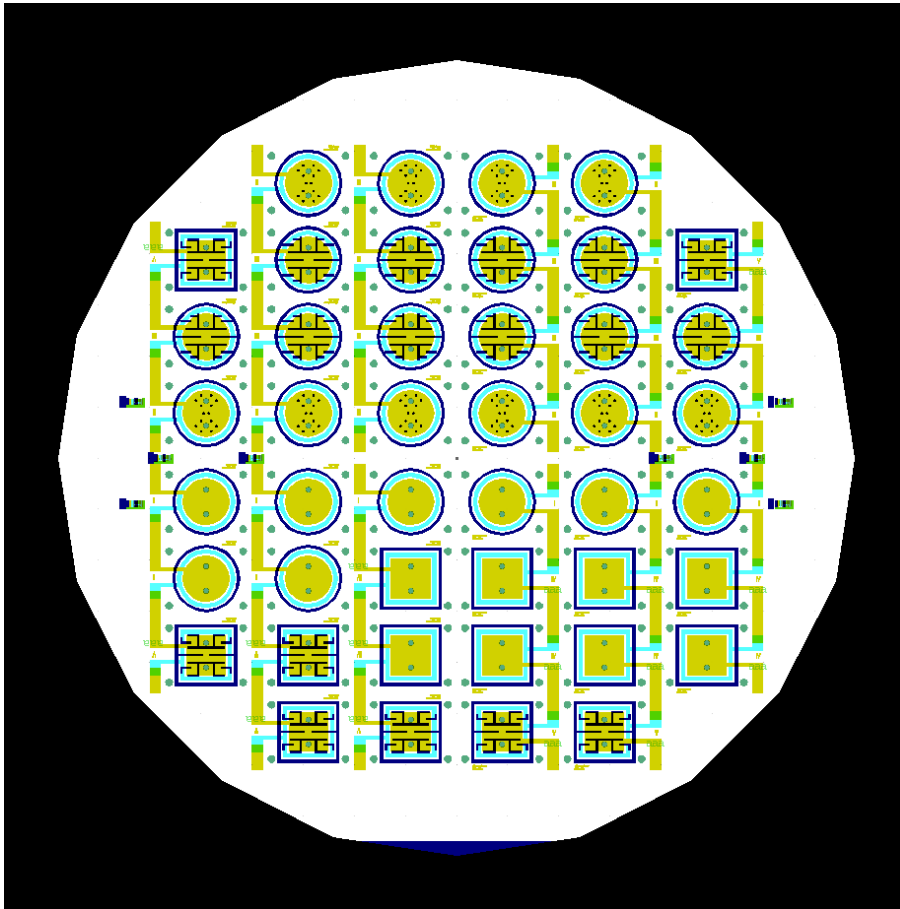
Figure 3.8. Design of 6" mask for microfabrication of 2ⁿᵈ generation electrodes.

Microfabrication was performed in cleanroom facilities of METU MEMS. The steps of the microfabrication are shown in Figure 3.9. As the first step, 6″ polished silicon wafer was cleaned and a Si_3N_4 layer was formed on both sides of the wafer to act as a mask during TMAH etching step. Then, the oxide layer was patterned with TMAH Etching Mask and the wafer was etched for ~150 µm with 25% TMAH at 80°C for 6 hours. After stripping the Si_3N_4 with reactive ion etching (RIE), a fresh SiO_2 was coated on front side of the wafer by plasma-enhanced chemical vapor deposition (PECVD) to provide passivation.

Cr/Au layers (30 nm / 300 nm) were sputtered and patterned respectively by the standard photolithography process by coating photoresist (PR) on the wafer and

exposing it with Gold Layer Forming Mask under UV light. Consecutively, Cr/Ag layers (30 nm / 300 nm) were sputtered and patterned respectively by the standard photolithography process by coating photoresist on the wafer and exposing it with Silver Layer Forming Mask under UV light. Then, the sacrificial silver layer was removed by lift-off technique.

The through-holes were drilled via deep reactive-ion etching (DRIE) after patterning with photolithography using DRIE Mask for Through Holes. Before dicing, a protective photoresist layer was coated on the wafer to protect the electrode surfaces from debris formed during dicing step. After the process on the wafer was finished, it was diced into 44 electrodes as seen in Figure 3.10 showing the microfabricated wafer with TMAH etching at different steps of the process. The silver layers on diced electrodes were chlorinated just before experiments to get AgCl layers. After this step, the electrodes were ready to be used in µMFC assembly in pairs. Chemicals and equipment used during the mentioned microfabrication are given the Table.

1st and 2nd generation electrodes had very similar process flows. 1st generation electrodes were microfabricated by METU BioMEMS researchers before the start of this study. There were two differences between the processes except the electrode designs. TMAH etching depth was ~50 µm for the 1st generation electrodes and ~150 µm for the 2nd generation electrodes. Furthermore, SiO_2 was used for 1st generation microfabrication and Si_3N_4 was used for 2nd generation microfabrication as a mask during TMAH etching.
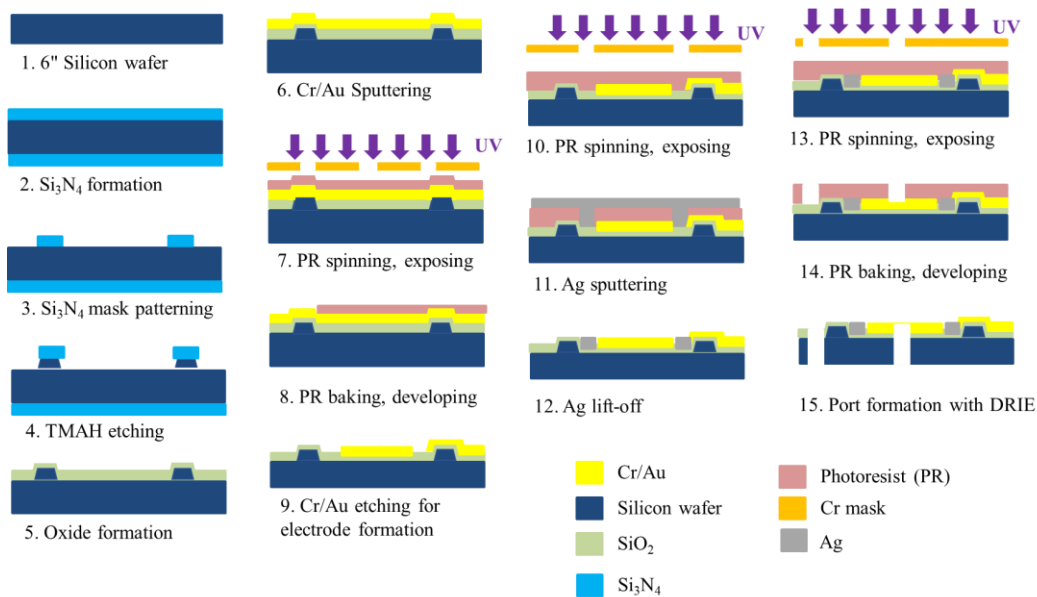
Figure 3.9. Microfabrication steps for 2nd generation electrodes with TMAH etching.
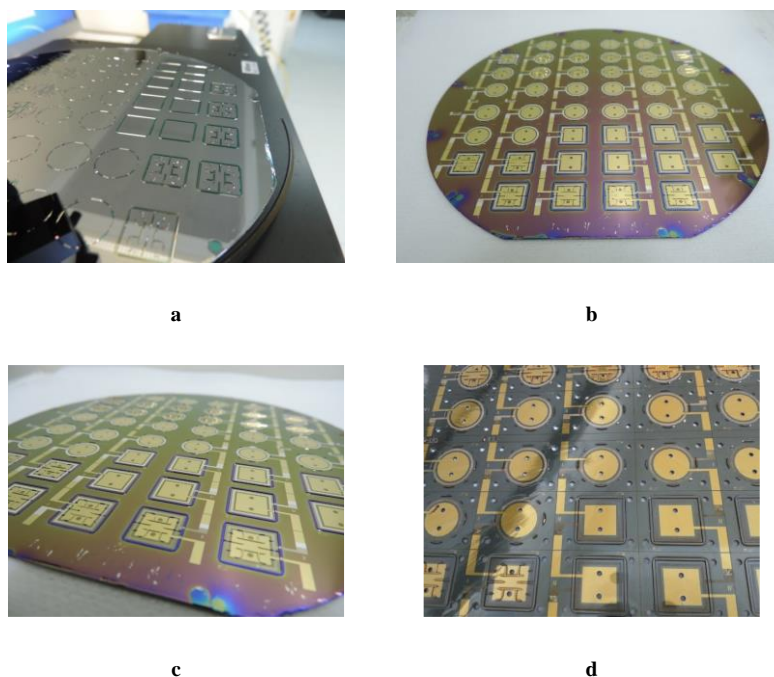
Figure 3.10. Microfabricated 2nd generation electrodes. a: TMAH etched silicon wafer; b, c: Silicon wafer after sputtering of gold layers and before dicing; d: Close-up of diced wafer with protective photoresist layer on top.

Table 3.1. Chemicals and equipment used during microfabrication.

| Category	Items
Chemicals	SPR220-3, S1813, MF24-A, SVC14, HF, TMAH, Transene gold etchant, Cr etchant, H_2SO_4, Piranha solution, Acetone, IPA, DI water
Equipment	STS PECVD, AJA sputter, EVG620 Exposure / Aligner, STS Pegasus DRIE, ACS 200 auto coater, NanoPlas O_2 plasma, IBC Branson O_2 plasma, Dektak profilometer, Dicer, Spinner, Optical microscope, Hot plate, Oven, Wet benches

Between the microfabrication steps, the wafer was inspected via optical microscope to check for any microfabrication flaws. After TMAH etching step of the wafer for 6 hours and 153 µm depth was achieved. However, when the formed 3D structures were inspected, it was observed that corners of right-angled shapes were under etched, and they were blunt (Figure 3.11). However, there were no collapses. Angled walls of round electrodes with respect to wafer flat were damaged. Alignment marks also were damaged, and the shapes were not as designed. Although it was expected that TMAH would cause under etch due to long etching duration for ~150 µm depth, it was more than expected. This problem could be meliorated by a new mask design, also the depth of the of the etch could be decreased.

a   **b**   **c**

d   **e**   **f**
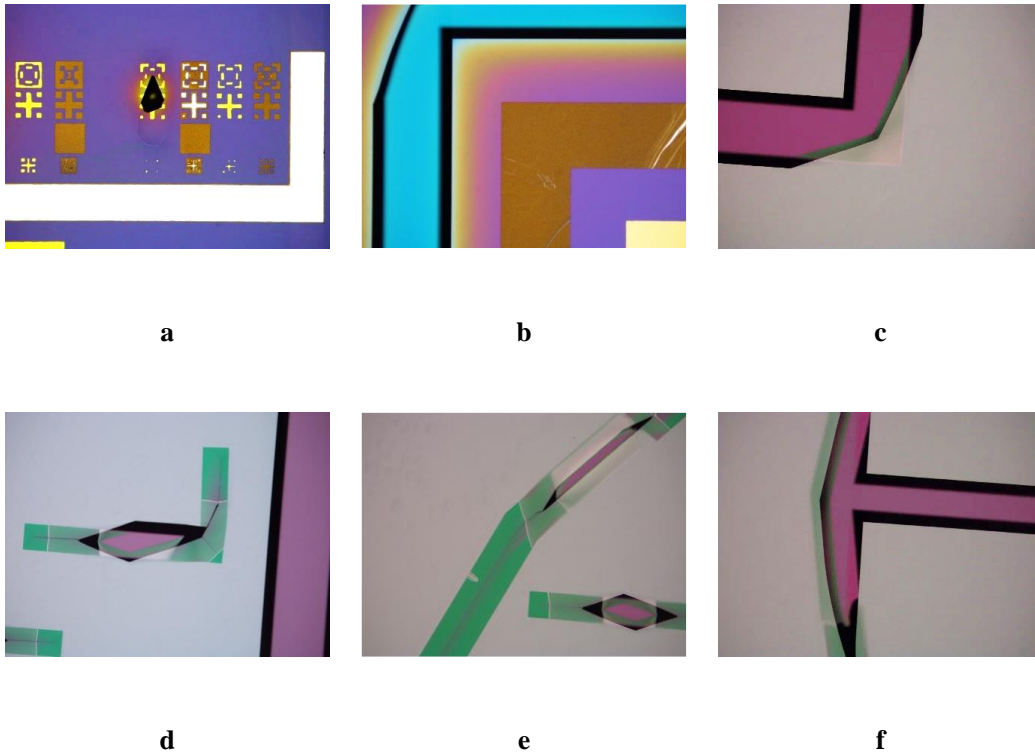
Figure 3.11. Challenges faced during TMAH etching of 2nd generation microfabrication. a: Over etching of TMAH mask alignment mark; b, c: Blunt outside corners of right-angled walls; d: Over etching of thin right-angled walls; e, f: Over etching of round walls.

At this point, it was decided to continue microfabrication of new batch of wafer without TMAH etching. Same microfabrication steps were used omitting the TMAH etching. Figure 3.12 shows microfabrication process steps and Figure 3.13 shows the images of the wafer at the start with oxide formation and at the final step with metal layers on.
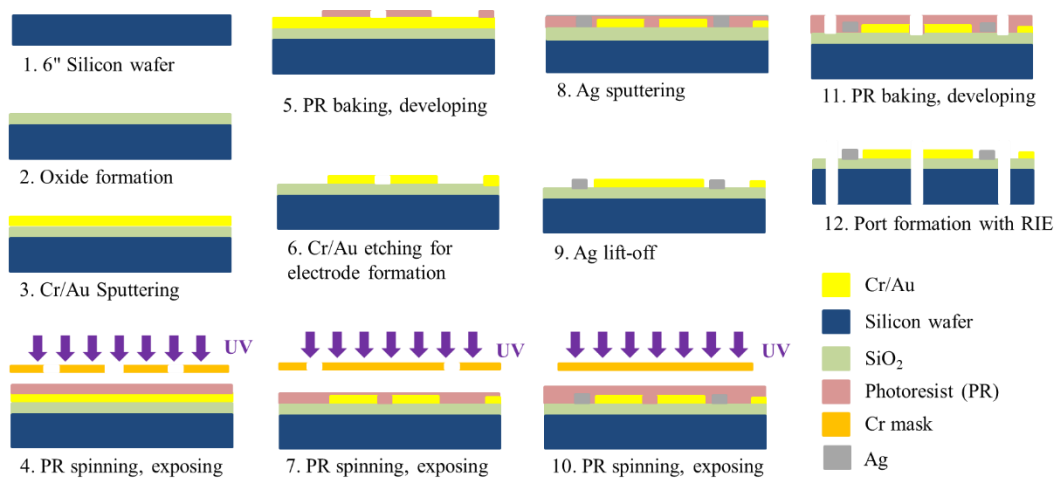
Figure 3.12. Microfabrication steps for 2nd generation electrodes without TMAH etching.

a   **b**
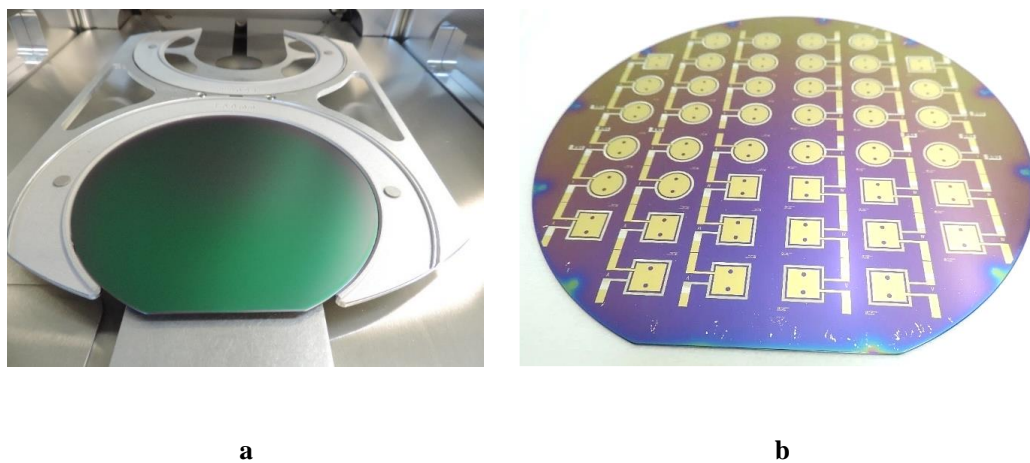
Figure 3.13. Microfabrication steps of 2nd generation electrodes without TMAH etching. a: Silicon oxide coated wafer; b: completed wafer before dicing.

The difference of shaping reservoir walls with etching from different microfabrication batches is shown on Figure 3.14.
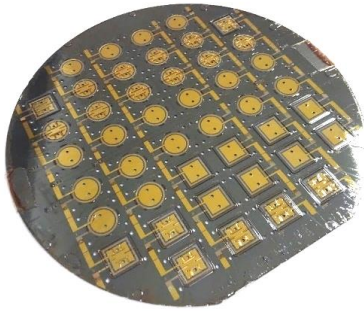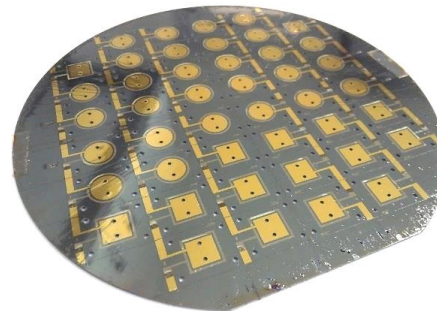
a   b
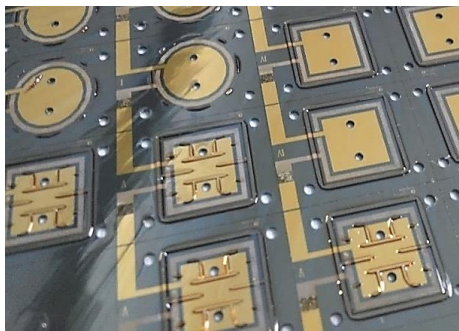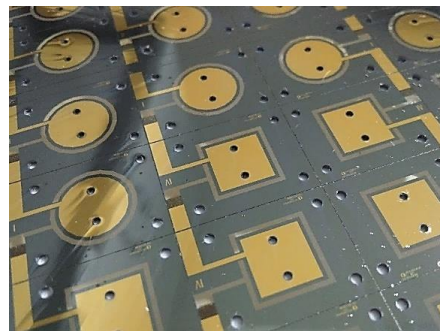
c   d

Figure 3.14. Comparison of 2nd generation electrodes from different batches. a, c: Silicon oxide coated wafer; b, d: without TMAH etching.

After the completion of the microfabrication, silicon wafer was diced into 44 electrodes. Figure 3.15 shows the diced round electrode with planar gold and silver active regions.
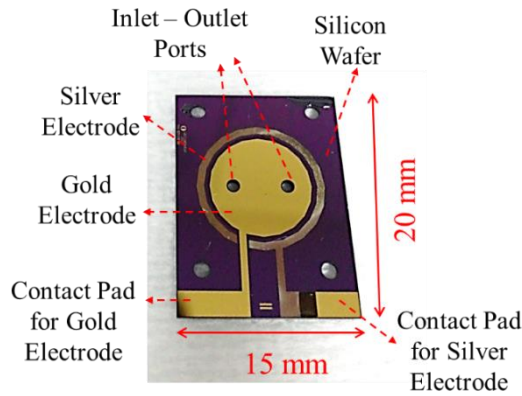
Figure 3.15. Diced 2nd generation electrode without walls.

3.1.3 Third Generation Wide-footprint Electrodes

After the experiments performed with 2nd generation electrodes, it was decided that μMFC assembly requires improvement. This improvement details are given in section 3.2. To comply with the assembly changes, electrode footprint needed to be widened. Electrode active area and dimensions were kept constant. The microfabrication facility has opportunities to operate with both 6" and 4" masks. During the microfabrication of new batch, the main equipment was set to work with 4" masks. Thus, new mask was designed on a 4" template as shown on Figure 3.16.

a   b
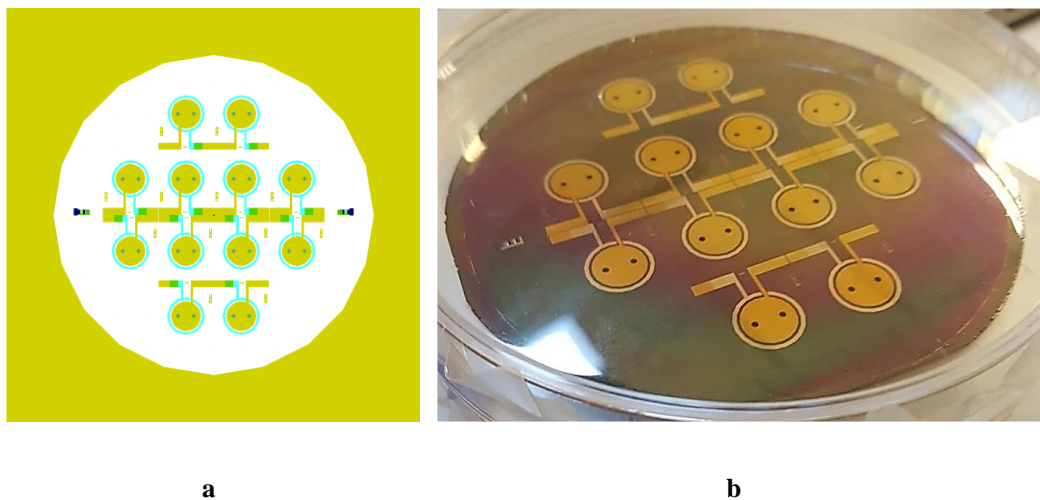
Figure 3.16. a: 3rd generation 4" mask; b: Diced 3rd generation wafer after dicing.

Figure 3.17 shows all the individual electrode designs used during the experiments.
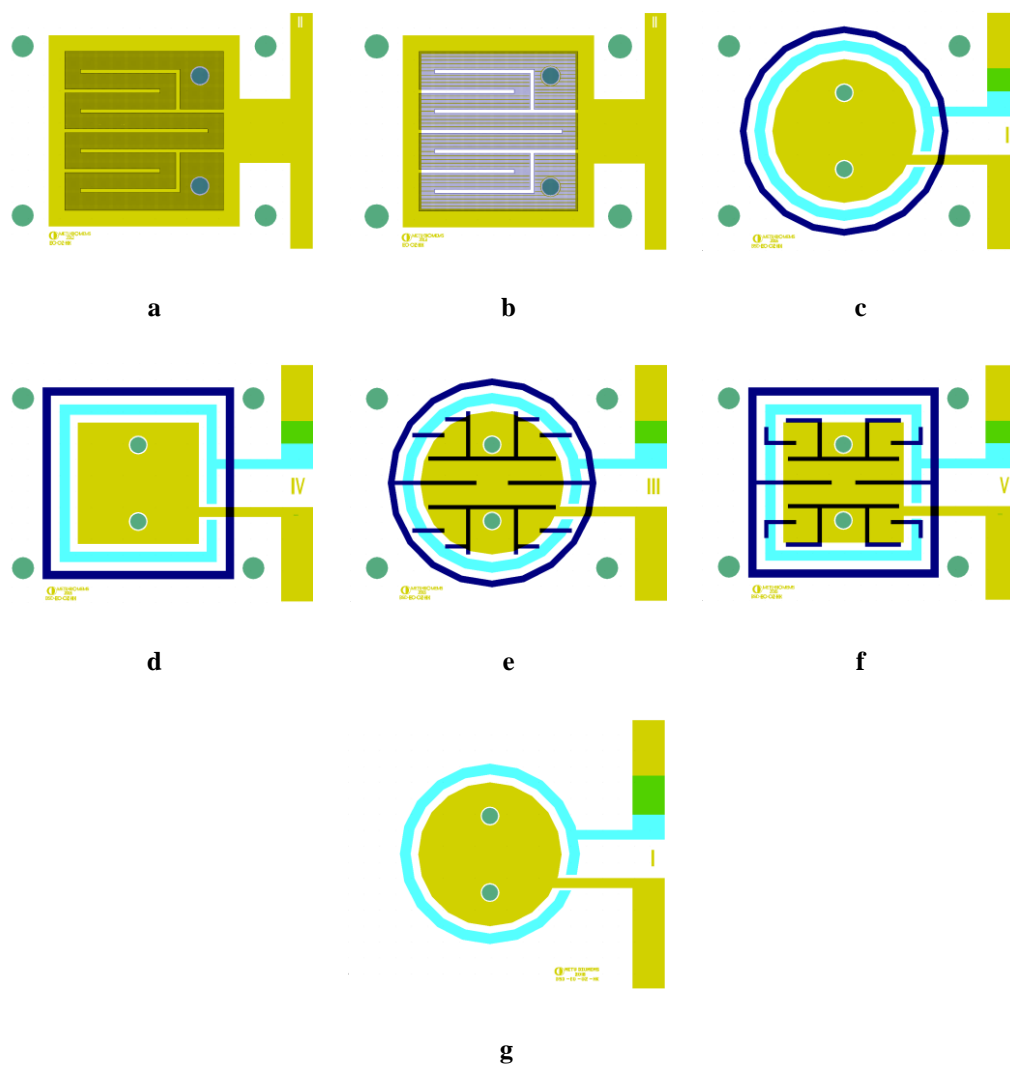
Figure 3.17. All the electrode designs used in the study. a: 1st Generation serpentine electrode; b: 1st Generation serpentine UME; c: 2nd Generation round electrode; d: 2nd Generation square electrode; e: 2nd Generation round electrode with channels; f: 2nd Generation square electrode with channels; g: 3rd Generation wide footprint round electrode.

3.2 Microfluidic Setup Design and Assembly

To operate the μMFC, the experimental setup was required to be connected to a digital multimeter for continuous recording of the voltage and to a syringe pump for feeding anolyte and catholyte separately to related chambers. To meet these requirements, different interfaces were designed for electrical and microfluidic connections throughout the study. In this regard, Figure 3.18 shows the designed schematic for μMFC assembly.
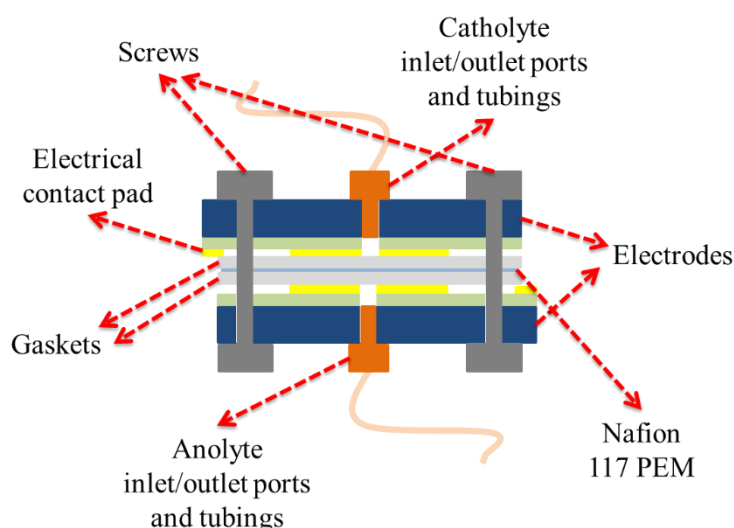
Figure 3.18. Designed schematic for μMFC assembly.

3.2.1 Deep Chamber Fuel Cells

For the assembly of 1st generation electrodes, two small pieces of Ice Cube polymer sheets (Freudenberg GmbH, 350 µm × 15 mm × 17 mm, with square holes at the center) were used as gaskets between the electrodes and Nafion 117 PEM, which separates the anode and cathode chambers. There are thinner PEM options in the market but Nafion 117 was available in the research facilities. Also, it was the most

studied PEM in literature for MFCs which helped the compare the study results easily. The channel thickness was defined by these thick gaskets. When two electrodes on substrates faced each other at 180°, the gold contact pads were exposed for electrical wiring. The contact pad on these electrodes were small so when thick wiring was soldered on, they stripped the gold layer, rendering it unusable. Thus, the electrical connections were attached by clamps on the contact pads. However, this was not a robust solution.

Through holes were drilled through the silicon substrate for anolyte and catholyte feeding via microfluidic connection. CapTite microfluidic bonded port connectors made of polyetherimide (Ultem®, LabSmith), was bonded to each port on back side of electrodes using epoxy adhesive (LS-EPOXY, LabSmith) for the interface between tubing and chamber. CapTite one-piece fitting and two-piece adapter made of PEEK (LabSmith) were attached to one end of tubing pieces with epoxy adhesive. Flexible, transparent, and sterile tubing pieces (OD 1/16", ID 1/32") from venipuncture kits were used after removing their needle. Transparent tubing helped observation of biofilm forming inside the tubing due to low flow rate. The other end of tubing had Luer Lock connector and a closing cone which provided easy attachment to syringes. 10 mL and 50 mL sterile disposable syringes were used (Genject). All the mentioned components are shown in Figure 3.19.
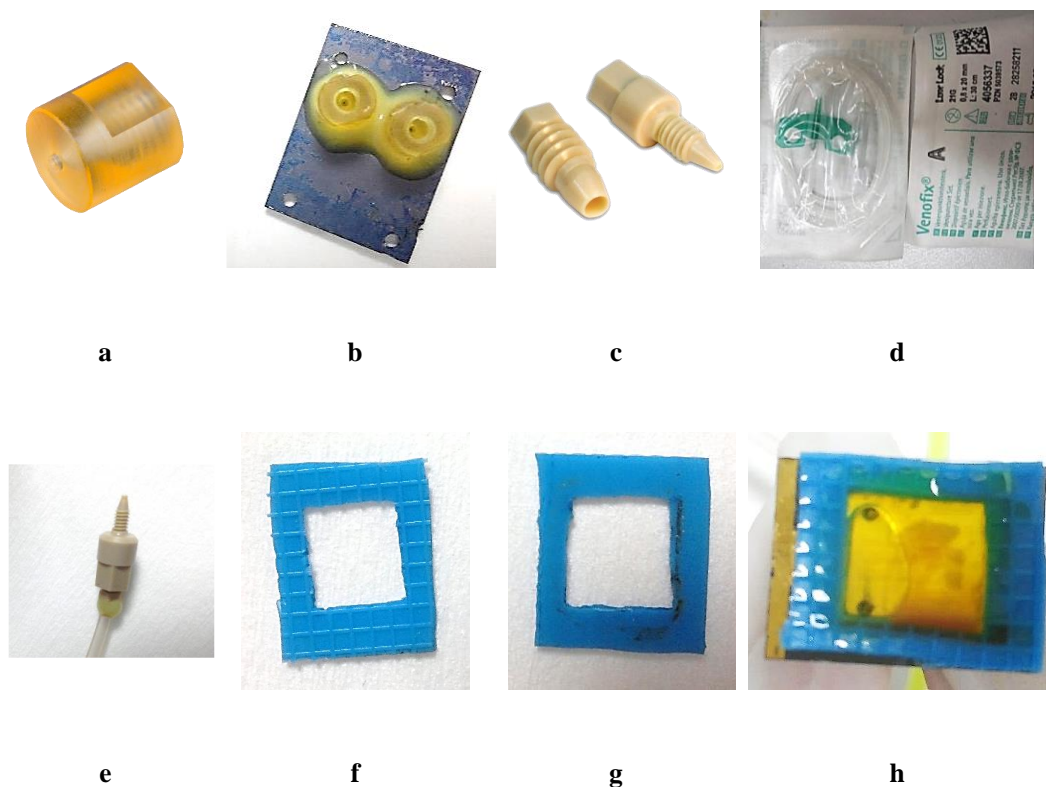
Figure 3.19. Components of Deep Chamber μMFC. a: CapTite bonded-port connector; b: port connectors bonded to back of electrode; c: CapTite fitting; d: tubing; e: microfluidic connector attached tubing; f, g: Front and back sides of Ice Cube polymer sheets shaped to be used as gaskets (0.35 mm,); **h:** Liquid inside the chamber formed between electrode and PEM during disassembly.

There were through holes at the corners for screws to keep the assembly together. However, when metal crews were used, they damaged the silicon substrate and caused falling apart off the disassembly. As a result, all layers were manually stacked on top of each other (Figure 3.20) and tightly kept together by clamps instead of screws. Assembled μMFC had two chambers (96 μL for each chamber for assemblies with SE and S-UME), defined as anode and cathode chambers. The exposed conductive electrodes area per chamber differed among the designs.

<div align="center">
a   **b**
</div>
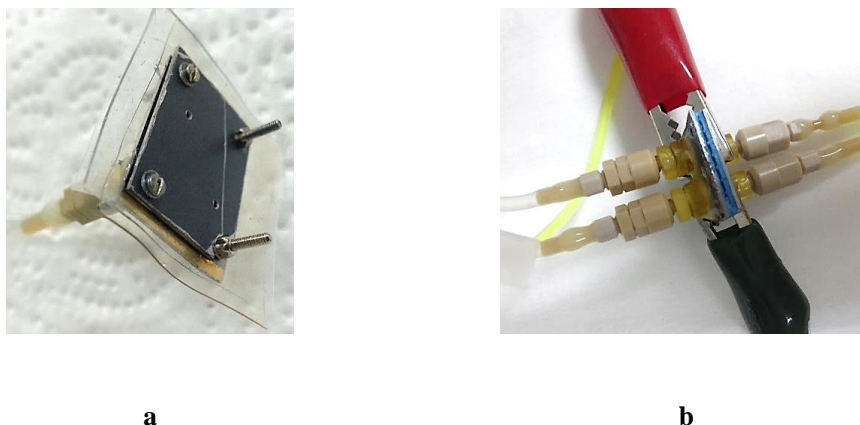
Figure 3.20.µMFC assembly options. a: initial trials with screws and without gaskets; b: Deep chamber µMFC

3.2.2   **Shallow Chamber Fuel Cells**

During the assembly of 1st generation electrodes, a thick gasket material is preferred. However, its thickness was higher than the etched chamber thickness, which prevented using the etched channels for flow manipulation. Thus, a thinner gasket was preferred for the studies with 2nd generation electrodes. Gel-Pak manufactures WF Gel-Film which is a gel layer bonded to a metalized polyester substrate material giving it a light gray appearance. It can be purchased at different film thickness from 170 to 560 µm. It can adhere to several types of surfaces.

For the assembly of 2nd generation electrodes, two small pieces of Gel-Pak WF 1.5-X4 gel films (170 µm × 15 mm × 17 mm, with round or square holes at the center) were used as gaskets between the electrodes and Nafion 117 PEM, which separates the anode and cathode chambers. The channel thickness was defined by these thin gaskets. When two electrodes on substrates faced each other at 180°, the gold contact pads were exposed for electrical wiring. The contact pad on these electrodes were bigger than 1st generation electrodes so soldering on gold contact pads was possible.

Through holes were drilled through the silicon substrate for anolyte and catholyte feeding via microfluidic connection. CapTite microfluidic bonded port connectors

made of polyetherimide (Ultem®, LabSmith), was bonded to each port on back side of electrodes using epoxy adhesive for the interface between tubing and chamber. CapTite one-piece fitting and two-piece adapter made of PEEK (LabSmith) were attached to one end of tubing pieces with epoxy adhesive. Flexible, transparent, and sterile tubing pieces (OD 1/16", ID 1/32") from venipuncture kits were used after removing their needle. Transparent tubing helped observation of biofilm forming inside the tubing due to low flow rate. The other end of tubing had Luer Lock connector and a closing cone which provided easy attachment to syringes. 10 mL and 50 mL sterile disposable syringes were used (Genject). All the mentioned components are shown in Figure.

| a | b | c | d |

| e | f | g | h |
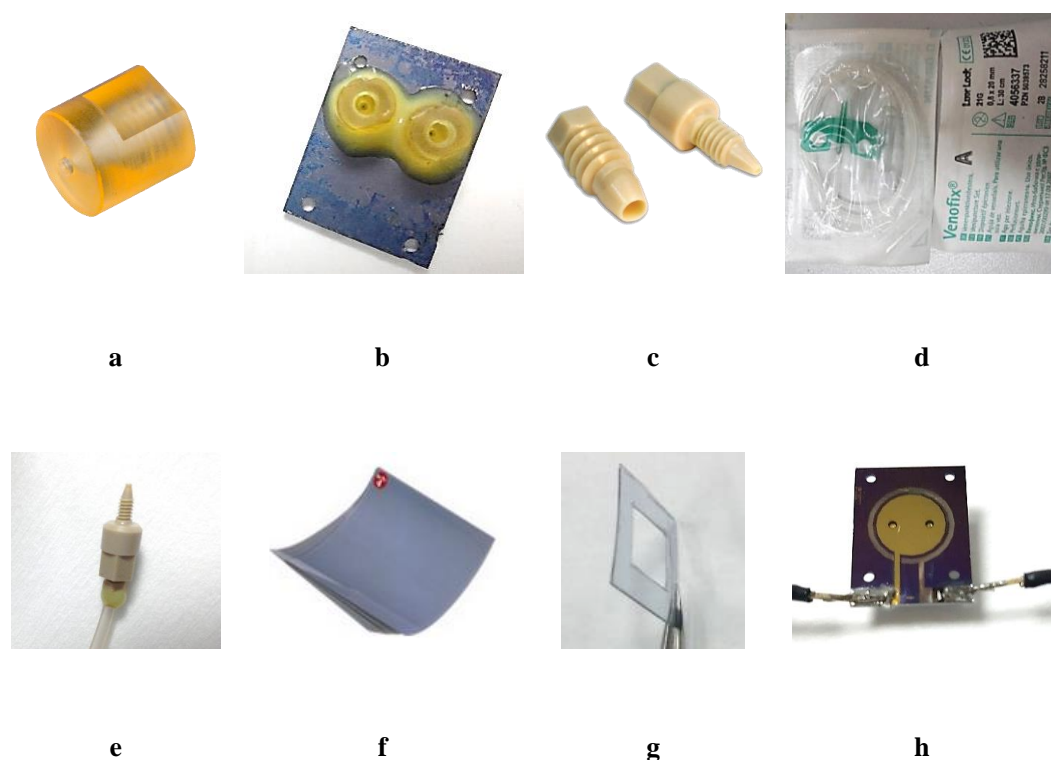
Figure 3.21. Components of Shallow Chamber µMFC. a: CapTite bonded-port connector; b: Port connectors bonded to back of electrode; c: CapTite fitting; d: Tubing; e: Microfluidic connector attached tubing; f: WF Gel-Film (Gel-Pak) sheets; g: WF Gel-Film piece shaped as a frame to be used as gasket (170 µm thick); h: Round electrode with soldered wiring to contact pads.

Although there were through holes at the corners for screws to keep the assembly together in 2nd generation electrodes too, all layers were manually stacked on top of each other (Figure) and tightly kept together by clamps instead of screws. Assembled µMFC had two chambers (10.4 µL for each chamber for assemblies with round electrodes), defined as anode and cathode chambers. The exposed conductive electrodes area per chamber differed among the designs.
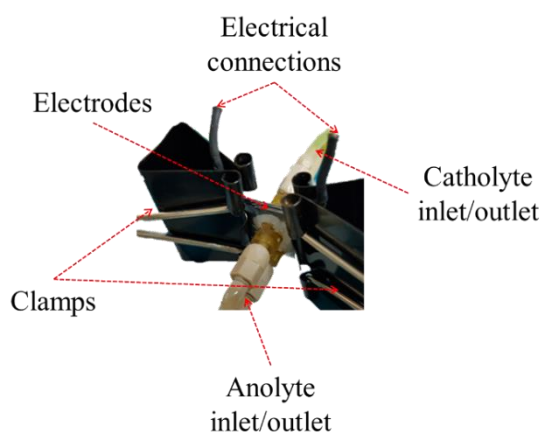
Figure 3.22. Assembled shallow chamber µMFC.

3.2.3   Implementation of Fuel Cell Case

During the experiments with shallow chamber µMFCs, there were some challenges faced. First, clamps did not always provide a tight assembly of the MFC. They were prone to leakage and required adjustment often during operation. Also, electrical connections were not stable even the with soldering. Clamps damaged the soldered parts time to time. Moreover, electrical noise was high during impedance measurements due to poor wiring. Furthermore, during the surface modification experiments, modified gold anode surfaces got damaged if microfluidic port was attached later than modification. Microfluidic ports got sometimes damaged during surface modification with thiols solved in ethanol. This caused liquid leakage.

To solve these problems, a fuel cell case was designed. It was made of an acetal homopolymer (Delrin® by Dupont, Wilmington, DE, USA). It had non-stiff touch so that it would not damage fragile silicon electrode edges.

It included two pieces of same electrode holder with recessed areas to place electrodes. For the assembly, two pieces of Gel-Pak WF 1.5-X4 gel films were used as gaskets between the electrodes, and Nafion 117 PEM, which separates the anode and cathode chambers, was used as proton exchange membrane. All layers were manually stacked on top of each other (Figure 3.23).
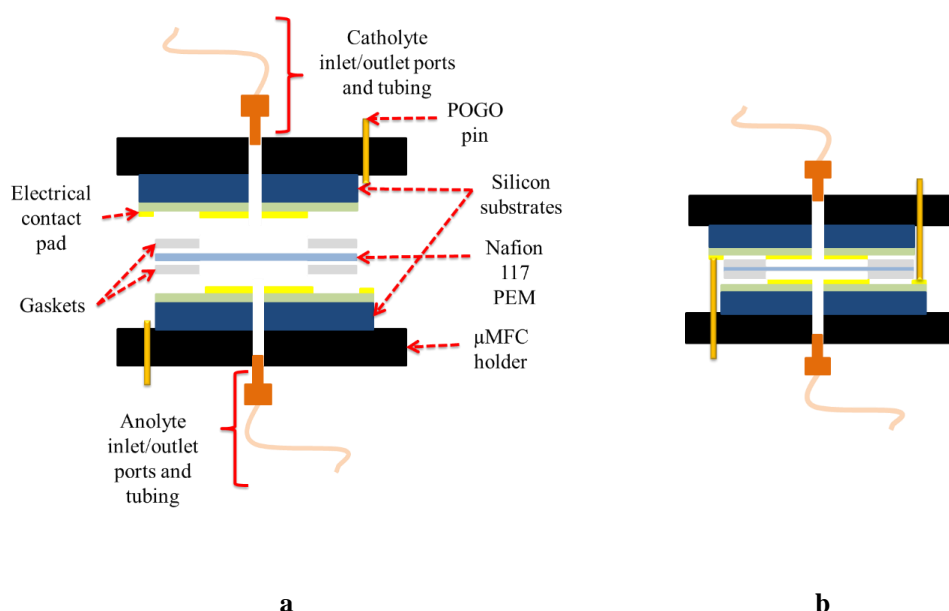
Figure 3.23. Schematic of µMFC. a: extended view; b: assembled view.

Assembled µMFC case had two chambers (10.4 µL each), defined as anode and cathode chambers. The active electrode area per chamber was 0.61 cm^2. The microfluidic inlet and outlet of the µMFC were connected from the outside of the holder via finger-tight PEEK (polyether ether ketone) fittings (IDEX Health & Science) and capillary fused silica tubing (ID 150 µm, Postnova Analytics GmbH, Landsberg am Lech, Germany). Capillary fused silica tubing pieces were connected

to luer lock syringes by appropriate PEEK connectors (IDEX Health & Science) for a tight fitting.

Electrical connections were made by inserting pogo pins (spring-loaded electrically conductive pins) (OD 0.66 mm, FIXTEST GmbH, Engen, Germany) from the outside of the µMFC holder to electrical contact pads of both anode and cathode electrodes. Figure 3.24 depicts the components of µMFC holder.

a

b

c

d
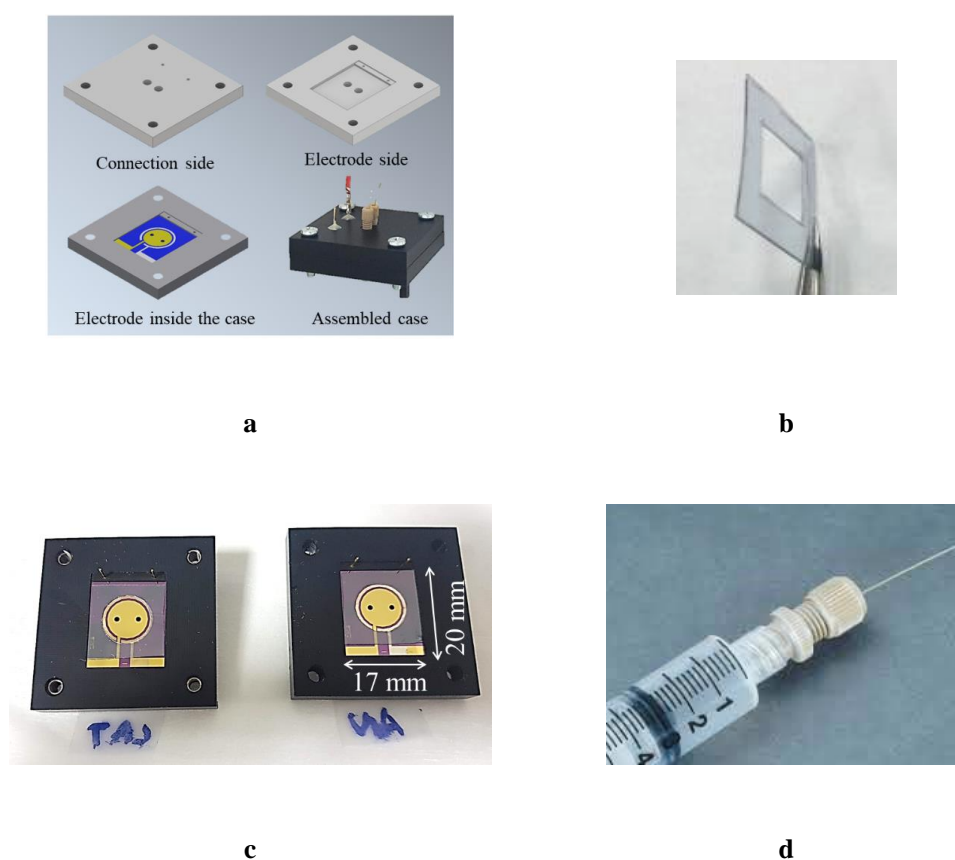
Figure 3.24. Components of µMFC Case. a: Schematics of holder design and assembled case; b: Gel-Pak gasket; c: Electrodes placed inside the holders; d: Syringe, luer-lock connector, and fused silica tubing.

Figure 3.25 shows the comparison of assembled shallow chamber µMFC and µMFC case. The case had a compact design. It was less prone to leakage and electrical connection problems.
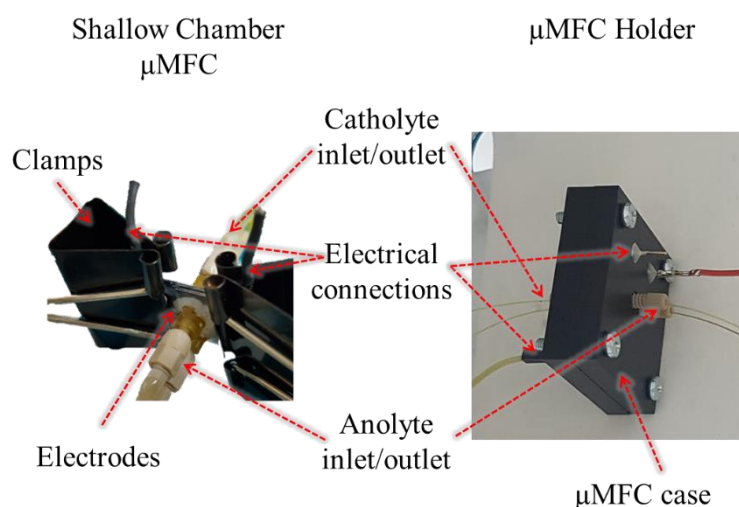
Figure 3.25. Comparison of assembled shallow chamber µMFC and µMFC case.

3.2.4   Macro MFC

To compare the operational advantages and disadvantages of the macro and microscale MFCs, a macro MFC was designed (Figure 3.26). It was made of plexiglass to make the visual inspection possible throughout the experiments. Each chamber had 35 mL volume formed by inserting Nafion 117 PEM between the chambers. Two pieces of PDMS gaskets were inserted between the PEM and chamber edges to prevent leakage. Screws provided a tight assembly. The microfluidic connections were glued on the sides of each chamber. The flow was supplied by the two-channel syringe pump. Thin cables were inserted through the holes for electrical connection between the breadboard and the electrodes in each chamber. 1 cm x 1cm gold substrates were used as anode and cathode. They were soldered to cables. Macro MFC setup also included digital multimeter and computer for data recording.
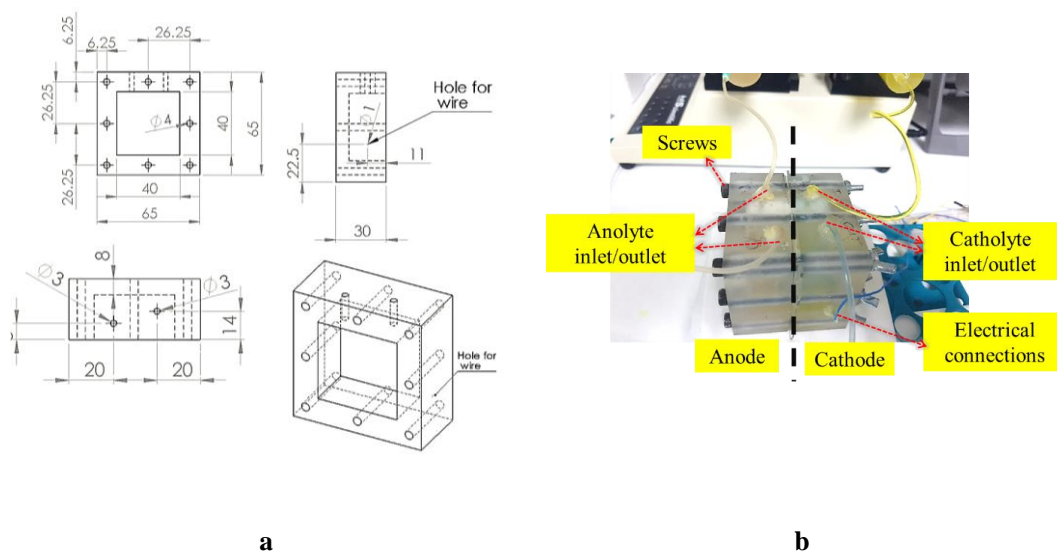
Figure 3.26. Macro MFC. a: Technical drawings; b: assembled plexiglass macro MFC with microfluidic and electrical connections.

3.2.5   Flow Cell

To investigate the biofilm formation and the interaction of bacteria with different surfaces, a flow cell was designed. To make the visual inspection possible throughout the experiments, it was made of plexiglass. It had a reservoir to place the bare gold or surface-modified gold substrates inside. The cover had two holes on the outside for continuous medium supply by syringe pump. PDMS gasket frame with 2 mm thickness was sandwiched between the reservoir edges and the cover to prevent leakage (Figure 3.27). The assembly was kept close by large plastic clamps.
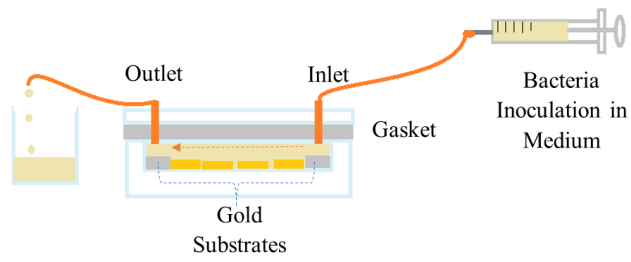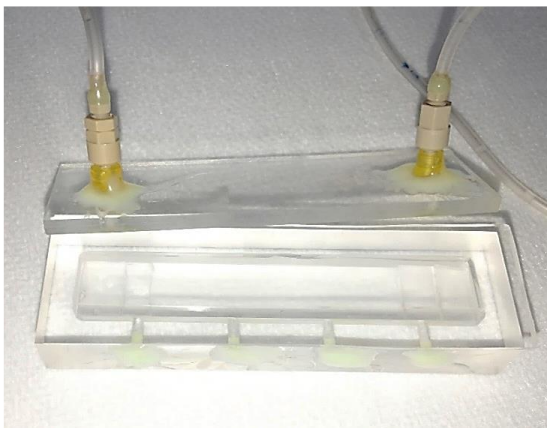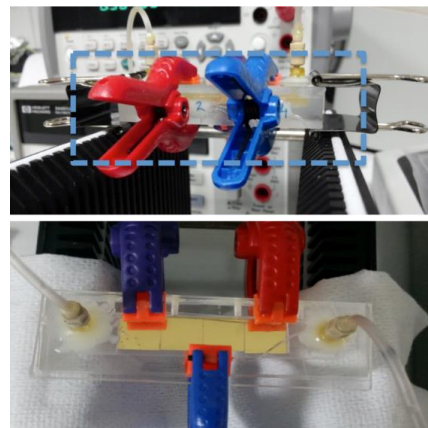
Figure 3.27. Flow cell. a: Technical drawings; b: fabricated plexiglass reservoir and cover with microfluidic connections; c: assembled plexiglass flow cell with microfluidic connections and gold substrates inside.

CHAPTER 4

EXPERIMENTAL STUDIES

After the microfabrication of the electrodes and the assembly of the fuel cells as defined in Chapter 3, the experimental studies continued as explained in this chapter. Electrodes from different generations were investigated separately but the experimental conditions were the same unless stated otherwise.

4.1   Materials

All the plastic wares (Petri dishes, pipette tips, cell spreaders, inoculation loops, syringes falcon tubes and other reservoirs) used throughout the study were sterile and single use only.

0.1 M phosphate buffer solution was prepared by dissolving 12 g of NaH_2PO_4 in 1000 mL of DI water. Then, its pH was adjusted to 7.5 by addition of 1 M NaOH.

Aerobic culture medium was prepared by dissolving 30 g of Tryptic Soy Broth (TSB) in 1000 mL of DI water. Then, it was sterilized in an autoclave at 121°C for 15 min. It was stored at +4°C to avoid contamination.

Agar medium was prepared by dissolving 40 g of Tryptic Soy Agar (TSA) in 1000 mL of DI water. Then, it was sterilized in an autoclave at 121°C for 15 min. When it was cooled down to 45°C, it was poured into sterile Petri dishes. The Petri dishes were sealed and stored at +4°C to avoid contamination.

20 mM lactate medium was prepared by mixing the following chemicals in the given concentrations: 20 mM lactate (1.49 mL/L), 28 mM NH_4Cl (1.5 g/L), 1.34 mM KCl (0.1 g/L), 5 mM NaH_2PO_4 (0.6 g/L), 0.7 mM $NaSO_4$ (0.1 g/L), 1 mM $MgSO_4.7H_2O$ (0.246 g/L), 20 mM PIPES (6.047 g/L), 52 mM NaCl (3.04 g/L), 0.2 mM $CaCl_2$ (0.022 g/L), 1 mL trace mineral solution (ATCC). Then the volume was completed to 1000 mL by adding DI water and pH was adjusted to 7.0. Later, it was sterilized in an autoclave at 121°C for 15 min. After adding 1 mL vitamin solution, it was stored at +4°C to avoid contamination.

100 mM $K_3Fe(CN)_6$ solution was prepared by dissolving 32.9 g of $K_3Fe(CN)_6$ in 1000 mL of 0.1 M PBS (pH 7.5) solution. Then, it was sterilized in an autoclave at 121°C for 15 min. It was stored at room temperature by covering the bottle with aluminum foil to prevent photocatalytic degradation.

50% glycerol solution for the storage of bacteria culture at -80°C was prepared by mixing glycerol and DI water in equal volumes. Then, it was sterilized in an autoclave at 121°C for 15 min. It was stored at room temperature.

2% glutaraldehyde solution for the fixation of bacteria on the surfaces was prepared by mixing 25% glutaraldehyde stock solution (Grade I, 25% in H_2O, Sigma Aldrich, St. Louis, MO, USA) with DI water.

Nafion 117 proton exchange membrane was pretreated before usage to clean. After cutting into 5 cm x 5 cm pieces, it was boiled at 80°C in 3% H_2O_2 for 1 hour. Then, it was rinsed in DI water. At the second step, it was boiled at 80°C in DI water for 2 hours. Then, it was boiled at 80°C in 0.5M H_2SO_4 for 1 hour. After rinsing again in DI water, it was stored completely immersed in DI water to preserve the moisture level until usage.

Polydimethylsiloxane (PDMS) gasket was prepared by mixing 10 units of Sylgard 184 pre-polymer and 1 unit of curing agent per weight. After mixing vigorously in a cup, it was kept in a desiccator to degas the bubbles for 30 min. Then, it was cured for 30 min at 70°C in Petri dishes. It was important to pour the viscous liquid inside

the dishes in ~2 mm thickness. After curing, the solidified PDMS was stored at room temperature.

Piranha solution was prepared by mixing concentrated sulfuric acid (H_2SO_4) an 30% hydrogen peroxide (aqueous H_2O_2) in 30:70 v/v ratio.

Dip-coating of Zeolite Beta40 on bare gold surfaces was done by Akata Kurç Research Group following their previous biosensor surface modifications [179], [180].

4.2 Bacterial Growth and Inoculation

Shewanella oneidensis MR-1 (ATCC, Manassas, VA, USA) which is a facultative anaerobic electrogenic bacterium was used during all the steps of the study. Glycerol stocks (stored at -80 °C) of the bacteria were grown on TSA at 30 °C for 24 h by the streak plate method using single-use plastic inoculation loops to obtain single colonies. Then, a single colony was cultured in TSB medium on a shaker (150 rpm) at 30 °C for 24 h under aerobic conditions in 1:10 volume ratio. 1000 µL of remaining bacteria solution was mixed with 225 µL of 50% glycerol solution to prepare new stock to be stored at -80 °C.

Bacteria growth was monitored by colony-forming unit (CFU) determination (~2.5 $\times 10^6$ CFU/mL). 1:10 bacteria solutions in TSB were prepared by serial dilution until reaching 10^{-6} dilution by addition of TSB. Then, the final solution was spread by cell spreader on TSA plates in replicates. After incubating the plates aerobically at 30 °C for 20-24 hours, single colonies on each plate was counted if they were between 30 and 300 colonies.

To be fed as the anolyte, fresh TSB and bacteria inoculum were mixed (1:1 v/v%). Throughout the operation, the inoculum ratio fed to the system was decreased and only pure TSB was fed after the third or fourth day.

Different stages of bacteria inoculum are presented in Figure 4.1.
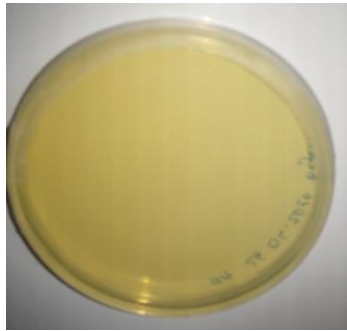
a
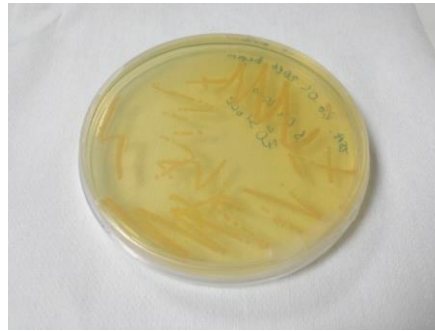
b

c
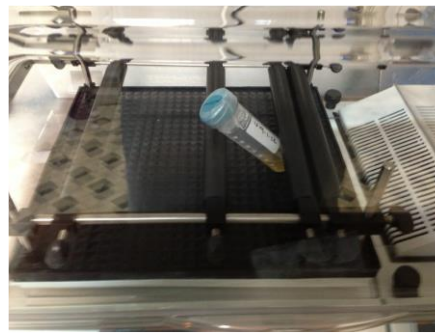
d
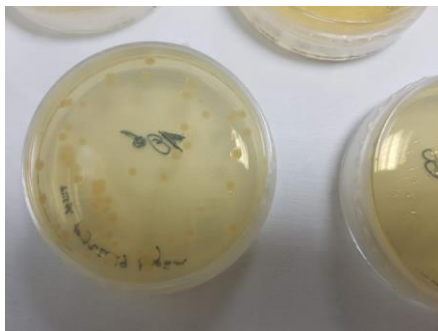
e
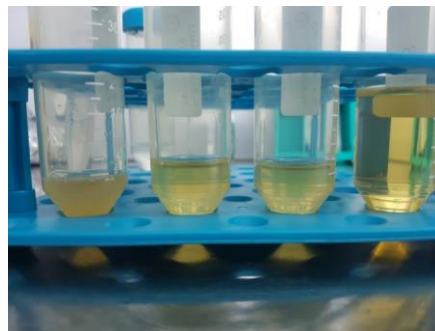
f

Figure 4.1. Cultivation and inoculation of bacteria in sterile environment. a: TSA prepared in Petri dish; b: bacteria colonies cultivated on TSA by streak plate technique; c: inoculation of bacteria colonies into TSB solution under sterile environment; d: Cultivation of bacteria in a shaker with temperature controlled environment; e: single colonies of the bacteria grown on TSA during CFU determination; f: different medium and bacteria solutions from left to right: one flask of 24 h grown bacteria in TSB, two flasks of bacteria just mixed with TS, pure TSB solution.

4.3 Operation of Microbial Fuel Cells

µMFCs described in Chapter 3 were assembled at different stages of the study. Figure 4.2 shows the assembled µMFCs from different phases. The initial experiments were done with Deep Chamber µMFCs using Serpentine and UME electrodes fabricated for 1st generation. During these initial tests, flow rates were compared and the values resulting in higher power output were used throughout the study.
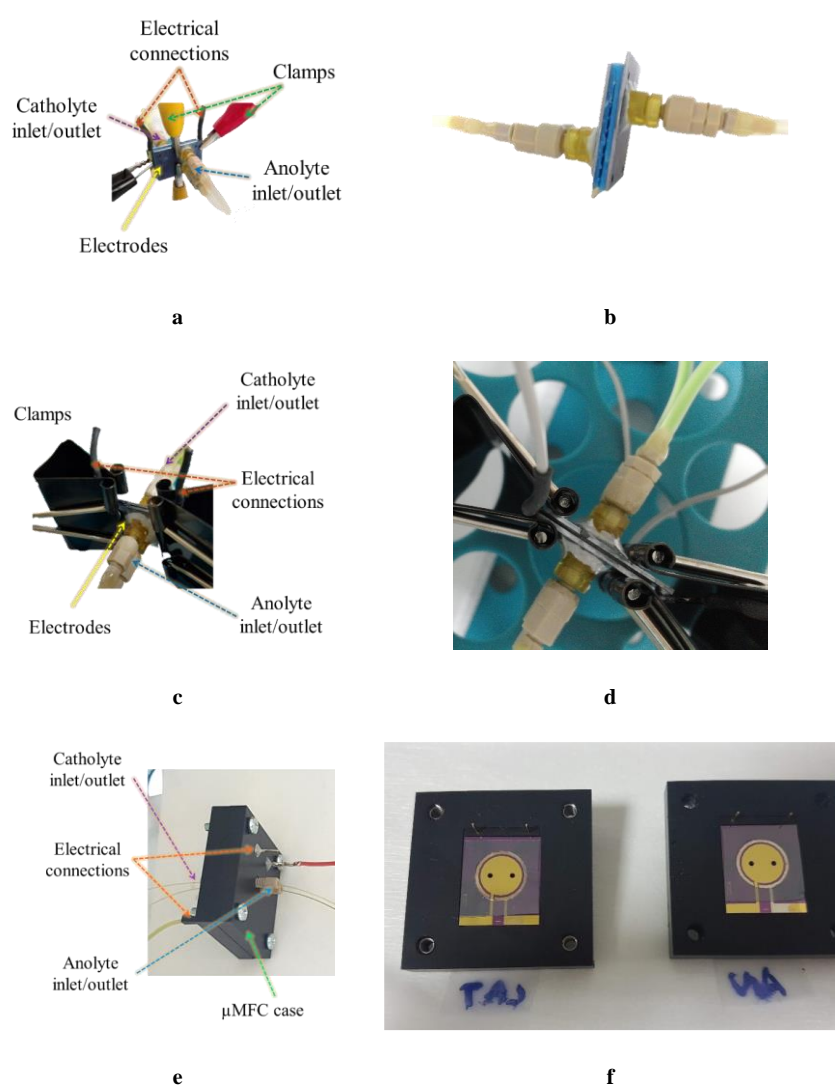
Figure 4.2. Assembly of µMFC at different stages of the study. a, b: Deep chamber µMFC; c, d: Shallow chamber µMFC; e, f: Shallow chamber µMFC with holder.

The assembled μMFCs were connected to experimental setup including a syringe pump with dual channel for flow control, a breadboard for electrical connections, digital multimeter connected to a computer to record the potential between the anode and cathode data across a load (or no load) continuously. The outlets of anolyte and catholyte from the fuel cell were collected in two different glass beakers as waste. The test setup is shown in Figure 4.3.
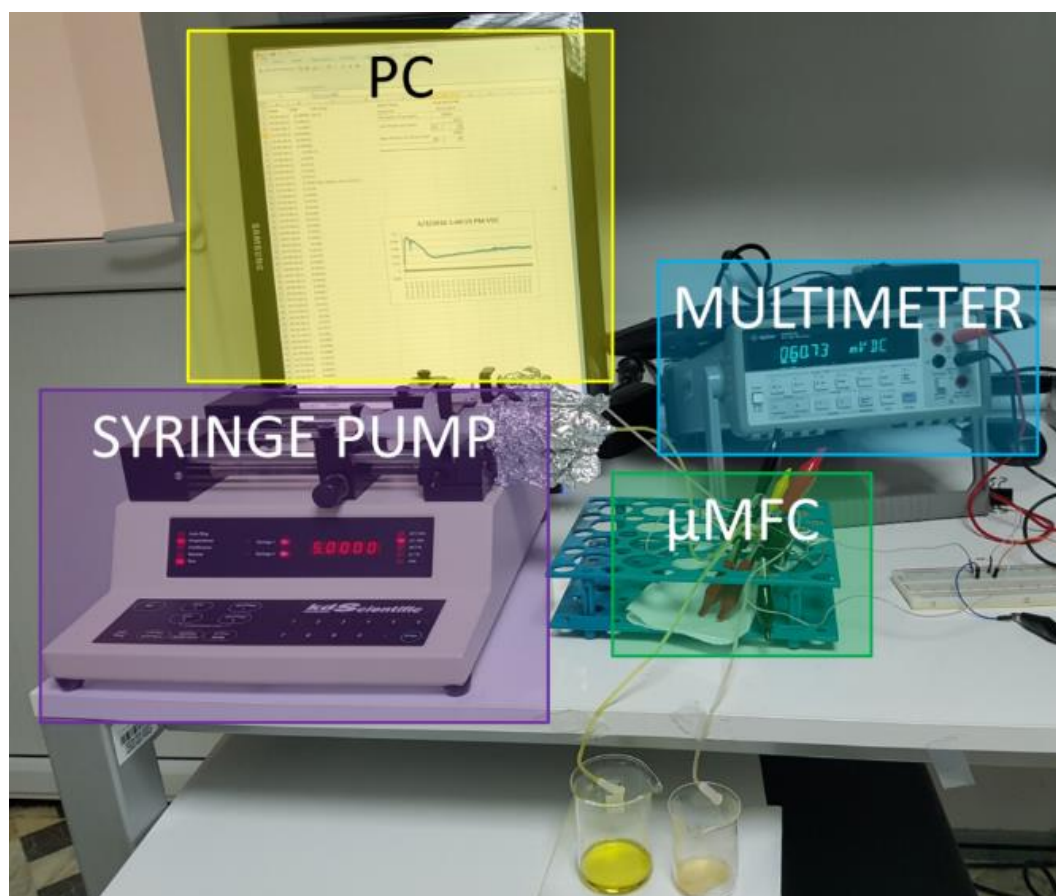
Figure 4.3. μMFC test set-up.

After the connection of μMFC to experimental setup, anolyte (bacteria in carbon-rich medium: TSB or lactate solution) and catholyte ($K_3(FeCN)_6$) solutions were continuously fed to anode and cathode chambers at different flow rates, independently. The μMFCs were operated at 25 ± 1 °C in a temperature-controlled

room under anaerobic conditions via the help of sealing gaskets between the anode and cathode chambers. Different µMFC assemblies were connected to varying external loads or operated under open circuit voltage conditions. The potential between the anode and the cathode was measured continuously via a digital multimeter with a data acquisition system and the data were recorded every 1 min via Keysight IntuiLink interface.

To compare the operational advantages and disadvantages of the macro and microscale MFCs, macro MFC made of plexiglass was operated with the same anolyte (bacteria in TSB) and catholyte (100 mM $K_3Fe(CN)_6$). The assembly (Figure) was done as described in Chapter 3. Figure shows the macro MFC during the operation.

a   b
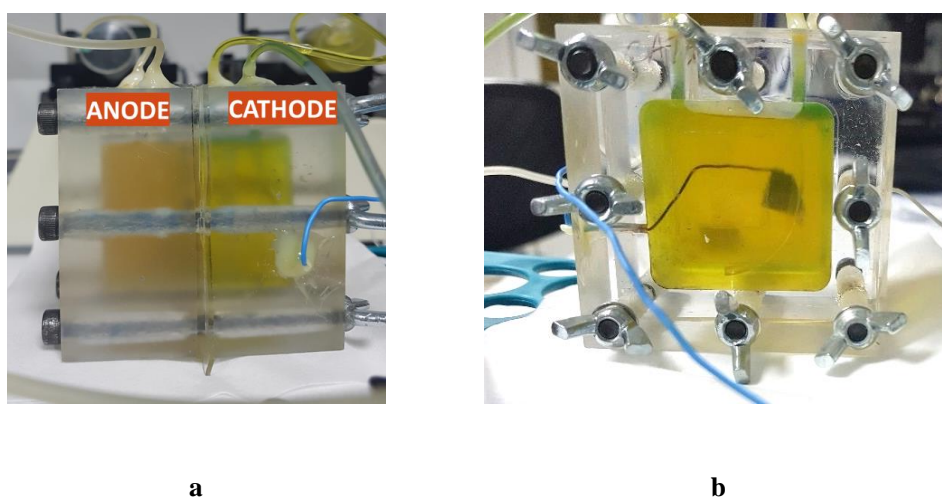
Figure 4.4. a: Macro MFC under operation. b: view from cathode chamber side.

For the initial investigation of interaction between the bacteria and bare or modified gold surfaces, a flow cell was assembled as described in Chapter 3. 1 cm x 1 cm bare gold and modified gold substrates were placed inside the flow cell. After sealing with PDMS gasket and cover (Figure 4.5), bacteria in TSB solution was fed to flow cell at 2 mL/min to fill it. When, the cell was full, the flow rate was decreased to 15 µL/min and kept constant. It was operated for 8 days at 25 ± 1 °C in a temperature-

controlled room. During the operation, biofilm formation was checked visually from the transparent cover. After the operation, the flow cell was disassembled and the surfaces were fixed with Scanning Electron Microscopy fixation procedure (Section 4.6).
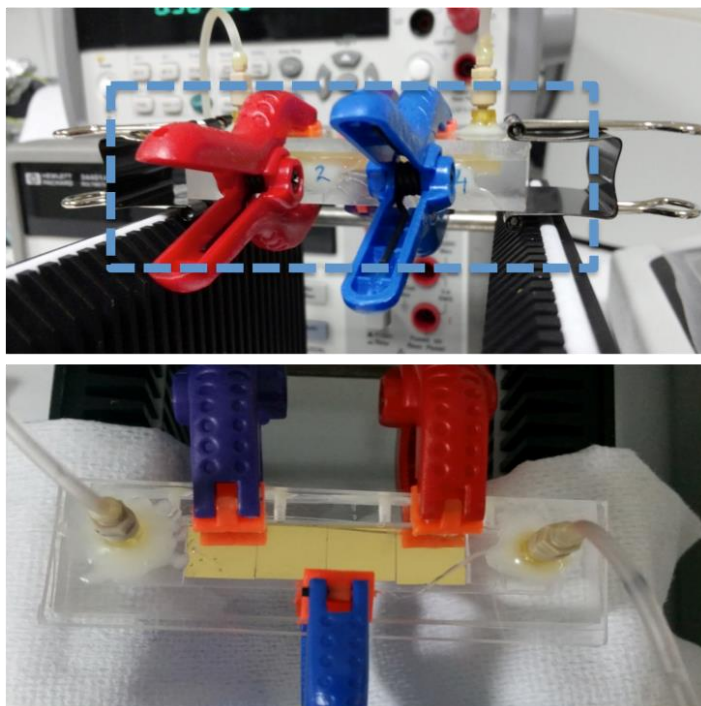
Figure 4.5. Flow cell for bacteria-surface interaction studies.

4.4   Modification and Characterization of Electrodes

Fabricated µMFC electrodes had gold and silver layers. During some of the experiments, these layers required surface modification. Following the modification procedure, surface conditions were characterized by different methods.

4.4.1   Chlorination of Planar Reference Electrode and Cyclic Voltammetry

Second and third generation μMFC electrodes had annular silver layers to be used for the adaptation of planar reference electrode. After the microfabrication of μMFC electrodes, silver layers were chlorinated to be used as miniature Ag/AgCl reference electrode. First, oxide layer on top of silver was removed by electrochemical cathodic cleaning method. μMFC electrode was dipped in KCl solution. Silver layer on top of μMFC electrode was used as working electrode. Platin substrate (0.5 cm x 1 cm) was used as counter electrode. A commercial Ag/AgCl reference electrode (Metrohm) was used as reference electrode. They were connected to Autolab PGSTAT204. Then, they were scanned between -2.0 V and -1.0 V with cyclic voltammetry (CV) for 5-8 min. During this step, hydrogen (cathode) and oxygen (anode) were formed. After rinsing with DI water for 3 min, μMFC electrode was dipped in 0.1 M$FeCl_3$ for 30 seconds. After rinsing with DI water, it was stored in saturated AgCl solution for overnight.

Chlorinated planar reference electrode was characterized using cyclic voltammetry with Autolab PGSTAT204. The round gold layer on round μMFC electrode was used working electrode and platin substrate (0.5 cm x 1 cm) was used as counter electrode. The electrodes were dipped in 1 mM $K_3Fe(CN)_6$ solution. Then, the working electrode was scanned at 25, 50, 100 and 200 mV/s scan rates between +0.5 V and 0.1 V. The experiment was repeated with the commercial Ag/AgCl reference electrode for the comparison of CV curves.

To check the voltage drift levels of the planar reference electrode, the chlorinated electrode was used for CV measurements at 50 mV/s scan rate in 1 mM $K_3Fe(CN)_6$ solution day by day. The CV experimental setup is given in Figure 4.6.

a   b

c   d
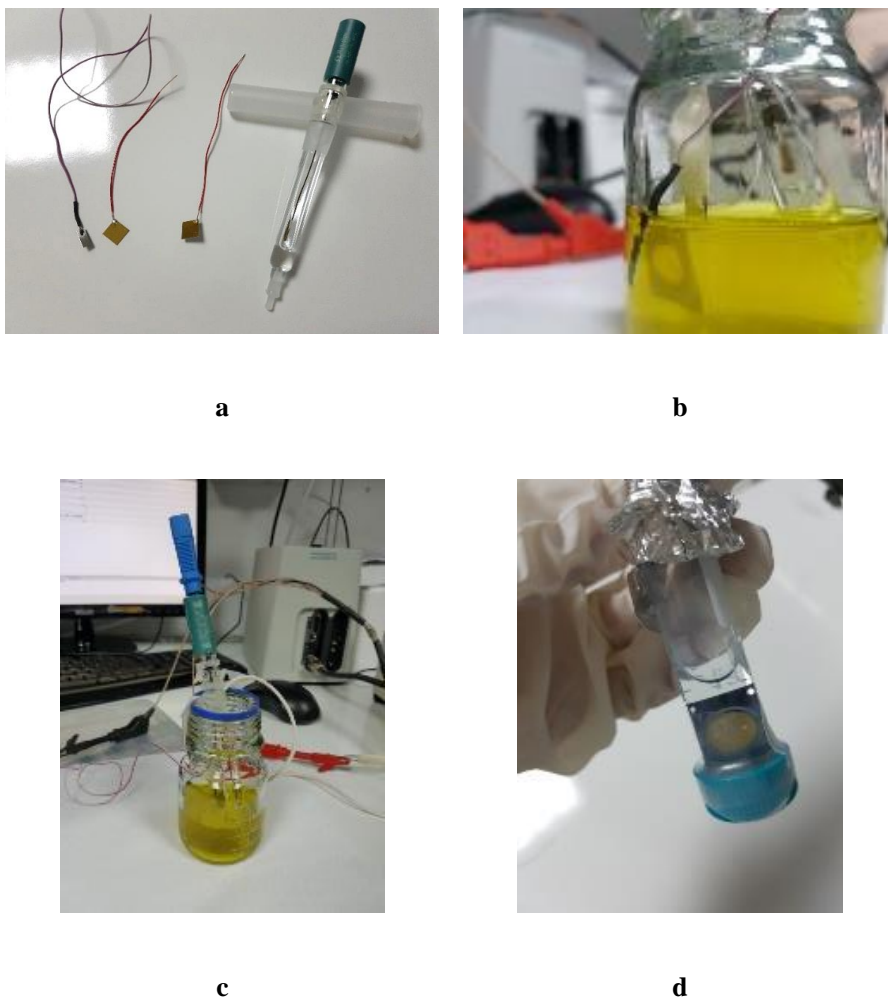
Figure 4.6. a: Electrodes used in CV experiments, platin and gold substrates as counter electrode, commercial Ag/AgCl reference electrode; b, c: CV test set-up; d: storage of the electrode in KCl solution.

4.4.2   Surface Modification of Gold with Thiols

To enhance the bacterial attachment on the surface, gold anode surfaces were modified with alkanethiols having different functional groups and chain lengths: amine terminated cysteamine (CYS), 3-mercaptopropionic acid (3-MPA) and 4-aminothiophenol (4-ATP), and carboxyl terminated 11-mercaptoundecanoic acid (11-MUA) (Sigma-Aldrich, St. Louis, MO, USA) (Figure).

74
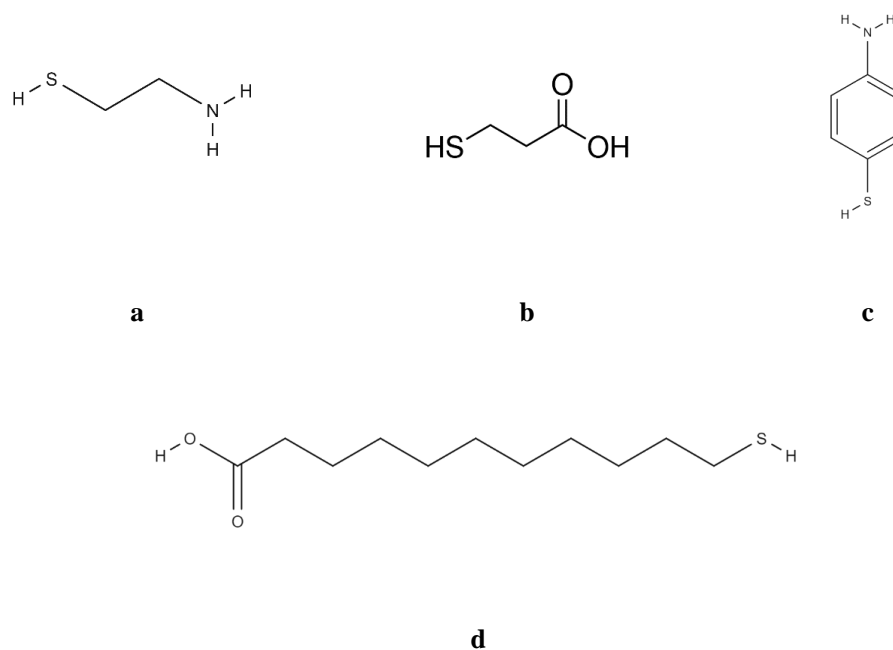
Figure 4.7. Thiol molecules used in the study. a: cysteamine; b: 3-mercaptopropionic acid; c: 11-mercaptoundecanoic acid; d: 4-aminothiophenol.

The quality of the self-assembled monolayer (SAM) to be formed on the gold surface is affected by gold surface cleanliness, solvent type, immersion time in solution, and concentration of the functional group in the solution. To obtain a good coverage on the gold surface, the procedure was completed as per the manufacturer's instructions [181]. First, all the glassware was cleaned in piranha solution, and protective photoresist layers on top of the gold electrodes were removed by immersion in acetone and IPA, respectively. Alkanethiol solutions with a 5 mM concentration were prepared separately in pure ethanol. For 11-MUA, the pH was adjusted to ~2. For CYS, 3-MPA and 4-ATP, the pH was adjusted to ~12. The cleaned electrodes were immersed and incubated in either CYS, 3-MPA, 11-MUA, or 4-ATP solutions for approximately 48 h after sealing with Parafilm (Figure). Later, the electrodes were rinsed with ethanol and dried with a stream of dry nitrogen gas [32,33]. The

functionalized surfaces were characterized with different techniques to check the coating characteristics.
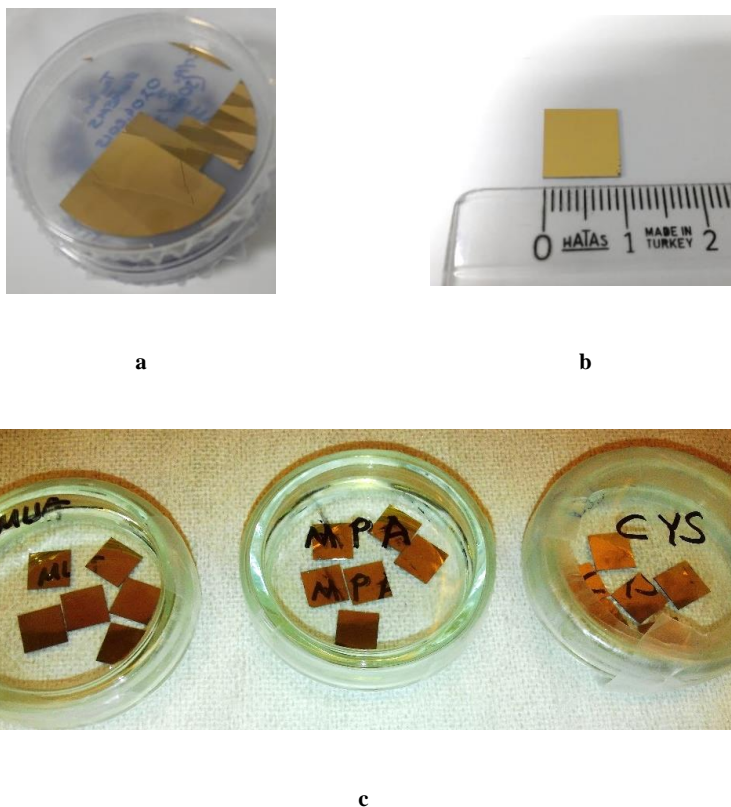
Figure 4.8. a: Gold sputtered 4" silicon wafer; b: 1 cm x 1 cm diced gold substrate; c: 1 cm x 1 cm gold surfaces during incubation in different SAM solutions.

4.4.3 Contact Angle Measurement

The functionalized 1 cm x 1 cm surfaces were characterized with contact angle measurement (KVS Attention Theta, METU Central Laboratory). The water contact angle was measured at room temperature using the sessile drop method by dropping 5 µL of water on both modified and unmodified surfaces. The contact angle was measured 5 seconds after the deposition of a drop by analyzing the image profile of the drop.

4.4.4   Atomic Force Microscopy

The atomic force microscopy (AFM), which is used in the research of micrometer and nanometer scale surfaces, provides detailed information about surface topography by using the force between the tip of a cantilever and the atoms of the examined surface. For the analysis of functionalized 1 cm x 1 cm surfaces, the Veeco Multimode V device in the METU Central Laboratory was used in "tapping" mode, and the surface was examined with a cantilever having 330 kHz resonant frequency. Then, the roughness values obtained from the software of the instrument were compared.

4.5   Characterization of Microbial Fuel Cells

The start-up time of the biofilm formation was determined using the voltage versus time plot, from the point when the voltage started to increase dramatically. The biofilm formation was accepted as having stopped when the voltage reached a steady value. During the operation of the μMFC, polarization curves and EIS data were collected.

4.5.1   Linear Voltammetry and Polarization Curves

The polarization curve (voltage vs current plots) was obtained by changing the external resistors between 1 MΩ and 0.5 kΩ at five-minute intervals while recording the voltage. Linear fitting of the curve in the ohmic loss region resulted in the total internal resistance of the μMFC. The current through the resistors was calculated via Ohm's law, $I = V/R$, and the output power was obtained via Joule's law, $P = V \times I$. Current and power densities were normalized to the anode area and anode chamber volume given at Table 4.1 for each electrode and MFC design.

Table 4.1. Normalization dimensions for different MFCs.

µMFC Type	Electrode	Active Anode Area	Overall Anode Volume
Deep Chamber µMFC	Serpentine	1.08 cm^2	96 µL
Deep Chamber µMFC	S-UME	0.28 cm^2	96 µL
Shallow Chamber µMFC	Square	0.55 cm^2	9.4 µL
Shallow Chamber µMFC	Round	0.61 cm^2	10.4 µL
Macro MFC	Square substrate	1 cm^2	35 mL

4.5.2 Electrochemical Impedance Spectroscopy

The EIS measurements were performed with a two-electrode mode using the Autolab PGSTAT204 potentiostat/galvanostat Frequency Response Analyzer (FRA) module (Metrohm, Switzerland) under open circuit conditions. The instrument is shown in Figure 4.9. Although the fabricated µMFC electrodes had silver layers to be used as the Ag/AgCl reference electrode after chlorination, this planar reference electrode was not suitable for long-term studies. Therefore, anode impedance spectra were obtained using the anode as the working electrode and the cathode functioning as both the reference and counter electrodes in a frequency range of 1 MHz to 0.1 Hz with a sinusoidal signal of a 10 mV amplitude. The data were fitted to an equivalent electrical circuit using the Autolab impedance analysis software Nova 1.11.

| a | b | c |
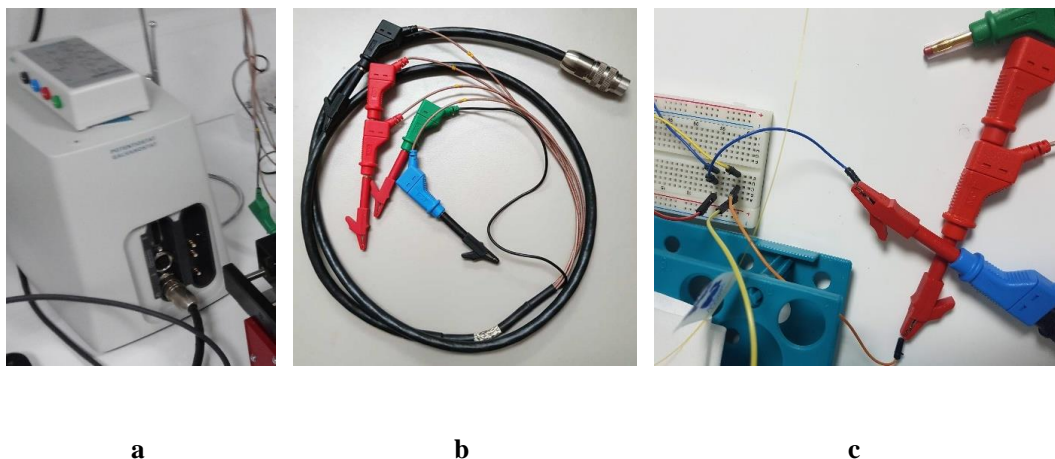
Figure 4.9. a: Autolab PGSTAT204 (Metrohm); b: shielded cables for the potentiostat; c: connection on breadboard

4.6   Characterization of Biofilm by Scanning Electron Microscopy

To investigate the relation between the characteristics of biofilm formed on anodes during μMFC operation and the power output of the system, anodes were treated for further biofilm characterization after the disassembly of the fuel cell.

The anodes from μMFCs and gold substrates from flow cell experiment were disassembled and rinsed in phosphate buffer saline (PBS) solutions. Adherent bacteria on the anodes were fixed in a 2% glutaraldehyde solution for at least 24 hours at 4 °C (glutaraldehyde solution, Grade I, 25% in H_2O, Sigma Aldrich, St. Louis, MO, USA). Samples were then dehydrated by serial 10-min transfers through 50, 70, 90, and 100% ethanol. A thin Au-Pd film with a thickness of 3 nm was deposited onto the sample by sputtering to improve the conductivity for Scanning Electron Microscope (SEM) imaging. Prepared samples were examined at 10 kV-30 kV using an SEM (FEI Quanta 400 F, METU Central Laboratory).

CHAPTER 5

RESULTS AND DISCUSSION

There were more than 50 separate MFC systems operated during the study. Some of them were excluded from the analysis due to the problems they faced such as leakage, data loss caused by power outage of laboratory and contamination of the bacteria or anolyte. Experiments were performed in three phases with respect to three electrode generations. Both the electrode properties and the assembly architecture were improved step by step to solve the previous challenges faced.

During the operation of μMFC systems, it was observed that the sudden voltage fluctuations were mainly due to bubbles entered the anode or cathode chambers. Their source was the bubbles formed in syringes during the operation of syringe pump (Figure 5.1). One of its reasons may be the aerobic respiration of the bacteria inoculum inside the syringe. To minimize this problem, status of supply syringes was closely followed and replaced often. Also, when the bubbles were observed in the tubing, flow rate was increased to flush the bubbles as soon as possible. However, it was noted that higher flow rates may damage the biofilm inside anode chamber. Thus, flow rate during flushing did not exceed 20 μL/min.

Figure 5.1. Bubbles formed inside anolyte supply syringe.

It was observed that high fluctuations of temperature inside the laboratory affected the performance of the systems because bacteria show better performance around 30°C. However, it was not possible to keep the laboratory warm. Instead it kept around 25°C via central air conditioning system.

5.1   Microfabricated Electrodes

μMFC electrodes designed for different phases of the study were successfully microfabricated in different microfabrication batches as given with details in Chapter 3. There were three generation of electrodes. First generation electrodes were used for comparison of operational parameters. Second and third generation electrodes were used to identify the effect of different acclimatization techniques and surface modification of anode on the μMFC performance.

Planar Reference Electrode

After the microfabrication of 2nd and 3rd generation electrodes, silver layers on these μMFC electrodes were successfully chlorinated following the removal of oxide layer (Figure 5.2a) to be used as a miniature planar reference electrode. However, it was observed that during MFC operation, the chlorinated silver layer gets damaged. When the electrode was kept in 3 M KCl for longer duration to achieve a thicker layer, it was observed that the silver layer was peeled off completely as seen in Figure 5.2d. Further enhancement of chlorination of reference electrode is suggested for future studies.
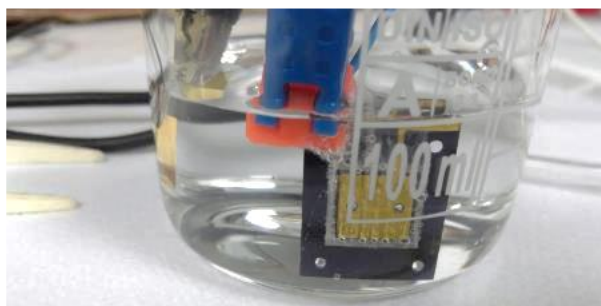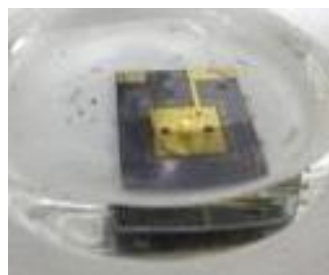
Figure 5.2. Chlorination of silver electrode. a: Removal of oxide layer on silver electrode; b: Unprocessed silver layer; c: Chlorinated silver electrode; d: Stripping of AgCl layer due to over incubation inside 3 M KCl.

There was an apparent drift in miniature reference electrode after multiple usage as seen in Figure 5.3. It was also compared with a macro scale commercial reference electrode. Their performance was different. This was due the fact that planar reference electrode was not in touch with a saturated AgCl solution for replenishment. It was evident that more detailed development of the planar reference electrode was necessary. Thus, it was omitted in the study after a couple of trials. For future studies, it is suggested to focus on solving this problem which will be very beneficial for electrochemical study of fuel cells in micro scale.
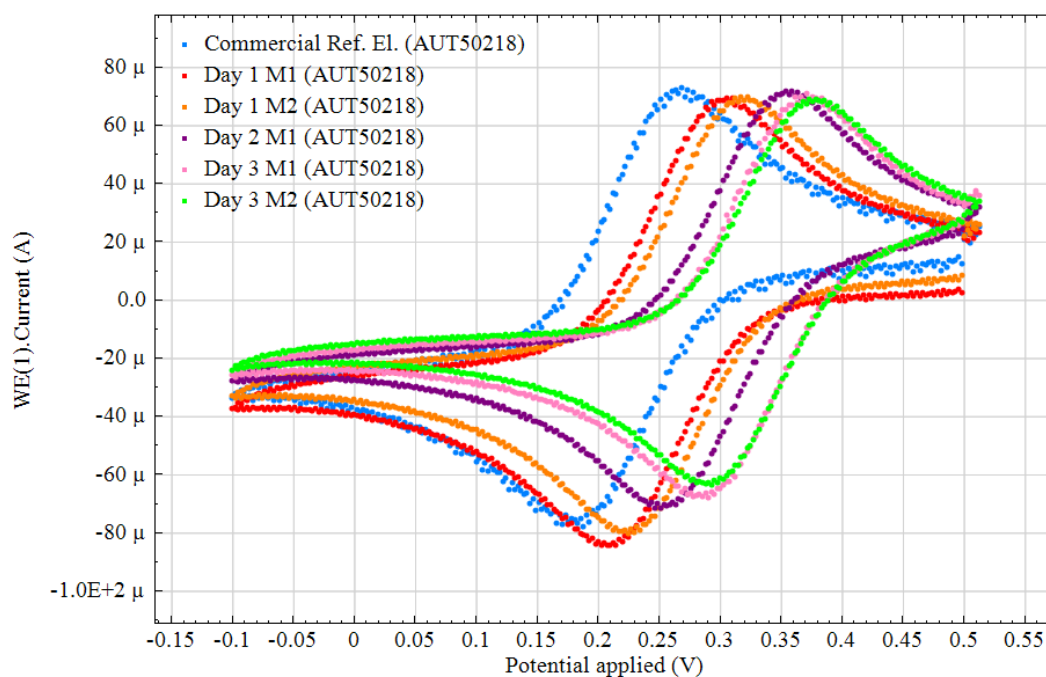
Figure 5.3. Comparison of CV plots of microscale planar Ag/AgCl reference electrode (red: day 1 measurement 1, orange: day 1 measurement 2, purple: day 2, pink: day 3 measurement 1, green: day 3 measurement 2) and commercial Ag/AgCl reference electrode (blue) at 50 mV/s scan rate.

µMFC Electrode after Disassembly

All the electrodes were investigated after the disassembly of the µMFC systems. Figure 5.4 shows some of the anode and cathode electrodes which had problems observed after disassembly. In Figure 5.4a, a cathode electrode is seen with catholyte filling the chamber created by PEM and thick blue gaskets of both anode and cathode sides. There was some precipitation of catholyte inside the chamber. To prevent this higher flow rates were adopted later.

Figure 5.4b shows biofilm formed following flow streamlines on anode surface. It seemed biofilm covered almost all the electrode, but it was more apparent along the streamlines probably due to better nutrient circulation there. This µMFC was operated for weeks and it showed the stripping of the silver layer around the gold

84

electrode due to EIS studies repeated several times. For future studies, it is suggested to form a thicker and more durable silver layer.

Figure 5.4c shows the anode and 5.3d shows the cathode of the same system. Due to prolonged EIS studies, gold layer is stripped off on the anode which was the working electrode. Brownish regions here are the remnants of the biofilm. However, the gold layer was intact on cathode which was used as counter electrode during EIS measurements.

Figure 5.4e shows the cathode of a µMFC where cathode was used as working electrode during EIS measurements. This electrode had both stripped gold layer and silver layer problems.

Most of the mentioned problems were corrected by enhancement of the experimental conditions along the study.

a   b

c   d   e
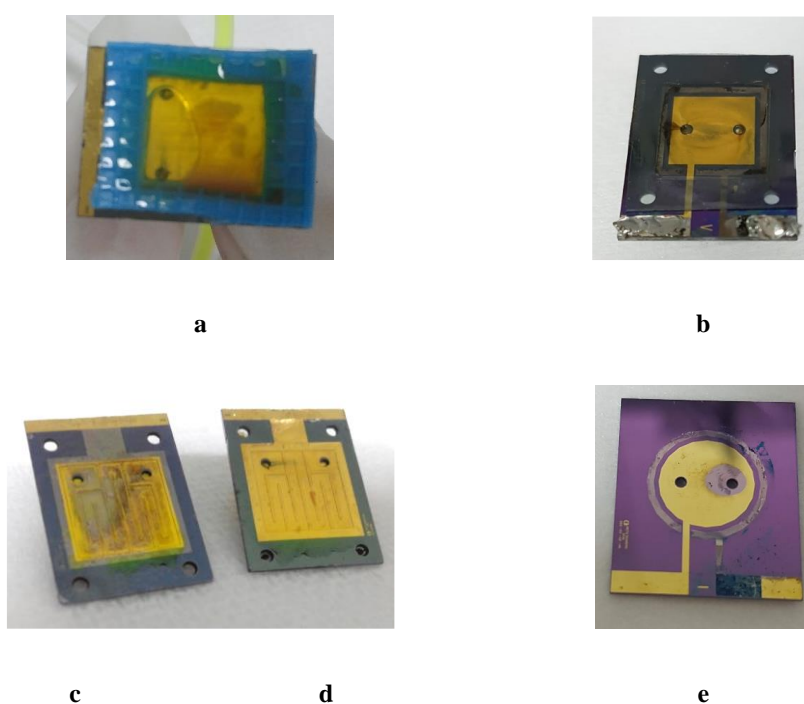
Figure 5.4. After disassembly status of µMFC components. a: residue inside cathode chamber; b: biofilm formed following the flow streamlines on anode; c: stripped gold layer anode; d: intact gold on cathode; e: stripped gold layer on cathode after EIS studies.

5.2   Performance of Deep Chamber µMFCs

First generation electrodes were used for comparison of anolyte type and anolyte flow rate in deep chamber µMFC assemblies. Also, performances of µMFCs assembled SE and S-UME were compared. Voltage change with respect to flow rate change was followed in µMFC experimental setup (Figures 5.5. and 5.6). For this part of the study, one µMFC assembled with SE and one µMFC assembled with S-UME were operated under same conditions simultaneously but independently for 40 days. They were fed from the same inoculum and the operational changes were applied on both systems at the systems. After starting the system with TSB as the anolyte, it was replaced with 30 mM and 40 mM lactate solutions gradually to acclimatize the bacteria to new nutrient. Both systems were started at OCV conditions and different loads were added to systems to check the current generation. Power and polarization curves were obtained with polarization studies.
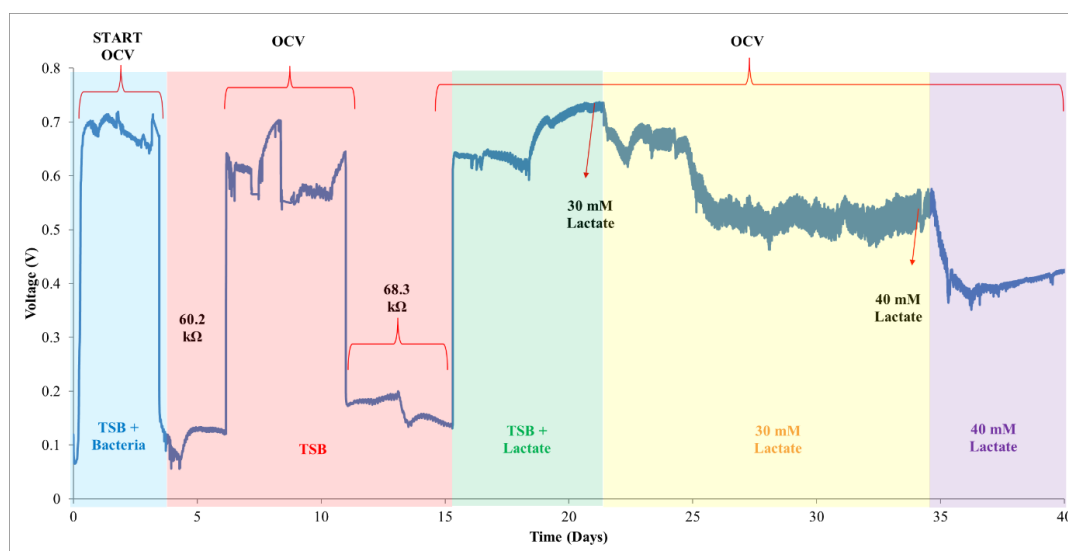
Figure 5.5. Operation of an µMFC with SE for 40 days. System was started at OCV conditions and fed with different anolytes were throughout 40 days.
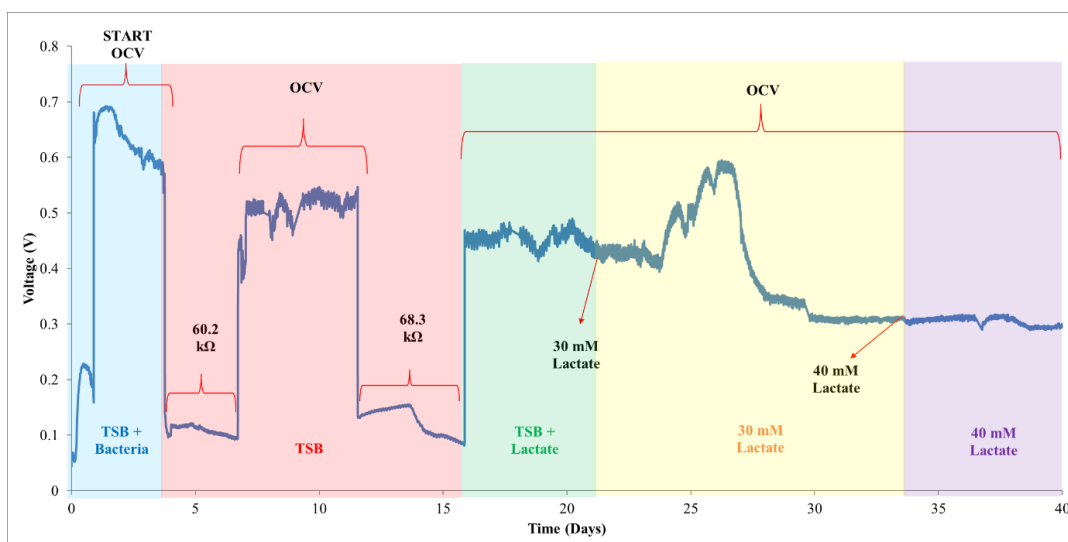
Figure 5.6. Operation of an μMFC with S-UME for 40 days. System was started at OCV conditions and fed with different anolytes were throughout 40 days.

5.2.1 Effect of Electrode Shape

When the Figures 5.5 and 5.6 were compared to examine the effect of electrode type, it was apparent that μMFC with S-UME resulted in lower voltage output than μMFC with SE at the same conditions. Both OCV (~630 mV) and voltage (~100 mV) under load were lower in μMFC with S-UME than OCV (~680 mV) and voltage (~110 mV) under load of μMFC with SE. Furthermore, the time to reach maximum voltage at the start was longer for this system. This was due to higher effective electrode area on the SE. Furthermore, as it can be observed in both figures, OCV values did not reach theoretical limit of 1.1 V due to activation losses occurring inside the fuel cells. This can be improved by adopting by adding catalysts on electrode surface.

Polarization and power curves of a μMFC with SE obtained after fourth day of operation are given in Figure 5.7. The three characteristic regions stemming from activation, ohmic and concentration losses are visible. As explained above, there was a sharp decrease due to activation losses. The power curve shows that maximum power obtained was ~0.55 μW when the load on the system was 24.8 kΩ. Internal

87

resistance was calculated from the linear region of polarization curve as 24.3 kΩ. This result supports that maximum power from the system can be obtained when the load is equal the internal resistance of the system.
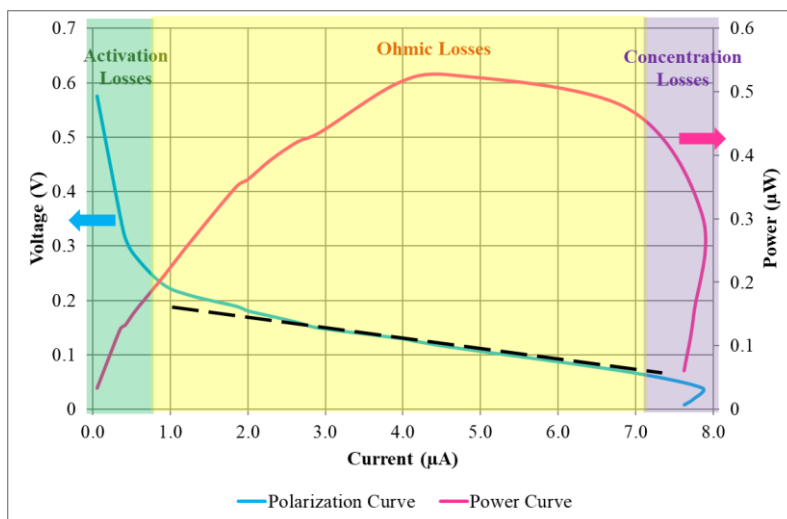
Figure 5.7. Polarization and power curves of SE operated 2 µL/min anolyte flow rate with the regions showing the losses. Dashed black line present the linear region where internal resistance of the system was calculated.

Although higher anolyte flow rate meant more fresh substance for bacteria to oxidize, it was observed that higher flow rates damaged the biofilm formed on anode surfaces. Creating channel structures on electrode surface may help the effective distribution of nutrients without the need of high flow rates. While sweeping the flow rates, performances of SE and S-UME µMFCs were compared at different flow rates as seen in Figures 8a-8d. Lower flow rate gave higher power output and lower internal resistance for µMFC assembled with SE. However, µMFC assembled with S-UME resulted in similar power output and internal resistance with high and low flow rate. This can be attributed to low sensitivity of the performance to parameters due to small effective anode area.

Figures 8e and 8f show the comparison of SE and S-UME µMFCs at the same conditions. SE µMFC had more than two times higher power output and its inertial resistance (24 kΩ) was lower than the internal resistance (70 kΩ) of S-UME µMFC.
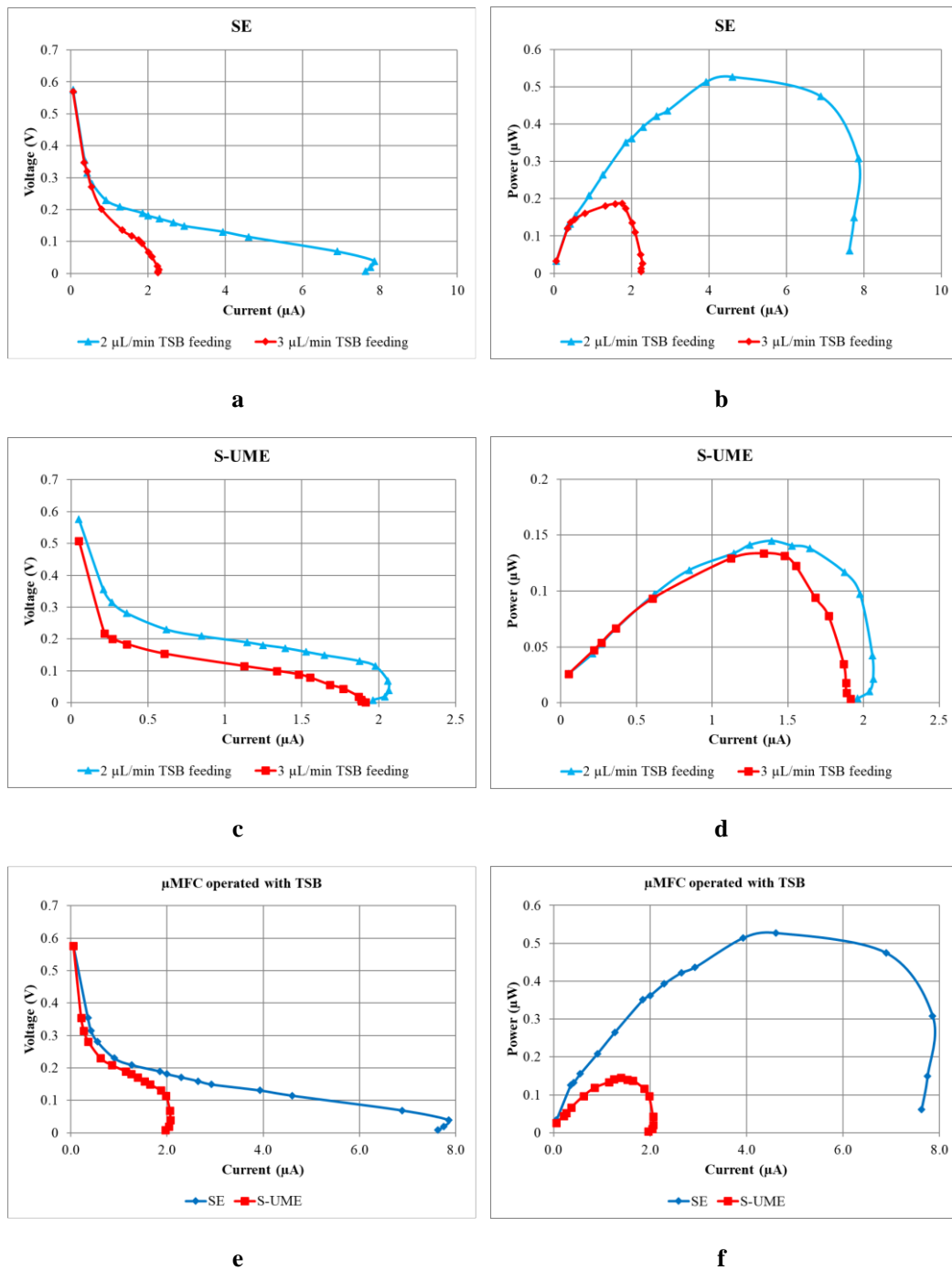
Figure 5.8. a, b: Polarization and power curves of μMFC with SE; c, d: Polarization and power curves of μMFC with SE; e, f: Comparison of μMFC systems assembled with SE and S-UME operated at the same conditions.

5.2.2   Effect of Anolyte Type and Concentration

Lactate at different concentrations (30 mM and 40 mM) and TSB were compared as the anolyte. When the lactate solution was used as the anolyte, bacteria required a gradual change of the anolyte from TSB to lactate to acclimate the new conditions. This affected the start-up duration of the system. Thus, after comparing the effect of anolyte with TSB and different concentrations of lactate solution, following studies were continued with TSB as the anolyte.

During the comparison of anolyte type, µMFCs assembled with 1st generation electrodes were operated for 40 days (Figures 5.5 and 5.6). The systems were fed with TSB for two weeks, then it was replaced with lactate solution gradually. When the lactate was fed to system, voltage readings of both systems decreased. This was mostly due to the difference in the contents of both solutions, TSB solution is richer in nutrient than lactate solution. Another reason suggested for the lower voltage observed in lactate fed µMFCs was the lower conductivity of lactate solutions with respect to TSB as seen in Table 5.1. Electrical conductivity of lactate solutions decreases with increasing lactate concentration. Although 40 mM lactate solution had more nutrient for bacteria than 30 mM lactate solution, it resulted in slightly lower power output due to lower conductivity.

Table 5.1. Conductivity of anolyte solutions.

Anolyte	Electrical Conductivity (20°C)
TSB	10.23 mS/cm
20 mM Lactate	7.92 mS/cm
30 mM Lactate	7.82 mS/cm
40 mM Lactate	7.77 mS/cm
50 mM Lactate	7.74 mS/cm

When the lactate solution was fed to systems for longer duration (~1 week), it was observed that bacteria got used to consume lactate more effectively and voltage values reached similar values obtained during TSB feeding phase.

Figure 5.9 shows the power and polarization curves for both SE and S-UME µMFCs operated with different lactate concentrations. The internal resistance increases with increasing lactate concentration and power output decreases consecutively for both systems.
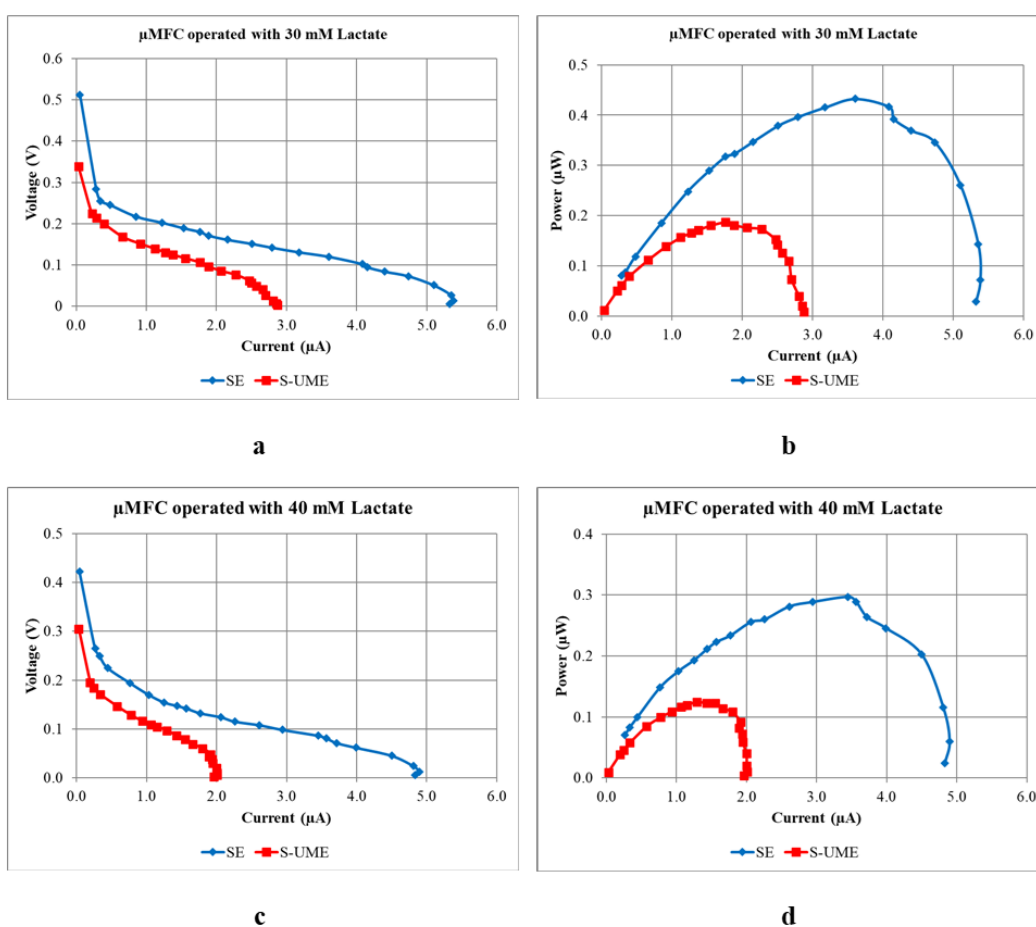
Figure 5.9. Comparison of µMFC systems assembled with SE and S-UME operated at the same conditions with differing anolyte concentrations.

Effect of using TSB and different lactate concentrations for µMFC system assembled with SE is compared in Figure 5.10. TSB fed system has resulted higher power output. Furthermore, open circuit potential was lower in lactate fed systems during polarization measurement which shows a very high overpotential with internal currents and fuel crossover. Different substrates that can be oxidized by *S. oneidensis* MR-1 can be studied in future studies to get higher power output.

a   b
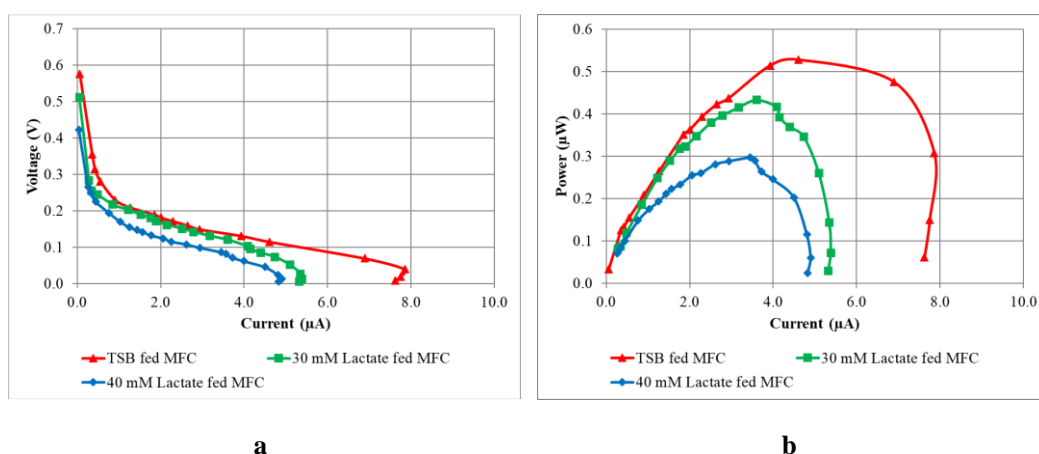
Figure 5.10. Comparison of polarization and power curves of µMFC systems assembled with SE operated with different anolytes.

Quantitative comparison of performances for 1st generation electrodes are summarized in Table 5.2. It is important to note that SE and S-UME µMFCs had same anode chamber volumes but their effective electrode areas were different. Thus, when areal densities are compared S-UME µMFC seems better due to lower effective electrode area. However, it would be more meaningful to compare the volumetric densities for actual performance.
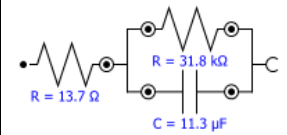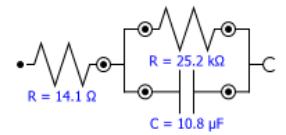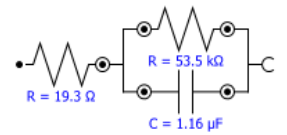
Table 5.2. Performance comparison of 1st generation electrodes with different anolytes.

Anolyte	System	Power (µW)	Current (µA)	Volumetric Power Density (µW/cm³)	Volumetric Current Density (µA/cm³)	Areal Power Density (µW/cm²)	Areal Current Density (µA/cm²)	Internal Resistance (kΩ)
TSB	SE	0.53	7.6	5.5	80	0.49	7.0	24.8
	S-UME	0.15	2.1	1.5	22	0.51	7.3	70
Lactate : TSB (1:1)	SE	0.52	7.6	5.5	80	0.48	7.0	25
	S-UME	0.19	2.9	2.0	30	0.69	10.1	51
30 mM Lactate	SE	0.43	5.4	4.5	56	0.40	5.0	29
	S-UME	0.19	2.9	2.0	30	0.66	10.1	55
40 mM Lactate	SE	0.30	4.9	3.1	51	0.27	4.5	29
	S-UME	0.12	2.0	1.2	21	0.44	7.1	61

Table 5.3 shows the comparison of EIS analysis performed on SE and S-UME µMFCs operated with 30 mM lactate as anolyte. For SE µMFC, the measurement was repeated for a wider frequency range to check the effect of processed occurring at lower frequencies. However, it should be noted that sweeping of lower frequency ranges result in prolonged measurement time which damages the thin planar gold electrodes. The EIS data was modeled with Simplified Randle's Circuit. The internal resistance values obtained with this model from the measured data were compared with the values calculated from polarization curves. The results were similar and

wider range measurement for SE µMFC was slightly closer to polarization data. In all three systems electrolyte resistance values (13.7, 14.1 and 19.3 kΩ) obtained from the model were similar as expected. Also, they were approximately 1000 times smaller than total internal resistance of the systems. This shows that electrolyte did not have a limiting effect on the performance. Moreover, it is observed that capacitance of SE system (10.8 µF) was higher UME system (1.16 µF). This result may yield a conclusion that charge storage in the biofilm for SE system was better.

Table 5.3. EIS analysis for different µMFCs fed with 30 mM lactate.

	SE µMFC	SE µMFC	S-UME µMFC
Frequency Range	0.01 Hz - 1 MHz	0. 1 Hz - 1 MHz	0. 1 Hz - 1 MHz
R(RC) Equivalent Circuit	R = 13.7 Ω, R = 31.8 kΩ, C = 11.3 µF	R = 14.1 Ω, R = 25.2 kΩ, C = 10.8 µF	R = 19.3 Ω, R = 53.5 kΩ, C = 1.16 µF
Internal Resistance Obtained with EIS	31.8 kΩ	25.2 kΩ	53.5 kΩ
Internal Resistance Obtained with Polarization Curve	29 kΩ	29 kΩ	55 kΩ

5.3   Performance of Shallow Chamber µMFCs

In the second part of the study, shallow chamber µMFCs were used with second generation electrodes. In this part, the aim was to investigate the start-up conditions of the systems so the µMFCs were operated for one to two weeks. Voltage-time plot

of a 2nd generation μMFC system assembled with round electrode and operated at OCV conditions is presented in Figure 5.11. The start-up time of the biofilm formation was similar to 1st generation μMFCs. After 70 hours, the maximum OCV (~650 mV) was reached.
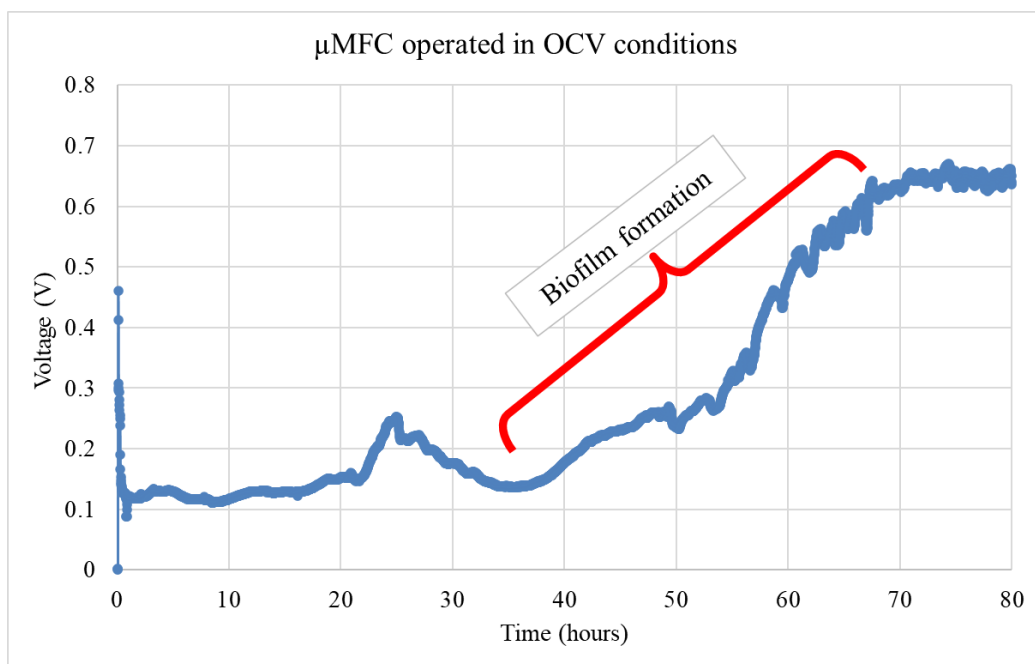
Figure 5.11. Voltage-time plot of a 2nd generation μMFC system operated at OCV conditions. Biofilm formation started after 30 hours and the maximum OCV was obtained after 70 hours. Round bare gold anode was used.

Figure 5.12 compares the polarization and power curves of 1st and 2nd generation μMFCs. While 1st generation system resulted in 0.5 μW power output, 2nd generation system showed almost three times higher performance (~1.4 μW). Furthermore, since the anode volume (10.4 μL) of the 2nd generation μMFCs was approximately 10 times smaller than the anode volume (96 μL) of the 1st generation μMFCs (10.4 μL), shallow chamber electrode resulted in ~25 times more power in terms of volumetric power density. The internal resistances were 19 kΩ for shallow chamber μMFC and 24 kΩ for deep chamber μMFC.

| a | b |
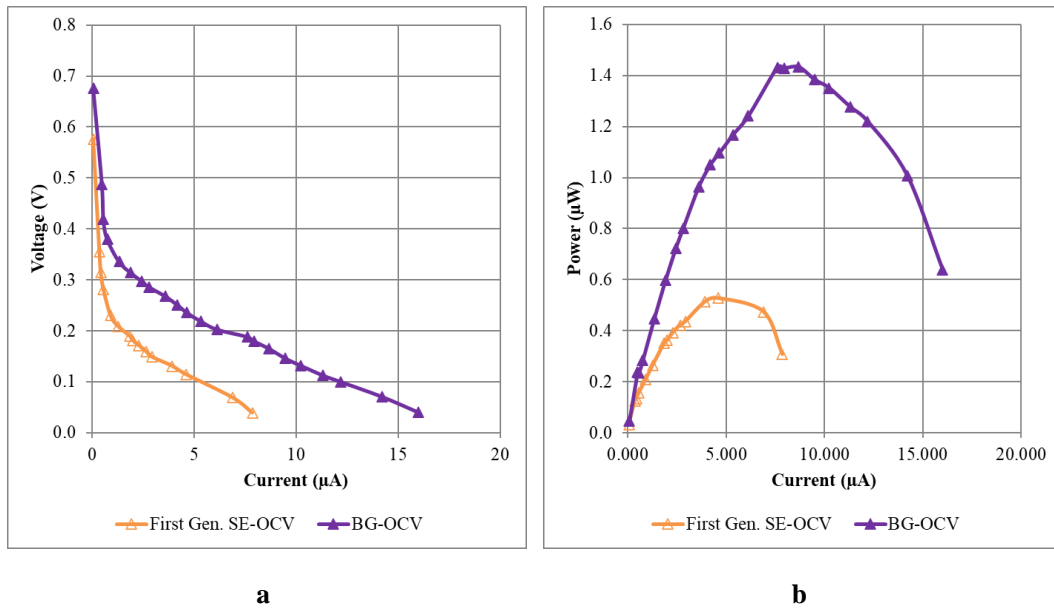
Figure 5.12. Comparison of polarization and power curves of 1st (SE) and 2nd generation (round) µMFC systems operated with TSB under OCV conditions.

5.3.1 Comparison of Different Acclimatization Strategies

To facilitate the bacterial attachment on anode surfaces better, different acclimatization strategies were adopted. Separate µMFCs were started under different loads and compared with µMFC operated at OCV conditions. Also, two separate µMFCs were started under positive and negative poised potential conditions (Table 5.4).

96

Table 5.4. µMFC systems operated in the study comparison of for acclimatization.

System	Acclimatization Condition
BG-OCV	µMFC started under OCV conditions
BG-10	µMFC started under 10 kΩ load
BG-25	µMFC started under 25 kΩ load
BG-50	µMFC started under 50 kΩ load
-200 mV PP	µMFC started with +200 mV PP
+200 mV PP	µMFC started with +200 mV PP

Figure 5.13 shows the operation of a µMFC system under 25 kΩ load for three days. It can be concluded from this figure that the biofilm formation starts around 30 hours and reached the maximum level around 45 hours. This duration may belong for practical applications, but it is much shorter than macroscale microbial fuel cells which sometimes takes weeks to start-up.
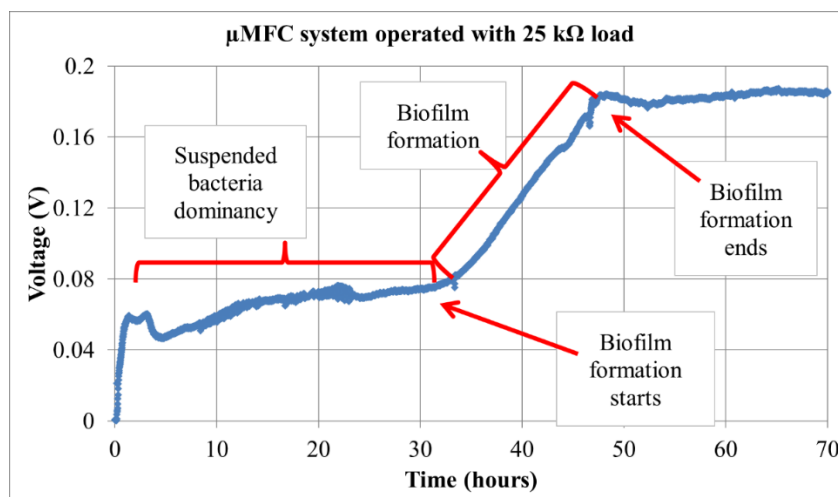
Figure 5.13. Voltage-time plot of a µMFC system acclimatized under 25 kΩ load. Voltage during the initial ~30 hours obtained with the activity of suspended planktonic bacteria. Biofilm formation causes an increase in voltage until a mature biofilm formed after ~45 hours.

μMFCs assembled with either square or round electrodes were compared in terms of start-up time. Both systems were fed with the same inoculum and operated under same conditions. The voltage readings were similar for both μMFCs as seen in Figure 5.14. However, it was observed that there were more fluctuations of voltage in μMFC with square electrodes. This may be due to non-uniform anolyte distribution in the corners of the electrode surface or the bubbles stacked inside the anode chamber.
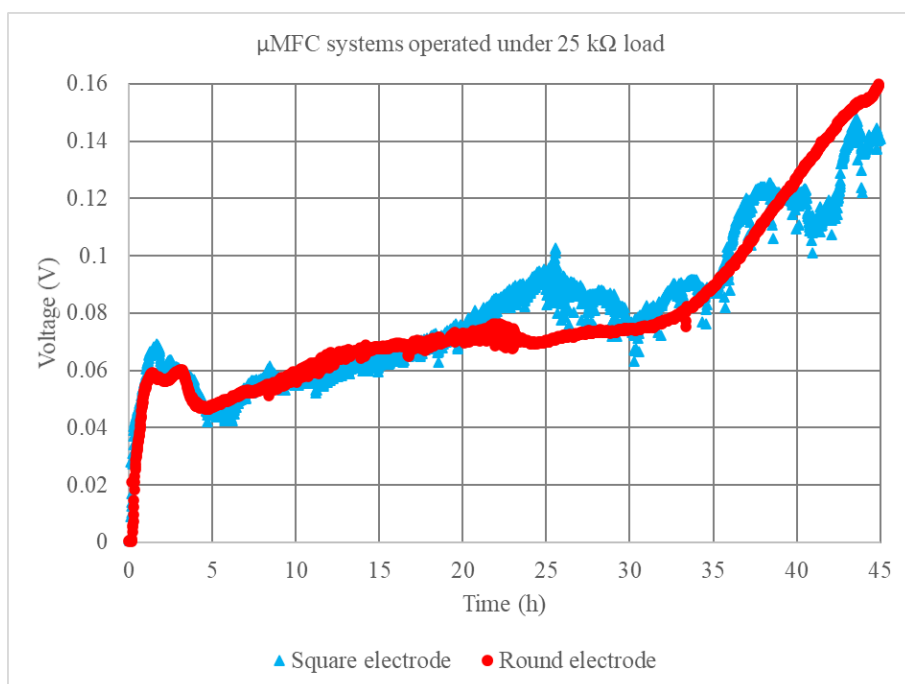
Figure 5.14. Comparison of μMFCs assembled with either square or round electrodes. The voltage readings were similar for both μMFCs.

Another acclimatization technique adopted in the study was application of poised potential (PP) on anode. Both positive and negative poised potential acclimatization of the μMFC for 24 hours was studied. Although the results showed improvement, acclimatization period increased the start-up time eventually (Figure 5.15). After potential application was ceased, the voltage started to fluctuate dramatically and reached maximum OCV after 20 hours. Table 5.5 compares the start-up time and time to reach maximum voltage for the μMFC acclimatized under different conditions. Although time to reach maximum OCV was fastest for poised systems,

it should be noted that 24 hours of acclimatization period was spent without power output.
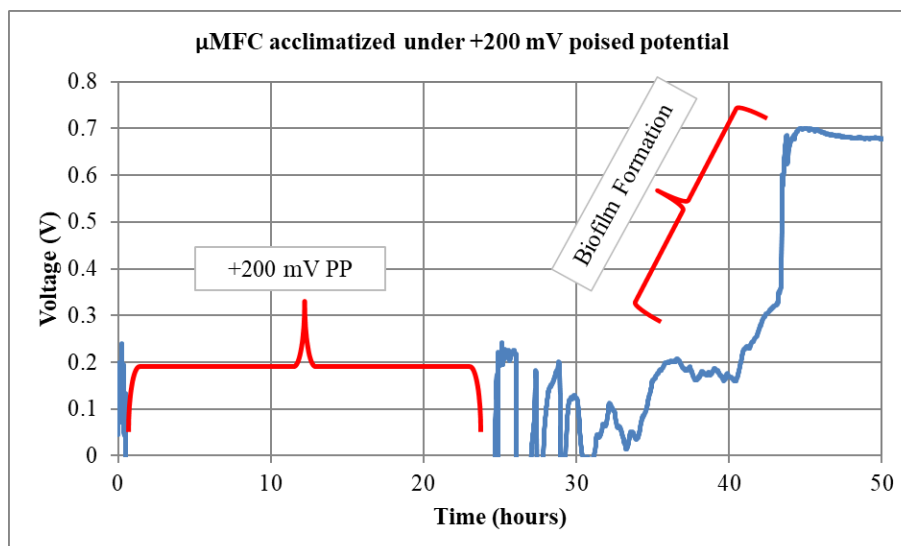
Figure 5.15. Voltage-time plot of an μMFC system acclimatized under +200 mV poised potential. Biofilm formation starts 10 hours after poised potential was stopped but 24 hours of acclimatization was necessary. Round bare gold anode was used.

Table 5.5. Comparison of start-up time with different acclimatization conditions.

System	Start-up time	Time to reach maximum power
BG-OCV	36 hours	70 hours
BG-10	31 hours	84 hours
BG-25	30 hours	48 hours
BG-50	25 hours	50 hours
-200 mV PP	7 hours	21 hours
+200 mV PP	10 hours	20 hours

To evaluate the performance of the μMFCs, polarization study was performed. Figure 5.16 shows the polarization and power curves for six different μMFC systems with different acclimatization conditions. It was observed that during these studies the open circuit potential was low (400 mV) for μMFC poised with -200 mV which shows a very high overpotential with internal currents and fuel crossover.
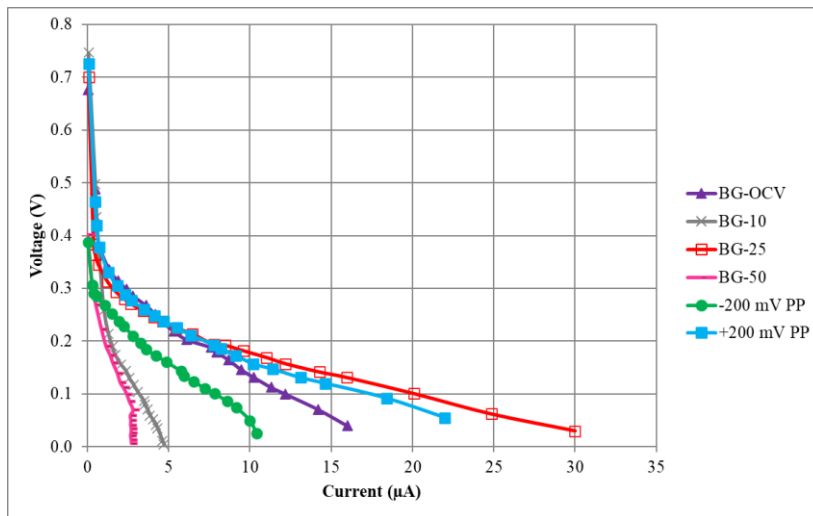
a
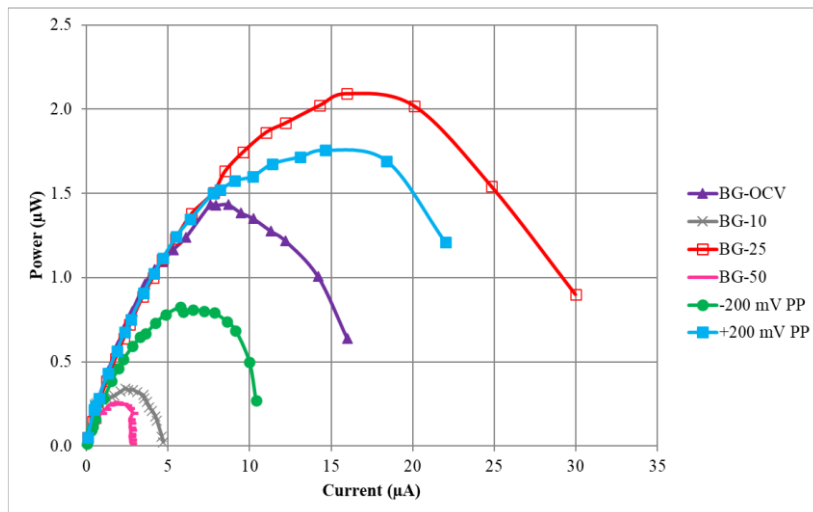
b

Figure 5.16. Polarization (a) and power (b) curves for six separate µMFC systems operated under different loads.

µMFC system poised with +200 mV was investigated with EIS technique in depth using the planar reference electrodes on anode and cathodes (Figure 5.17). for this µMFC, internal resistance was calculated as 8.5 kΩ. Equivalent circuit modelling of the measured EIS data resulted in internal resistance of ~4.5 kΩ. The difference

between the internal resistance values can be explained with the fitting precision of the model. The model can be further improved to obtain a closer internal resistance value.
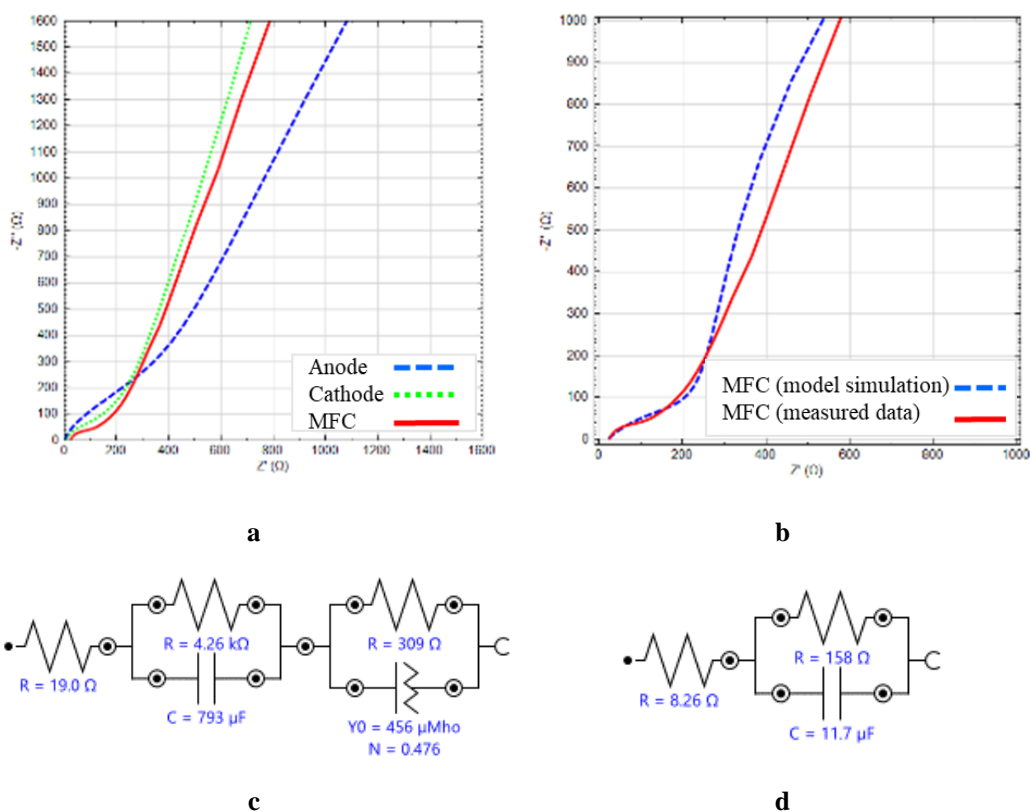
Figure 5.17. EIS analysis of µMFC system poised with +200 mV. a: Nyquist plots for anode, cathode, whole MFC; b: Nyquist plots of simulated MFC spectra using equivalent circuit model and measured MFC data; c: equivalent circuit derived for whole from measurement data; d: equivalent circuit for cathode chamber.

5.4   Effect of Surface Modification

One of the strategies to improve the performance of µMFCs was to modify the gold surfaces to make them more favorable for bacterial attachment. In this regard, gold anodes were modified with different functional groups. Power output and start-up time of µMFCs assembled with the modified anodes were compared.

5.4.1 Characterization of Modified Surfaces

Alkanethiol modified gold surfaces having carboxylic or amine functional groups are known to result in more hydrophilic character compared to bare gold surfaces. Table 5.6 shows the contact angle values for different surfaces. Carboxyl groups are amongst hydrophilic functional groups. Since the introduction of carboxylic acid on the surface lead to an increase in the hydrophilicity, the water contact angle decreased approximately 11 degrees for 11-MUA modified surface and 5 degrees for 3-MPA modified surface, which is in good agreement with the literature [182], [183]. Functionalization with amine terminated alkanethiols also lead to a decrease in the water contact angle. Water molecules can interact with amine groups by forming hydrogen bonds, justifying the modification of the surface. Introduction of amine groups were found to increase hydrophilicity also in other studies [184].

Table 5.6. Contact angle measurements.

Surface	Contact Angle
Bare gold	65°
Gold surface modified with cysteamine	52°
Gold surface modified with 3-MPA	60°
Gold surface modified with 11-MUA	53.7°
Gold surface modified with 4-ATP	52°

The surface roughness was investigated with AFM and the results are given below (Figure 5.18). RMS roughness values showed that bare gold surface was the least rough surface ($R_q=0.79\pm0.03$). Cysteamine modification resulted in 8% increase in roughness and 11-MUA modification resulted in 10% increase in roughness with respect to bare gold roughness.
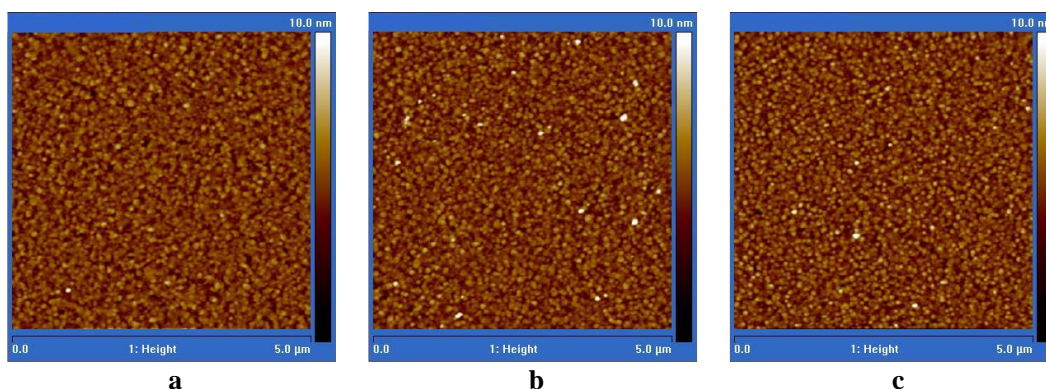
Figure 5.18. AFM images for A: bare gold surface, R_q=0.79±0.03; B: cysteamine modified, R_q=0.85±0.08; C: 11-MUA modified surface, R_q=0.87±0.05.

5.4.2   Investigations in Flow Cell

Before operating the μMFCs with surface modified anodes, the interaction between the bacteria and the modified gold substrates were investigated inside the flow cell designed. The modified gold surfaces and a bare gold surface were placed inside the flow cell. After filling the flow cell with bacteria inoculum in TSB at 2 mL/min flow rate, it was fed for 8 days continuously at 15 μL/min flow rate. After third day, the biofilm formation was observed inside the flow cell (Figure 5.19). After eighth day, the flow cell was disassembled, and the biofilm on surfaces were fixed as described in Chapter 4 for further analysis.

To examine the biofilm on surfaces, SEM and optical microscopy techniques were used. During these investigations, a bare gold surface not processed in flow cell was also studied as a control surface.
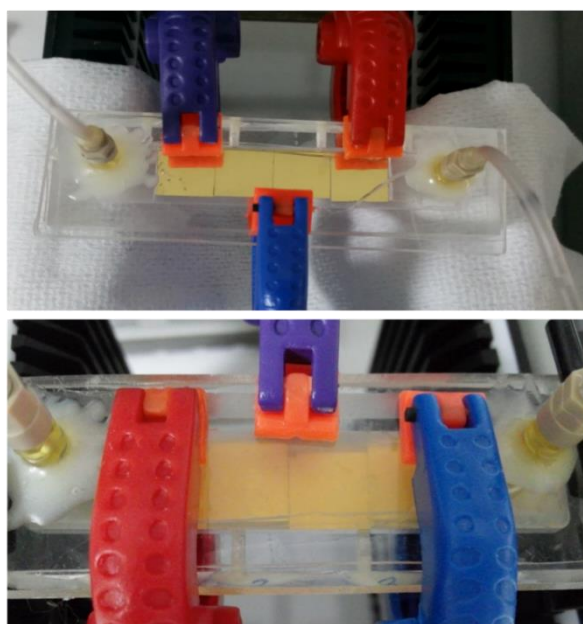
Figure 5.19. Flow cell. a: before feeding bacteria solution; b: after one week of operation.

In SEM technique, the surface under investigation needs to be electrically conductive, and it may be provided by coating a thin layer conductive material. However, it is sometimes preferred not to coat the biological samples. Also, it may be preferable to used lower vacuum levels inside SEM chambers to protect the sample. Thus, in this phase of the study, low vacuum was used and bacteria on surfaces were not coated with conductive layers. Figure 5.20 shows the density of *Shewanella oneidensis* MR-1 grown on all the surfaces including a control surface processed in flow cell. Although single bacteria were apparent on the surfaces, a thick biofilm was not observed. This may be due to the damages occurred during disassembly of the flow cell. Qualitative analysis showed the highest density was on cysteamine modified surface and bacteria were longer. The lowest density was on 3-MPA modified surface. It was noted that the resolution was not good enough to examine the bacteria more closely. It was probably because of low vacuum conditions and lack of conductive layer.
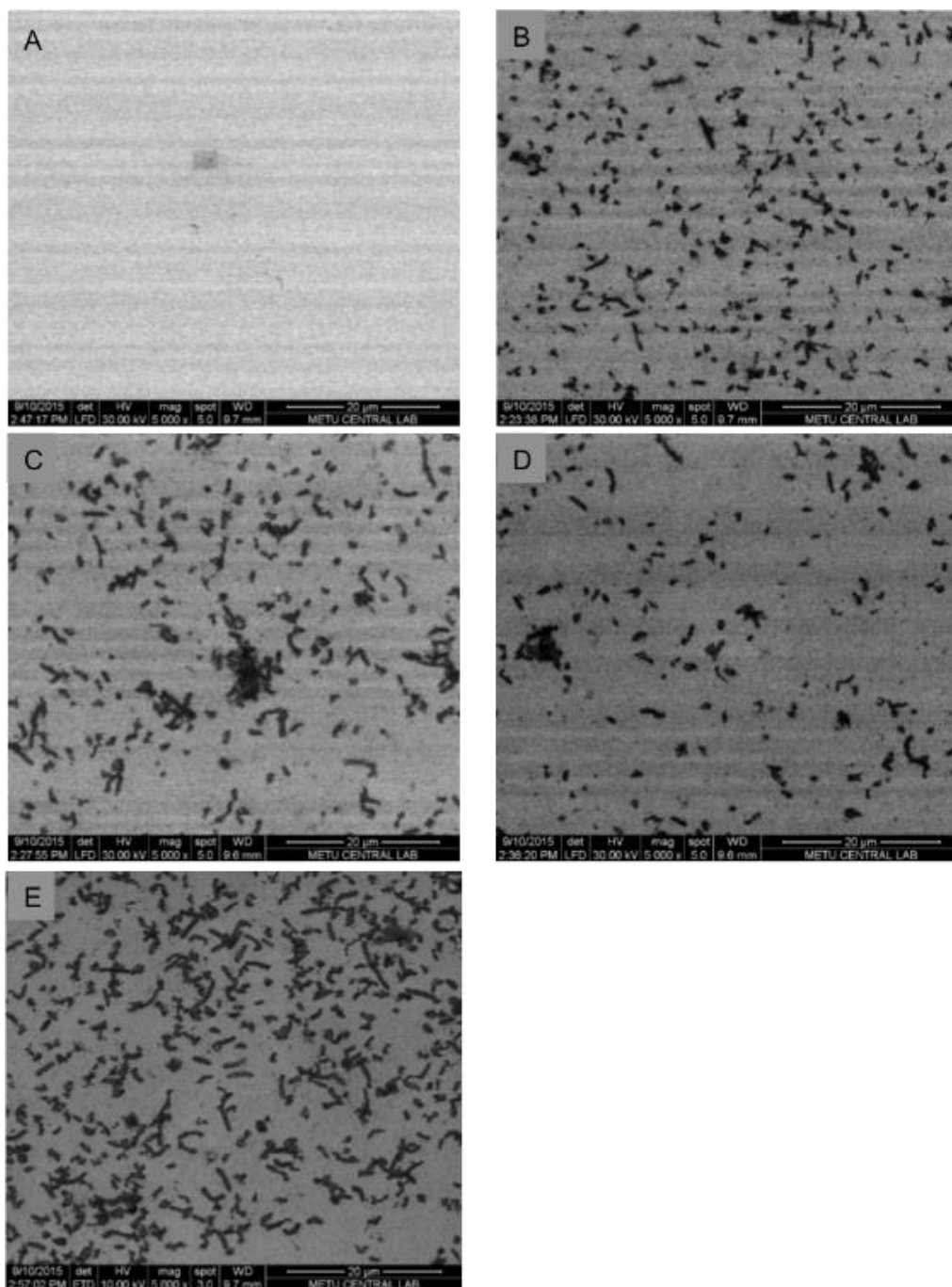
Figure 5.20. SEM images (30,000 kV) showing the bacterial density on different surfaces at 5000X magnification. A: Bare gold surface not processed in flow cell presented as a control surface; B: Bare gold surface processed in flow cell; C: Gold surface modified with 11-MUA; D: Gold surface modified with 3-MPA; E: Gold surface modified with cysteamine after processing in flow cell.

After investigation with SEM, the same surfaces were also examined under optical microscopy to check the bacterial density on the surfaces (Figure 5.21). The results were similar to SEM results. *Shewanella oneidensis* MR-1 grown on all the surfaces processed in flow cell but biofilm coverage of whole surfaces was not observed.
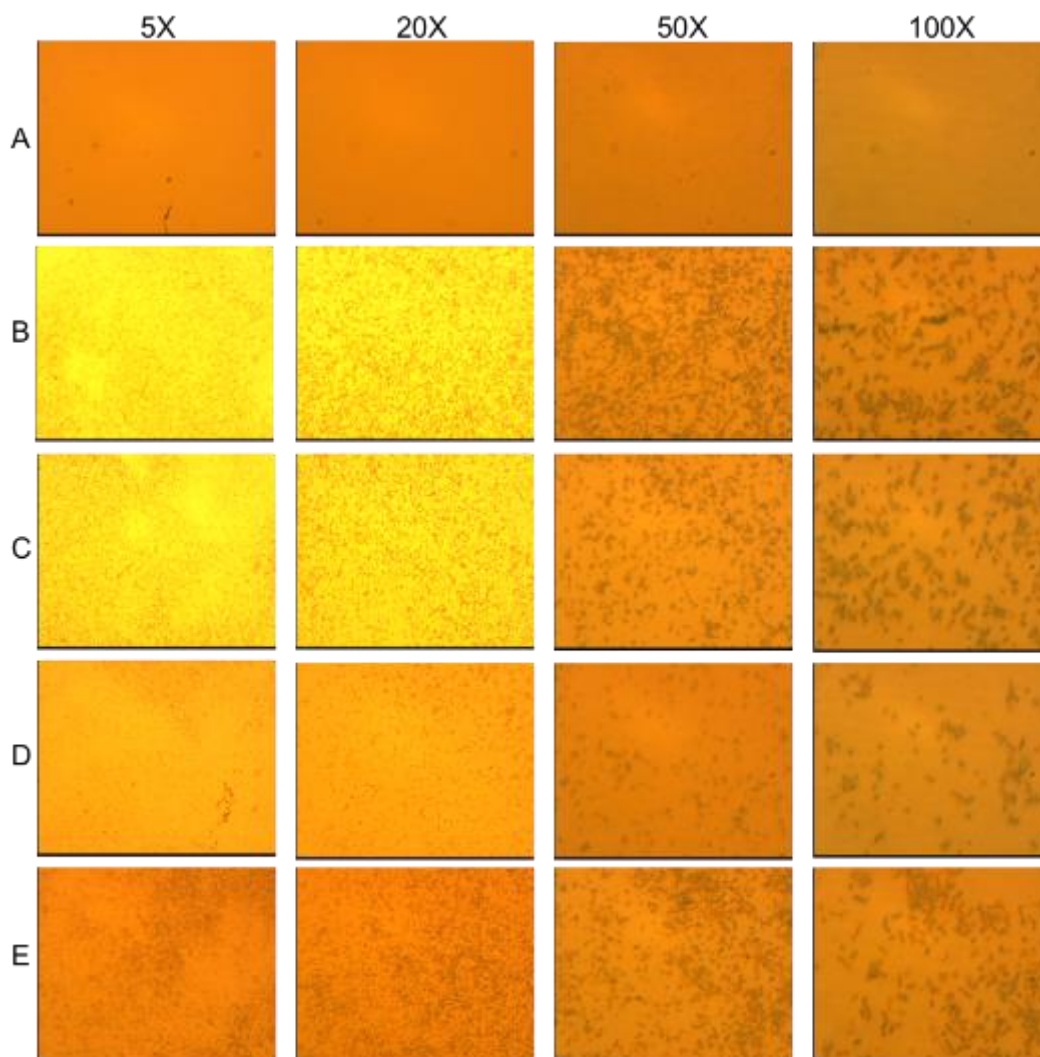
Figure 5.21. Optical microscopy images showing the bacterial density on different surfaces in 5, 20, 50 and 100X magnifications. A: Bare gold surface not processed in flow cell presented as a control surface; B: Bare gold surface processed in flow cell; C: Gold surface modified with 11-MUA; D: Gold surface modified with 3-MPA; E: Gold surface modified with cysteamine after processing in flow cell.

5.4.3 Effect on the Fuel Cell Performance

To study the effect of modified anodes, different µMFC assemblies were connected to 25 kΩ external loads or operated under open circuit voltage conditions. All the systems were operated under anaerobic conditions via the help of sealing gaskets between the anode and cathode chambers. The characteristics of µMFC systems operated in the study are presented in Table 5.7.

Table 5.7. µMFC systems operated in the study.

System	Surface Treatment	Acclimatization Condition
BG-OCV	Bare gold	Under OCV conditions
BG-25	Bare gold	Under 25 kΩ load
CYS-OCV	Gold surface modified with Cysteamine	Under OCV conditions
CYS-25	Gold surface modified with Cysteamine	Under 25 kΩ load
MUA-OCV	Gold surface modified with 11-MUA	Under OCV conditions
MUA-25	Gold surface modified with 11-MUA	Under 25 kΩ load
ATP-OCV	Gold surface modified with 4-ATP	Under OCV conditions

Shewanella oneidensis MR-1 used in the study can be simultaneously found as planktonic cells and adherent cells forming the biofilm in fuel cells, and both types can generate electricity alongside each other [37]. However, adherent cells on the anode are the main contributor to current generation in most cases [38]. Rozenfeld *et al.* showed that the biofilm on the anode provided most of the power output rather than planktonic bacteria in different micro electrolysis cells [39].

In accordance with the mentioned literature, when introduced in the anode chamber, planktonic bacteria started oxidation of the fuel, causing a potential difference between the electrodes in this study. When the bacteria started to accumulate on the gold anode surface, the biofilm gradually formed. There was a rapid increase in voltage after some lag time, as shown in Figure 6. This lag time is associated with

the time needed to establish initial bacteria-anode electron transfer. This increase was more apparent for the systems operated under OCV (BG-OCV, CYS-OCV, and MUA-OCV) than the systems operated under load (BG-25 and CYS-25). This can be observed in the voltage versus time plots of the µMFCs in Figure 5.22. CYS-25 and BG-25 system voltages started to increase after inoculation and kept increasing until reaching a maximum stable voltage value.
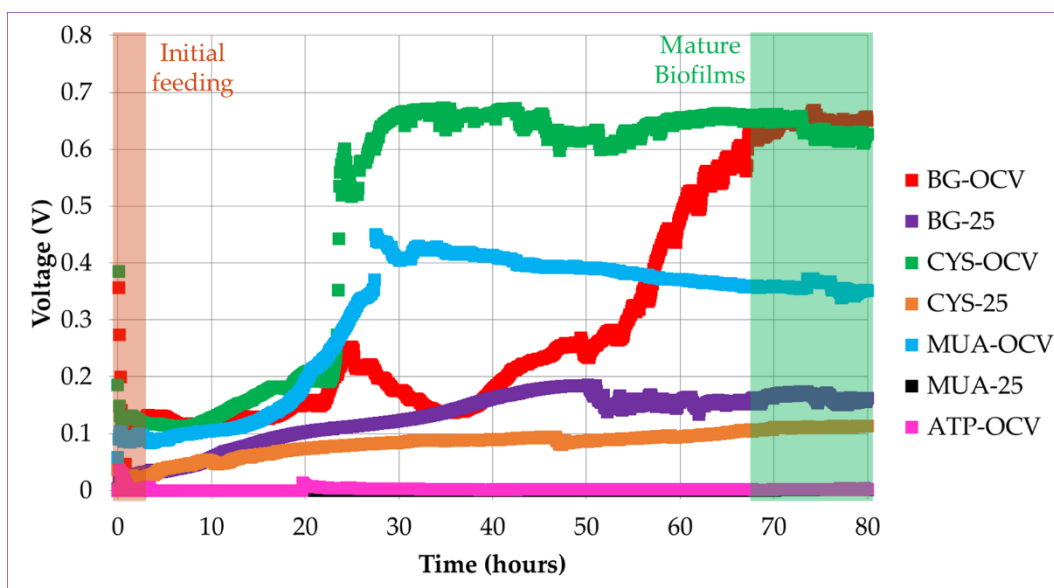
Figure 5.22. Voltage versus time plots for different µMFC systems during the start-up period (the voltage for the MUA-25 system was close to ATP-OCV).

The time needed to reach 90% of the maximum stable voltage was determined as the start-up time. In our previous study, the acclimatization of µMFCs under a load resulted in a shorter start-up time [27]. In accordance with the previous results, in the study presented here, µMFCs with an unmodified anode (BG-25) resulted in a shorter start-up time when operated under load than BG-OCV. µMFCs functionalized with alkanethiols (CYS-OCV and MUA-OCV) displayed a greater than 50% shorter start-up time without the need of an operation under load with respect to the BG-OCV system. However, CYS-25 did not present advantages over CYS-OCV in terms of the start-up time. MUA-25 and ATP-OCV systems had very

108

low voltages, so it was not possible to determine their start-up times and a quantitative performance analysis could not be performed (Table 5.8).

After the maturation of all systems, electrochemical analyses were performed. Figure 5.23 shows the polarization and power output curves of the five µMFCs investigated. The polarization plots consist of three regions. In the first region, activation losses were observed. This was characterized by a drastic decrease in voltage under a low current. As stated in the literature, these losses occur during the transfer of electrons at the electrode surface due to the activation energy needed for oxidation and reduction reactions [40]. In the second region, the voltages for all the systems fell more slowly and the voltage drop had a linear relation with the current. This region is defined by the ohmic losses, which were both the resistance to the flow of electrons through the electrodes and interconnections, and the resistance to the flow of ions through anolyte, PEM, and catholyte. The slope of the linear part of the curve for ohmic losses defines the internal resistance value of the system. MUA-OCV had the highest internal resistance (214 kΩ), causing a very low power output. This can be explained by inefficient electron transfer through the anode and 11-MUA coating due to the long chain of this molecule. Internal resistances for CYS-25 (23 kΩ) and BG-OCV (19 kΩ) were in the same range, but BG-OCV had a higher power output (1.433 µW) because CYS-25 had not only a higher internal resistance, but also higher activation losses in the first region. As Figure 5.23b shows, the power outputs of BG-25 (2.093 µW) and CYS-OCV (2.000 µW) were close, but CYS-OCV had a 25% higher current value at the maximum power point due to a 33% lower internal resistance than BG-25. This demonstrated that CYS-OCV had a higher efficiency between the biofilm and anode surface, which may be due to better-quality biofilm formation. Concentration losses were dominant in the third region of the polarization curves, as can be observed in Figure 5.23. These losses occurred when the rate of mass transport of a chemical species by diffusion to the electrode surface inside the system limited the current production, mainly at high current densities, as stated by Logan *et al.* [40].
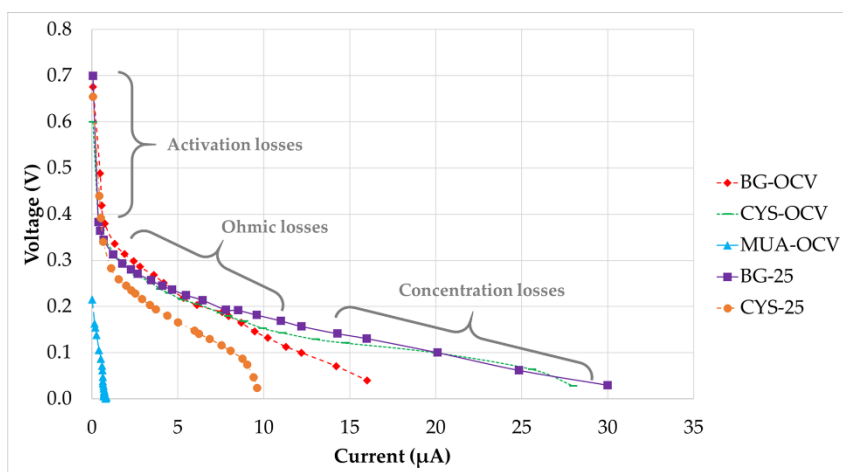
(a)
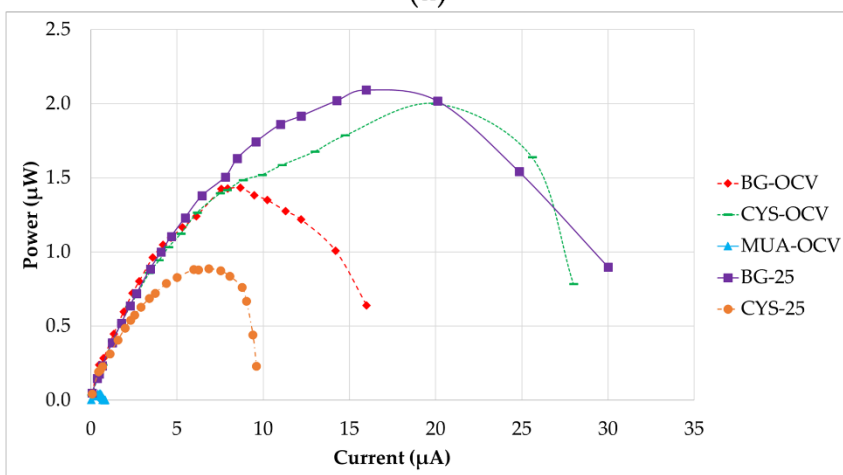
(b)

Figure 5.23. a: Polarization curves (the regions are shown approximately); b: power output curves.

Table 5.8 provides a comparison of the quantitative results presented in Figure 5.23 for µMFCs investigated in this study. Although MUA-OCV had a shorter start-up time, its power output was very low. The bacteria quickly adhered to the modified surface and resulted in a shorter start-up time; however, since 11-MUA has a long carbon chain, its electron conductivity is lower than that of CYS, which affects the performance of the fuel cell. CYS-OCV was found to be quite promising because its power output was as high as BG-25 and it had a short start-up time. This can be explained by the favorable bacterial attachment on the amine group and

rapid/uninhibited electron transfer due to the short carbon chain. On the other hand, ATP-OCV modified with 4-ATP did not generate power. Correspondingly, it is believed that phenol rings in 4-ATP might have inhibited bacterial growth, as some studies in the literature have claimed that phenols may have antimicrobial activity [41]. Furthermore, it was concluded that an increase in surface hydrophilicity had a positive effect on the power output in the case of the cysteamine-modified anode when BG-OCV and CYS-OCV were compared. Hydrophilicity makes surfaces more approachable for planktonic bacteria, as evidenced by [42,43], where an enhancement of the power output with an increase in the surface hydrophilicity was reported. However, it was observed in this study that hydrophilicity alone was not enough for this enhancement since modification with cysteamine and 3-ATP had a similar hydrophilicity, but different performance. It can be concluded that the functional group on the surface was also important, in addition to the hydrophilicity.

Table 5.8. Performance µMFC systems.

Parameter	BG-OCV	BG-25	CYS-OCV	CYS-25	MUA-OCV
Load during operation	OCV	25 kΩ	OCV	25 kΩ	OCV
Start-up time	70 h	48 h	30 h	42 h	27 h
Internal resistance	19 kΩ	8 kΩ	6 kΩ	23 kΩ	214 kΩ
Maximum power	1.433 µW	2.093 µW	2.000 µW	0.889 µW	0.046 µW
Current at max. power	8.684 µA	15.976 µA	20.000 µA	6.842 µA	0.527 µA

The results obtained established certain performance enhancement in terms of power and current densities and the start-up time with respect to similar microliter-scale microbial fuel cells with the same biocatalyst used in the literature. The power density ($315 \, \mu W/cm^3$) and start-up time (30 h) obtained with CYS-modified µMFCs (operated in an open circuit) were found to be better than in a similar literature study

carried out by Qian *et al.* [7] (Table 5.9). The power and current densities in this study were smaller than the densities of MFCs made of carbon paper by Vigolo *et al.* [44], but the start-up time was five times shorter. Bacteria usually prefer to adhere to carbon-based materials, but they are difficult to integrate in MEMS processes compared to gold as an electrode material. There are studies being conducted to adapt carbon-based electrodes to micro-scale MFCs [45], but their fabrication is not yet compatible with mass production solutions.

Table 5.9. Comparison of µMFC systems with the literature.

Parameter	BG-25	CYS-OCV	Qian *et al.*, 2009 [7]	Vigolo *et al.*, 2014 [44]
Bacteria	*S. oneidensis* MR-1	*S. oneidensis* MR-1	*S. oneidensis* MR-1	*S. oneidensis* *MR-1*
Fuel cell geometry	Double chamber with Nafion-117	Double chamber with Nafion-117	Double chamber with Nafion-117	Double chamber with Nafion-117
Process type	Continuous	Continuous	Batch	Continuous
Anode area	0.61 cm^2	0.61 cm^2	0.15 cm^2	0.5 cm^2
Anode volume	10.4 µL	10.4 µL	5 µL	5 µL
Chamber depth	170 µm	170 µm	100 µm	100 µm
Anode / Cathode materials	Au/Au	Au/Au	Au/Carbon cloth	Carbon paper/Carbon paper
Anolyte / Catholyte	TSB / K$_3$Fe(CN)$_6$	TSB / K$_3$Fe(CN)$_6$	TSB / K$_3$Fe(CN)$_6$	TSB / K$_3$Fe(CN)$_6$
Load	25 kΩ	OCV	100 Ω	100 kΩ
Start-up time	48 h	30 h	47 h	160 h (15 h lag time)

Internal resistance	8 kΩ	6 kΩ	30 kΩ	49 kΩ
Volumetric power density	330 µW/cm^3	315 µW/cm^3	15 µW/cm^3	900 µW/cm^3
Areal power density	3.4 µW/cm^2	3.3 µW/cm^2	0.15 µW/cm^2	9 µW/cm^2

EIS Characterization

Electrochemical Impedance Spectroscopy (EIS) is a technique widely used for the characterization of fuel cells to investigate electron transfer processes between interfaces. Its advantage over polarization curves is that EIS does not only give the total internal resistance of the fuel cell, but can also provide information about its components, such as the electrolyte resistance, charge transfer resistance, and diffusion resistance [46]. EIS forms the impedance spectra by applying an AC potential to an electrochemical cell and then measuring the current through this cell.

The µMFCs used in this study showed performance variations due to different resistances contained in their anode, cathode, electrolytes, and membrane. Figure 5.24 shows the Nyquist plots of overall fuel cells with a close-up view of the high-frequency region. When the Nyquist plots were compared, the primary observation was that the plots were formed by a distressed semi-circle (a characteristic of charge transfer process limitations) and a straight line in the low-frequency region, representing typical Warburg impedance (a characteristic of diffusion limitations). A distressed semi-circle is generally observed due to the combination of a capacitor element and a resistor element in parallel when fitting the EIS data. Determining the equivalent circuit of the system is crucial to interpreting these data. The Randles circuit is the most used equivalent circuit in the fitting of experimental data during EIS analysis. It is a model for a semi-infinite diffusion-controlled faradaic reaction to a planar electrode [47]. The diffusional resistance element (the Warburg

impedance) is in series with the charge transfer resistance. It also includes the solution resistance and a double-layer capacitor.

By analyzing the data after fitting with the Randles circuit, it was observed that the main influence on the impedance was due to the charge transfer resistance. This was especially apparent with the very high impedance value ($-Z$" = 46.7 kΩ) of MUA-OCV. Its high impedance hindered the mass transfer effect in the low-frequency region. This supports the results obtained from polarization curves showing that MUA-OCV had inefficient charge transfer. Charge transfer resistances calculated using the fitted data for BG-25, CYS-OCV, CYS-25, and MUA-OCV were 1.3, 1.2, 1.8, and 60 kΩ. These values differed from the ones obtained using polarization curves. This difference may be corrected by using more accurate equivalent circuit models. Although the general behaviors of BG-25, CYS-OCV, and CYS-25 were similar, cysteamine-modified μMFCs had more prominent mass transfer limitations, as demonstrated by the low-frequency region in the Nyquist plots. These results were consistent with the study of Rikame *et al.* [48], where they concluded that the modified graphite anodes showed decreased charge transfer and electrolyte resistances due to active materials.

As demonstrated in Figure 5.24b, the solution resistance values changed between 10 and 20 Ω, which were much lower than the total internal resistance values. Additionally, the same plot showed that systems had non-zero inductances as its effects are often seen at the highest frequencies (between 1 and 0.15 MHz in the study). Possible causes are the actual physical inductance of the wires and the electrode. It points out that for developing a more accurate model, an inductor can also be included in the equivalent circuit.
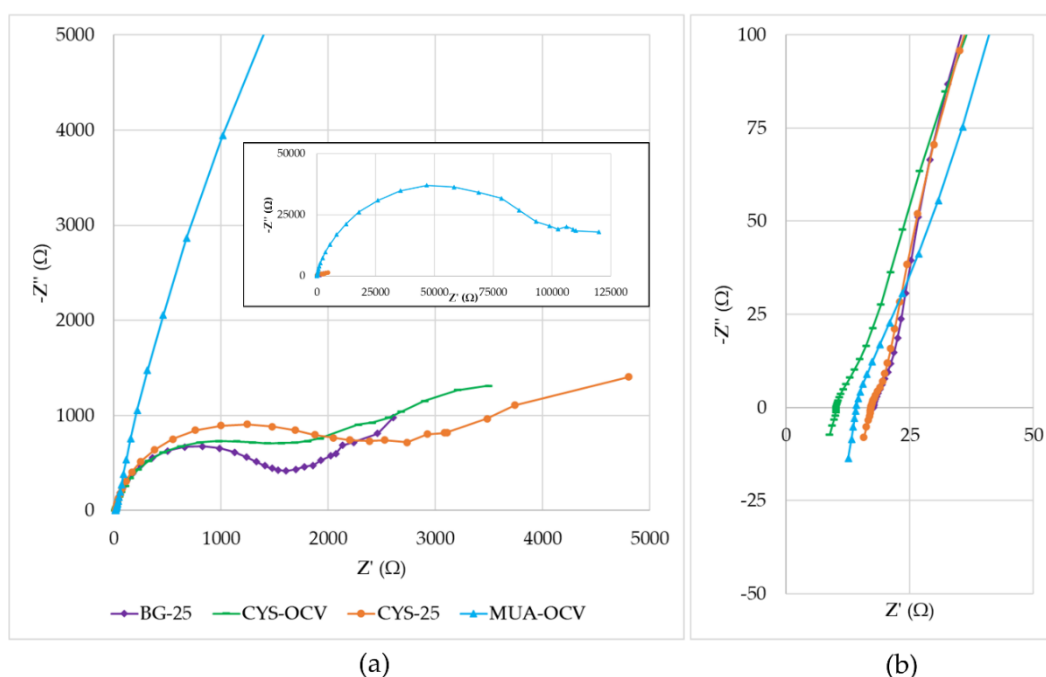
Figure 5.24. Nyquist plots: a: Inset is the full view, including the low-frequency range for MUA-OCV; b: close-up of the high-frequency region (1 MHz–5 kHz).

Characterization of Biofilms

After approximately two weeks of operation, μMFCs were disassembled and an SEM analysis of fixed gold anodes was performed. For three different μMFCs, SEM images showing *Shewanella oneidensis* MR-1 are given in Figure 5.25. CYS-25 and MUA-OCV systems resulted in very densely packed bacterial cells on the surface by stacking on top of each other. This was in good agreement with the relation between the start-up time and biofilm quality. Even though MUA-OCV produced a very low power output, it had a high-quality biofilm resulting in a shorter start-up time, which showed that 11-MUA does not inhibit biofilm growth, but electron transfer is inhibited by the long carbon chain of the molecule. The main difference between the appearances of biofilms was the amount of extracellular polymeric substances (EPS). MUA-OCV had less EPS and precipitated salts than CYS-25. The appearance of the bacteria was altered in some regions due to the fixation procedure. Furthermore, the treatment with ethanol might have washed away constituents, and dehydration might

have affected the structure and thickness of the biofilm. There were visible regions where the biofilm was peeled off from the gold layer due to the damage that occurred during EIS measurements. When observed at a higher magnification (20,000×), there were voids and cracks on the biofilm. These structures help the mass transport by forming water channels. These cracks were also observed with the *Shewanella oneidensis* MR-1 biofilm grown on gold by Qian *et al.* [8] and on graphene foam by Jiang *et al.* [45]. These voids also lead to imperfect contact between the bacteria and the gold surface, causing a decrease in the electrical conductivity of the biofilm matrixes, which lowers the performance of the fuel cell, as suggested by other studies [49–51].
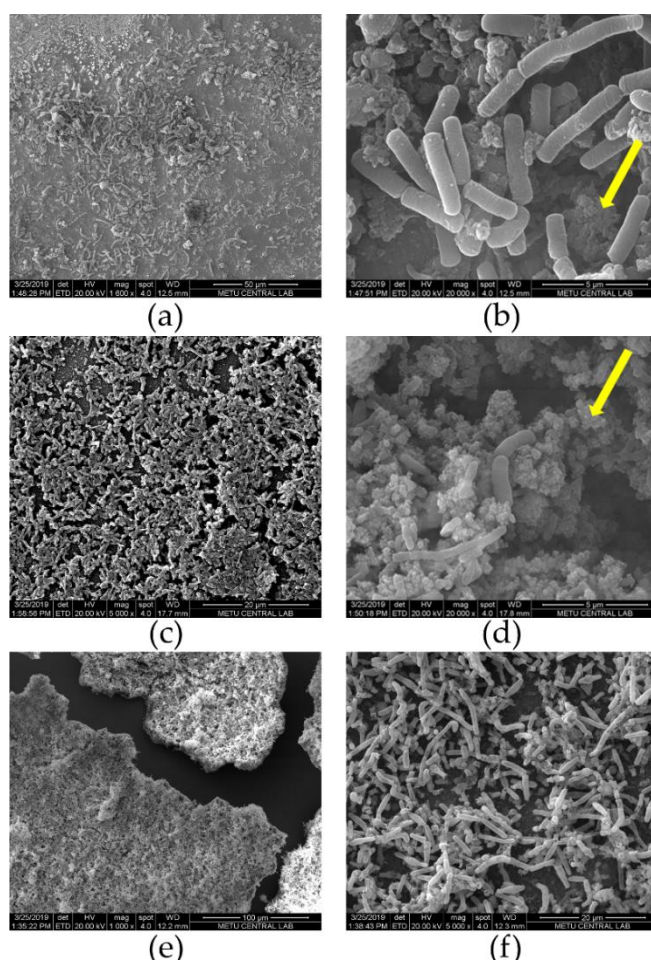
Figure 5.25. SEM images taken at 20 kV for different µMFC systems after the disassembly and fixation: (a, b) BG-25; (c, d) CYS-25; (e, f) MUA-OCV (arrows mark extracellular polymeric substances (EPS)).

5.5   Macro MFC

There were also experiments to compare the operational conditions of macro and micro scale MFCs. It was observed that air bubble formation inside anode and cathode chambers was a main problem in macro MFCs. Also, since electrode area to chamber volume ratio was small, it was difficult to distribute the fresh anolyte and catholyte around electrodes in macro MFCs.

One macro MFC with bare gold anode and one macro MFC with gold anode modified with Zeolite Beta40 were studied. Both systems were acclimatized with 1 kΩ load at the start. Zeolite modified macro MFC showed higher power output and lower internal resistance than bare gold macro MFC. This was a promising result for using zeolites in modification of anodes in MFC studies. However, due to the operational difficulties with dip-coated zeolite anodes, they could not be adopted to µMFCs to investigate their effect in these systems. The summary of the macro MFCs compared with high performance µMFCs developed in the second part of the study is given in Table 5.10. In terms of volumetric power and current densities, µMFCs showed higher performance although their higher internal resistances were higher.

Table 5.10. Comparison of macro MFCs and µMFCs developed in this study.

Parameter	BG-25	CYS-OCV	Macro MFC Bare Gold (acclimatized with 1 kΩ load)	Macro MFC Zeolite Beta40 (acclimatized with 1 kΩ load)
Volume	10.4 µL	10.4 µL	35 mL	35 mL
Anode Area	0.61 cm^2	0.61 cm^2	1 cm^2	1 cm^2
Internal Resistance	8 kΩ	6 kΩ	2.4 kΩ	0.6 kΩ
Power Density	3.4 µW/cm^2	3.3 µW/cm^2	3.9 µW/cm^2	155 µW/cm^2
Power Density	330 µW/cm^3	315 µW/cm^3	28 pW/cm^3	4.4 nW/cm^3
Current Density	26.1 µW/cm^2	32.7 µW/cm^2	14.3 µW/cm^2	455 µW/cm^2
Current Density	2515 µW/cm^3	3148 µW/cm^3	408 pW/cm^3	13 nW/cm^3

CHAPTER 6

CONCLUSIONS AND RECOMMENDATIONS

Microbial fuel cell, a special type of biological fuel cells, is a promising technology converting chemical energy into electrical energy utilizing microorganisms as biocatalyst to be used as renewable energy. They can be implemented to use for bioelectricity generation, wastewater treatment and sensing applications. However, microbial fuel cells require further increase in power generation for feasible implementation. Further research on bacteria, biofilm formation, electrode materials, and cell configurations could address several significant research gaps to obtain viable power density.

In this regard, the aim of this study was to develop a microbial fuel cell with microliter volume having high performance parameters as a power source. Within the scope of this work, effects of different parameters such as electrode surface characteristics and system operating conditions on the power density and start-up time were investigated.

Different microbial fuel cell architectures were designed with different chamber thicknesses and electrode shapes. Gold electrodes were microfabricated using silicon MEMS technology. After investigating the effects of geometry, the architecture of the fuel cell was finalized as a 10.4 µL double chamber microbial fuel cell with easy interfacing for microfluidic and electrical connections. The µMFCs fabricated were tested with selected exoelectrogenic bacteria (*Shewanella oneidensis* MR-1). Power density, start-up time and internal resistance were the primary parameters to compare between various µMFC systems using Linear Voltammetry, Polarization Curves and Electrochemical Impedance Spectroscopy. Anode surfaces were inspected using

SEM after fuel cell operation to compare the relation between biofilm formation and power generation.

The proposed study had the following outcomes:

- MEMS based microliter-volume, double-chamber microbial fuel cell was microfabricated and successfully operated under different conditions (batch or continuous feeding at different flow rates with different substrate types, operation under load or under OCV, positive or negative poised potential application at the start-up).

- The µMFC with improved architecture had successfully generated power in microwatt scale (~330 µW/cm^3).

- Surface modification with different functional groups on gold electrodes were compared with bare gold anodes and 50% reduction in start-up time was achieved with anodes modified with cysteamine and 11-MUA SAMs.

Consequently, the proposed study resulted in a compact µMFC design with higher power density than the similar literature studies.

As a future work, it is suggested the implementation of different architectural and operational parameters should be investigated based on the other potential applications also (biosensor for bacteria screening, water treatment, etc.) to improve their performance in diverse aspects and not only in power generation. Especially, a laminar flow µMFC microfabricated with silicon and glass can be designed and its surface can be modified with novel carbon materials like graphene. Since glass is transparent, it can help to study the biofilm formation under microscope during the operation.

There is still time to reach the maturation of microbial fuel cell technology. It can be foreseen that with further research in this field, microbial fuel cell technology can be commercially feasible.

REFERENCES

[1]   U. Schröder, "Discover the possibilities: microbial bioelectrochemical systems and the revival of a 100-year–old discovery," *J. Solid State Electrochem.*, vol. 15, pp. 1481–1486, 2011.

[2]   M. S. Alias, S. K. Kamarudin, A. M. Zainoodin, and M. S. Masdar, "Active direct methanol fuel cell: An overview," *Int. J. Hydrogen Energy*, vol. 45, no. 38, pp. 19620–19641, 2020.

[3]   R. Abbasi *et al.*, "Low-temperature direct ammonia fuel cells: Recent developments and remaining challenges," *Curr. Opin. Electrochem.*, vol. 21, pp. 335–344, 2020.

[4]   H. Su and Y. H. Hu, "Progress in low-temperature solid oxide fuel cells with hydrocarbon fuels," *Chem. Eng. J.*, vol. 402, p. 126235, 2020.

[5]   A. Heller, "Miniature biofuel cells," *Phys. Chem. Chem. Phys.*, vol. 6, pp. 209–216, 2004.

[6]   S. Srinivasan, *Fuel Cells - From Fundamentals to applications*. 2006.

[7]   A. F. Ghenciu, "Review of fuel processing catalysts for hydrogen production in PEM fuel cell systems," *Curr. Opin. Solid State Mater. Sci.*, vol. 6, pp. 389–399, 2002.

[8]   J. Larminie and A. Dicks, *Fuel cell systems explained*, 2nd ed., vol. 2. Chichester, UK: Wiley, 2003.

[9]   A. L. Walker and C. W. Walker Jr, "Biological fuel cell and an application as a reserve power source," *J. Power Sources*, vol. 160, pp. 123–129, 2006.

[10]   A. M. Kannan, V. Renugopalakrishnan, S. Filipek, P. Li, G. F. Audette, and L. Munukutla, "Bio-batteries and bio-fuel cells: leveraging on electronic charge transfer proteins," *J. Nanosci. Nanotechnol.*, vol. 9, pp. 1–13, 2009.

[11] W. R. Grove, "On a small voltaic battery of great energy; some observations on voltaic combinations and forms of arrangement; and on the inactivity of a copper positive electrode in nitro-sulphuric acid," *London, Edinburgh, Dublin Philos. Mag. J. Sci.*, vol. 15, no. 96, pp. 279–293, 1839.

[12] M. C. Potter, "Electrical Effects Accompanying the Decomposition of Organic Compounds," *Proc. R. Soc. B Biol. Sci.*, vol. 84, pp. 260–276, 1911.

[13] B. Cohen, "The Bacterial Culture as an Electrical Half-Cell," *J. Bacteriol.*, vol. 21, pp. 18–19, 1931.

[14] J. H. Canfield, B. H. Goldner, and R. Lutwack, "NASA Technical Report: Research on Applied bioelectrochemistry," Anaheim, 1963.

[15] M. H. Boyer, R. C. Bean, Y. H. Inami, E. R. Walwick, R. E. Kay, and W. C. Shepherd, "NASA Technical Report: Study of Basic Electrochemistry," 1963.

[16] A. T. Yahiro, S. M. Lee, and D. O. Kimble, "Bioelectrochemistry. I. Enzyme utilizing bio-fuel cell studies," *BBA - Spec. Sect. Biophys. Subj.*, vol. 88, pp. 375–383, 1964.

[17] J. L. Stirling *et al.*, "Microbial fuel cells," *Biochem. Soc. Trans.*, vol. 11, no. 4, pp. 451–453, 1983.

[18] H. P. Bennetto, J. L. Stirling, K. Tanaka, and C. A. Vega, "Anodic reactions in microbial fuel cells," *Biotechnol. Bioeng.*, vol. 25, pp. 559–568, 1983.

[19] S. D. Roller, H. P. Bennetto, G. M. Delaney, J. R. Mason, J. L. Stirling, and C. F. Thurston, "Electron-Transfer Coupling in Microbial Fuel Cells: 1. Comparison of Redox-Mediator Reduction Rates and Respiratory Rates of Bacteria," *J. Chem. Technol. Biotechnol. Biotechnol.*, vol. 34 B, pp. 3–12, 1984.

[20] R. M. Allen and H. P. Bennetto, "Microbial fuel-cells - Electricity production from carbohydrates," *Appl. Biochem. Biotechnol.*, vol. 39–40, pp. 27–40, 1993.

[21] D. R. Lovley, "Dissimilatory Fe(III) and Mn(IV) Reduction," *Microbiol. Rev.*, vol. 55, no. 2, pp. 259–287, 1991.

[22] S. Wilkinson, "'Gastrobots' - benefits and challenges of microbial fuel cells in food powered robot applications," *Auton. Robots*, vol. 9, pp. 99–111, 2000.

[23] S. Wilkinson and S. C. Campbell, "Green bug robots - Renewable environmental power for miniature robots," in *Proceedings of 4th IASTED international conference, robotics and manufacturing*, 1996, pp. 275–278.

[24] S. Wilkinson, "Gastronome - a pioneering food powered mobile robot," in *Proceedings of the 8th IASTED international conference, robotics and applications*, 2000.

[25] B. H. Kim, I. Chang, M. Hyun, H. J. Kim, and H. S. Park, "A biofuel cell using wastewater and active sludge for wastewater treatment," 2001.

[26] B. H. Kim, I. Chang, M. Hyun, H. J. Kim, and H. S. Park, "An electrochemical method for enrichment of microorganism, a biosensor for analysing organic substance and BOD," 2001.

[27] H. J. Kim, H. S. Park, M. S. Hyun, I. S. Chang, M. Kim, and B. H. Kim, "A mediator-less microbial fuel cell using a metal reducing bacterium, Shewanella putrefaciens," *Enzyme Microb. Technol.*, vol. 30, pp. 145–152, 2002.

[28] E. Kjeang, N. Djilali, and D. Sinton, "Microfluidic fuel cells: A review," *J. Power Sources*, vol. 186, pp. 353–369, 2009.

[29] M. Chiao, K. B. Lam, and L. Lin, "Micromachined microbial fuel cells," in *Micro Electro Mechanical Systems 2003, Kyoto*, 2003, pp. 383–386.

[30] C. M. Moore, S. D. Minteer, and R. S. Martin, "Microchip-based ethanol/oxygen biofuel cell," *Lab Chip*, vol. 5, pp. 218–225, 2005.

[31] M. Chiao, K. B. Lam, and L. Lin, "Micromachined microbial and

photosynthetic fuel cells," *J. Micromechanics Microengineering*, vol. 16, pp. 2547–2553, 2006.

[32] R. a. Rozendal, H. V. M. Hamelers, K. Rabaey, J. Keller, and C. J. N. Buisman, "Towards practical implementation of bioelectrochemical wastewater treatment," *Trends Biotechnol.*, vol. 26, no. 8, pp. 450–459, 2008.

[33] T. H. J. a Sleutels, A. Ter Heijne, C. J. N. Buisman, and H. V. M. Hamelers, "Bioelectrochemical systems: An outlook for practical applications," *ChemSusChem*, vol. 5, no. 6, pp. 1012–1019, 2012.

[34] T. Krieg, A. Sydow, U. Schröder, J. Schrader, and D. Holtmann, "Reactor concepts for bioelectrochemical syntheses and energy conversion," *Trends Biotechnol.*, vol. 32, no. 12, pp. 645–655, 2014.

[35] S. E. Oh, J. R. Kim, J. H. Joo, and B. E. Logan, "Effects of applied voltages and dissolved oxygen on sustained power generation by microbial fuel cells," *Water Sci. Technol.*, vol. 60, no. 5, pp. 1311–1317, 2009.

[36] S. Choi, "Microscale microbial fuel cells: Advances and challenges," *Biosens. Bioelectron.*, vol. 69, pp. 8–25, 2015.

[37] B. E. Logan, "Exoelectrogenic bacteria that power microbial fuel cells.," *Nat. Rev. Microbiol.*, vol. 7, no. 5, pp. 375–381, 2009.

[38] A. J. McCormick *et al.*, "Photosynthetic biofilms in pure culture harness solar energy in a mediatorless bio-photovoltaic cell (BPV) system," *Energy Environ. Sci.*, vol. 4, pp. 4699–4709, 2011.

[39] K. Rabaey and W. Verstraete, "Microbial fuel cells: novel biotechnology for energy generation," *Trends Biotechnol.*, vol. 23, no. 6, pp. 291–298, 2005.

[40] S. Mukherjee, S. Su, W. Panmanee, R. T. Irvin, D. J. Hassett, and S. Choi, "A microliter-scale microbial fuel cell array for bacterial electrogenic screening," *Sensors Actuators, A Phys.*, vol. 201, pp. 532–537, 2013.

[41]   H. Ren, H.-S. Lee, and J. Chae, "Miniaturizing microbial fuel cells for potential portable power sources: promises and challenges," *Microfluid. Nanofluidics*, vol. 13, pp. 353–381, 2012.

[42]   F. Qian, M. Baum, Q. Gu, and D. E. Morse, "A 1.5 µL microbial fuel cell for on-chip bioelectricity generation," *Lab Chip*, vol. 9, no. 21, p. 3076, 2009.

[43]   Y. Murata *et al.*, "Genome-wide expression analysis of yeast response during exposure to 4°C," *Extremophiles*, vol. 10, no. 2, pp. 117–128, 2006.

[44]   E. A. Parra and L. Lin, "Microbial fuel cell based on electrode-exoelectrogenic bacteria interface," *Proc. IEEE Int. Conf. Micro Electro Mech. Syst.*, pp. 31–34, 2009.

[45]   O. M. Vasyliv, O. I. Bilyy, Y. P. Ferensovych, and S. O. Hnatush, "Application of acetate, lactate, and fumarate as electron donors in microbial fuel cell," *Proc. SPIE*, vol. 8825, pp. 88250Q1-Q7, 2013.

[46]   J. K. Fredrickson *et al.*, "Towards environmental systems biology of Shewanella," *Nat. Rev. Microbiol.*, vol. 6, no. 8, pp. 592–603, 2008.

[47]   Y. A. Gorby *et al.*, "Electrically conductive bacterial nanowires produced by Shewanella oneidensis strain MR-1 and other microorganisms," *PNAS*, vol. 103, no. 30, pp. 11358–11363, 2006.

[48]   I. Ivanov, T. Vidaković-Koch, and K. Sundmacher, "Direct hybrid glucose–oxygen enzymatic fuel cell based on tetrathiafulvalene–tetracyanoquinodimethane charge transfer complex as anodic mediator," *J. Power Sources*, vol. 196, no. 22, pp. 9260–9269, 2011.

[49]   H. Cheng, Q. Qian, X. Wang, P. Yu, and L. Mao, "Electricity generation from carboxymethyl cellulose biomass: A new application of enzymatic biofuel cells," *Electrochim. Acta*, vol. 82, pp. 203–207, 2012.

[50]   R. L. Arechederra and S. D. Minteer, "Complete Oxidation of Glycerol in an Enzymatic Biofuel Cell," *Fuel Cells*, vol. 9, no. 1, pp. 63–69, 2009.

[51] I. Ivanov, T. Vidaković-Koch, and K. Sundmacher, "Recent Advances in Enzymatic Fuel Cells: Experiments and Modeling," *Energies*, vol. 3, no. 4, pp. 803–846, 2010.

[52] E. Katz and I. Willner, "A biofuel cell with electrochemically switchable and tunable power output," *J. Am. Chem. Soc.*, vol. 125, no. 22, pp. 6803–6813, 2003.

[53] M. Fischback *et al.*, "Enzyme precipitate coatings of glucose oxidase onto carbon paper for biofuel cell applications," *Biotechnol. Bioeng.*, vol. 109, no. 2, pp. 318–324, 2012.

[54] F. Sato *et al.*, "Enzyme-based glucose fuel cell using Vitamin K3-immobilized polymer as an electron mediator," *Electrochem. commun.*, vol. 7, no. 7, pp. 643–647, 2005.

[55] S. Kerzenmacher, J. Ducrée, R. Zengerle, and F. von Stetten, "Energy harvesting by implantable abiotically catalyzed glucose fuel cells," *J. Power Sources*, vol. 182, no. 1, pp. 1–17, 2008.

[56] D. Ivnitski, B. Branch, P. Atanassov, and C. Apblett, "Glucose oxidase anode for biofuel cell based on direct electron transfer," *Electrochem. commun.*, vol. 8, no. 8, pp. 1204–1210, 2006.

[57] X. Wu, F. Zhao, J. R. Varcoe, A. E. Thumser, C. Avignone-Rossa, and R. C. T. Slade, "A one-compartment fructose/air biological fuel cell based on direct electron transfer," *Biosens. Bioelectron.*, vol. 25, no. 2, pp. 326–331, 2009.

[58] D. Basu and S. Basu, "A study on direct glucose and fructose alkaline fuel cell," *Electrochim. Acta*, vol. 55, no. 20, pp. 5775–5779, 2010.

[59] S. Topcagic and S. D. Minteer, "Development of a membraneless ethanol/oxygen biofuel cell," *Electrochim. Acta*, vol. 51, no. 11, pp. 2168–2172, 2006.

[60] A. Ramanavicius, A. Kausaite, and A. Ramanaviciene, "Enzymatic biofuel

cell based on anode and cathode powered by ethanol," *Biosens. Bioelectron.*, vol. 24, no. 4, pp. 761–766, 2008.

[61]   G. T. R. Palmore, H. Bertschy, S. H. Bergens, and G. M. Whitesides, "A methanol/dioxygen biofuel cell that uses NAD+-dependent dehydrogenases as catalysts: application of an electro-enzymatic method to regenerate nicotinamide adenine dinucleotide at low overpotentials," *J. Electroanal. Chem.*, vol. 443, pp. 155–161, 1998.

[62]   Y. Ahn and B. E. Logan, "Domestic wastewater treatment using multi-electrode continuous flow MFCs with a separator electrode assembly design," *Appl Microbiol Biotechnol*, vol. 97, pp. 409–416, 2013.

[63]   M. Togo, A. Takamura, T. Asai, H. Kaji, and M. Nishizawa, "An enzyme-based microfluidic biofuel cell using vitamin K3-mediated glucose oxidation," *Electrochim. Acta*, vol. 52, no. 14, pp. 4669–4674, 2007.

[64]   M. Togo, A. Takamura, T. Asai, H. Kaji, and M. Nishizawa, "Structural studies of enzyme-based microfluidic biofuel cells," *J. Power Sources*, vol. 178, no. 1, pp. 53–58, 2008.

[65]   N. Mano, F. Mao, and A. Heller, "Characteristics of a miniature compartment-less glucose-O2 biofuel cell and its operation in a living plant," *J. Am. Chem. Soc.*, vol. 125, no. 13, pp. 6588–6594, 2003.

[66]   M. Rasmussen, R. E. Ritzmann, I. Lee, A. J. Pollack, and D. Scherson, "An Implantable Biofuel Cell for a Live Insect," *J. Am. Chem. Soc.*, vol. 134, no. 3, pp. 1458–1460, 2012.

[67]   D. R. Lovley, "Bug juice: harvesting electricity with microorganisms," *Nat. Rev. Microbiol.*, vol. 4, no. 7, pp. 497–508, 2006.

[68]   B. E. Logan *et al.*, "Microbial fuel cells: Methodology and technology," *Environ. Sci. Technol.*, vol. 40, no. 17, pp. 5181–5192, 2006.

[69]   R. W. Bradley, P. Bombelli, S. J. L. Rowden, and C. J. Howe, "Biological

photovoltaics: intra- and extra-cellular electron transport by cyanobacteria," *Biochem. Soc. Trans.*, vol. 40, no. 6, pp. 1302–1307, 2012.

[70] K. Y. Cheng, G. Ho, and R. Cord-Ruwisch, "Affinity of microbial fuel cell biofilm for the anodic potential," *Environ. Sci. Technol.*, vol. 42, no. 10, pp. 3828–3834, 2008.

[71] R. C. Wagner, S. Porter-Gill, and B. E. Logan, "Immobilization of anode-attached microbes in a microbial fuel cell," *AMB Express*, vol. 2, no. 1, p. 2, 2012.

[72] U. Schröder, "Anodic electron transfer mechanisms in microbial fuel cells and their energy efficiency," *Phys. Chem. Chem. Phys.*, vol. 9, no. 21, pp. 2619–2629, 2007.

[73] M. Zhou, H. Wang, D. J. Hassett, and T. Gu, "Recent advances in microbial fuel cells (MFCs) and microbial electrolysis cells (MECs) for wastewater treatment, bioenergy and bioproducts," *J. Chem. Technol. Biotechnol.*, vol. 88, no. 4, pp. 508–518, 2013.

[74] D. Xu and T. Gu, "Bioenergetics explains when and why more severe MIC pitting by SRB can occur," in *NACE International Corrosion 2011*, 2011, no. 11, pp. 1–21.

[75] D. H. Park and J. G. Zeikus, "Electricity generation in microbial fuel cells using neutral red as an electronophore," *Appl. Environ. Microbiol.*, vol. 66, no. 4, pp. 1292–1297, 2000.

[76] C. P. B. Siu and M. Chiao, "A microfabricated PDMS microbial fuel cell," *J. Microelectromechanical Syst.*, vol. 17, no. 6, pp. 1329–1341, 2008.

[77] H.-Y. Wang, A. Bernarda, C.-Y. Huang, D.-J. Lee, and J.-S. Chang, "Micro-sized microbial fuel cell: A mini-review," *Bioresour. Technol.*, vol. 102, no. 1, pp. 235–243, 2011.

[78] B. Min and B. E. Logan, "Continuous electricity generation from domestic

wastewater and organic substrates in a flat plate microbial fuel cell," *Environ. Sci. Technol.*, vol. 38, no. 21, pp. 5809–5814, 2004.

[79] S. Ishii, B. E. Logan, and Y. Sekiguchi, "Enhanced electrode-reducing rate during the enrichment process in an air-cathode microbial fuel cell.," *Appl. Microbiol. Biotechnol.*, vol. 94, no. 4, pp. 1087–94, 2012.

[80] V. Sharma and P. P. Kundu, "Biocatalysts in microbial fuel cells," *Enzyme Microb. Technol.*, vol. 47, no. 5, pp. 179–188, 2010.

[81] S. B. Velasquez-Orta, T. P. Curtis, and B. E. Logan, "Energy from algae using microbial fuel cells," *Biotechnol. Bioeng.*, vol. 103, no. 6, pp. 1068–1076, 2009.

[82] Z. Ren, T. E. Ward, and J. M. Regan, "Electricity production from cellulose in a microbial fuel cell using a defined binary culture," *Environ. Sci. Technol.*, vol. 41, no. 13, pp. 4781–4786, 2007.

[83] H. Ren, C. I. Torres, P. Parameswaran, B. E. Rittmann, and J. Chae, "Improved current and power density with a micro-scale microbial fuel cell due to a small characteristic length," *Biosens. Bioelectron.*, vol. 61, pp. 587–592, 2014.

[84] S. Choi *et al.*, "A μl-scale micromachined microbial fuel cell having high power density," *Lab Chip*, vol. 11, no. 6, pp. 1110–1117, 2011.

[85] J. Erben, A. Sido, E. Kipf, S. Thiele, and S. Kerzenmacher, "Improving current production of Shewanella oneidensis with electrospun anode materials," in *4th International Microbial Fuel Cell Conference, Australia*, 2013, vol. 132, no. September, p. 2013.

[86] C. R. Myers and K. H. Nealson, "Bacterial manganese reduction and growth with manganese oxide as the sole electron acceptor.," *Science (New York, N.Y.)*, vol. 240, no. 4857. pp. 1319–1321, 1988.

[87] E. Kipf *et al.*, "Systematic screening of carbon-based anode materials for

microbial fuel cells with Shewanella oneidensis MR-1," *Bioresour. Technol.*, vol. 146, pp. 386–392, 2013.

[88]   F. Golitsch, C. Bücking, and J. Gescher, "Proof of principle for an engineered microbial biosensor based on Shewanella oneidensis outer membrane protein complexes," *Biosens. Bioelectron.*, vol. 47, pp. 285–291, 2013.

[89]   H. H. Hau and J. A. Gralnick, "Ecology and Biotechnology of the Genus Shewanella," *Annu. Rev. Microbiol.*, vol. 61, no. 1, pp. 237–258, 2007.

[90]   K. Richter, M. Schicklberger, and J. Gescher, "Dissimilatory Reduction of Extracellular Electron Acceptors in Anaerobic Respiration," *Appl. Environ. Microbiol.*, vol. 78, no. 4, pp. 913–921, 2012.

[91]   J. You, X. A. Walter, J. Greenman, C. Melhuish, and I. Ieropoulos, "Stability and reliability of anodic biofilms under different feedstock conditions: Towards microbial fuel cell sensors," *Sens. Bio-Sensing Res.*, vol. 6, pp. 43–50, 2015.

[92]   R. A. Bouhenni *et al.*, "The role of Shewanella oneidensis MR-1 outer surface structures in extracellular electron transfer," *Electroanalysis*, vol. 22, no. 7–8, pp. 856–864, 2010.

[93]   S. T. Read, P. Dutta, P. L. Bond, J. Keller, and K. Rabaey, "Initial development and structure of biofilms on microbial fuel cell anodes," *BMC Microbiol.*, vol. 10, no. 1, p. 98, 2010.

[94]   D. Molognoni *et al.*, "Reducing start-up time and minimizing energy losses of Microbial Fuel Cells using Maximum Power Point Tracking strategy," *J. Power Sources*, vol. 269, pp. 403–411, 2014.

[95]   F. Qian and D. E. Morse, "Miniaturizing microbial fuel cells," *Trends Biotechnol.*, vol. 29, no. 2, pp. 62–69, 2011.

[96]   M. F. Cells, G. Scotti, P. Kanninen, T. Kallio, and S. Franssila, "Bulk-Aluminum Microfabrication for Micro Fuel Cells," *J.*

Microelectromechanical Syst., vol. 1, pp. 1–8, 2013.

[97] R. C. Sekol *et al.*, "Bulk Metallic Glass Micro Fuel Cell," *Small*, vol. 9, no. 12, pp. 2081–2085, 2013.

[98] D. Dávila, J. P. Esquivel, N. Sabaté, and J. Mas, "Silicon-based microfabricated microbial fuel cell toxicity sensor," *Biosens. Bioelectron.*, vol. 26, no. 5, pp. 2426–2430, 2011.

[99] Y. P. Chen *et al.*, "An innovative miniature microbial fuel cell fabricated using photolithography," *Biosens. Bioelectron.*, vol. 26, no. 6, pp. 2841–2846, 2011.

[100] F. Qian, Z. He, M. P. Thelen, and Y. Li, "A microfluidic microbial fuel cell fabricated by soft lithography," *Bioresour. Technol.*, vol. 102, no. 10, pp. 5836–5840, 2011.

[101] H. Hou *et al.*, "A microfluidic microbial fuel cell array that supports long-term multiplexed analyses of electricigens.," *Lab Chip*, vol. 12, no. 20, pp. 4151–4159, 2012.

[102] C. Wang, G. Jia, L. H. Taherabadi, and M. J. Madou, "A novel method for the fabrication of high-aspect ratio C-MEMS structures," *J. Microelectromechanical Syst.*, vol. 14, no. 2, pp. 348–358, 2005.

[103] D. Cecconet, S. Bolognesi, D. Molognoni, A. Callegari, and A. G. Capodaglio, "Influence of reactor's hydrodynamics on the performance of microbial fuel cells," *J. Water Process Eng.*, vol. 26, no. October, pp. 281–288, 2018.

[104] A. Fraiwan *et al.*, "Microbial Power-Generating Capabilities on Micro-/Nano-Structured Anodes in Micro-Sized Microbial Fuel Cells," *Fuel Cells*, vol. 14, no. 6, pp. 801–809, 2014.

[105] J. E. Mink and M. M. Hussain, "Sustainable design of high-performance microsized microbial fuel cell with carbon nanotube anode and air cathode," *ACS Nano*, vol. 7, no. 8, pp. 6921–6927, 2013.

[106] J. E. Mink, R. M. Qaisi, B. E. Logan, and M. M. Hussain, "Energy harvesting from organic liquids in micro-sized microbial fuel cells," *NPG Asia Mater.*, vol. 6, no. 3, pp. 1–5, 2014.

[107] J.-S. Park, S.-H. Park, S.-D. Yim, Y.-G. Yoon, W.-Y. Lee, and C.-S. Kim, "Performance of solid alkaline fuel cells employing anion-exchange membranes," *J. Power Sources*, vol. 178, no. 2, pp. 620–626, 2008.

[108] W. Cheng, C. Erbay, R. Sadr, and A. Han, "Dynamic Flow Characteristics and Design Principles of Laminar Flow Microbial Fuel Cells," *Micromachines*, vol. 9, no. 10, p. 479, 2018.

[109] H.-Y. Wang and J.-Y. Su, "Membraneless microfluidic microbial fuel cell for rapid detection of electrochemical activity of microorganism," *Bioresour. Technol.*, vol. 145, pp. 271–274, 2013.

[110] A. Fraiwan, D. F. Call, and S. Choi, "Bacterial growth and respiration in laminar flow microbial fuel cells," *J. Renew. Sustain. Energy*, vol. 6, no. 2, p. 023125, 2014.

[111] S. Choi and J. Chae, "An array of microliter-sized microbial fuel cells generating 100 μW of power," *Sensors Actuators A Phys.*, vol. 177, pp. 10–15, 2012.

[112] I. Ieropoulos, J. Greenman, and C. Melhuish, "Improved energy output levels from small-scale Microbial Fuel Cells," *Bioelectrochemistry*, vol. 78, no. 1, pp. 44–50, 2010.

[113] H. Hou, L. Li, Y. Cho, P. de Figueiredo, and A. Han, "Microfabricated Microbial Fuel Cell Arrays Reveal Electrochemically Active Microbes," *PLoS One*, vol. 4, no. 8, p. e6570, 2009.

[114] S.-E. Oh and B. E. Logan, "Voltage reversal during microbial fuel cell stack operation," *J. Power Sources*, vol. 167, no. 1, pp. 11–17, 2007.

[115] I. Ieropoulos, J. Greenman, and C. Melhuish, "Microbial fuel cells based on

carbon veil electrodes stack configuration and scalability," *Int. J. energy Res.*, vol. 32, pp. 1228–1240, 2008.

[116] J. An and H.-S. Lee, "Occurrence and Implications of Voltage Reversal in Stacked Microbial Fuel Cells," *ChemSusChem*, vol. 7, no. 6, pp. 1689–1695, 2014.

[117] P. Aelterman, K. Rabaey, H. T. Pham, N. Boon, and W. Verstraete, "Continuous electricity generation at high voltages and currents using stacked microbial fuel cells," *Environ. Sci. Technol.*, vol. 40, no. 10, pp. 3388–3394, 2006.

[118] Y. Yang, D. Ye, J. Li, X. Zhu, Q. Liao, and B. Zhang, "Biofilm distribution and performance of microfluidic microbial fuel cells with different microchannel geometries," *Int. J. Hydrogen Energy*, vol. 40, no. 35, pp. 11983–11988, 2015.

[119] T. Krieg, J. A. Wood, K. M. Mangold, and D. Holtmann, "Mass transport limitations in microbial fuel cells: Impact of flow configurations," *Biochem. Eng. J.*, vol. 138, pp. 172–178, 2018.

[120] T. M. Squires and S. R. Quake, "Microfluidics: Fluid physics at the nanoliter scale," *Rev. Mod. Phys.*, vol. 77, no. 3, pp. 977–1026, 2005.

[121] A. Fraiwan, S. Mukherjee, S. Sundermier, and S. Choi, "A microfabricated paper-based microbial fuel cell," *Proc. IEEE Int. Conf. Micro Electro Mech. Syst.*, no. i, pp. 809–812, 2013.

[122] S. Freguia, K. Rabaey, Z. Yuan, and J. Keller, "Electron and carbon balances in microbial fuel cells reveal temporary bacterial storage behavior during electricity generation," *Environ. Sci. Technol.*, vol. 41, no. 8, pp. 2915–2921, 2007.

[123] K. Y. Cheng, G. Ho, and R. Cord-Ruwisch, "Affinity of microbial fuel cell biofilm for the anodic potential," *Environ. Sci. Technol.*, vol. 42, no. 10, pp.

3828–3834, 2008.

[124] A. Mahadevan, D. a Gunawardena, and S. Fernando, "Biochemical and Electrochemical Perspectives of the Anode of a Microbial Fuel Cell," in *Technology and Application of Microbial Fuel Cells*, 2014, pp. 13–32.

[125] K. Rabaey, G. Lissens, and W. Verstraete, "Microbial fuel cells: performances and perspectives," in *Biofuels for fuel cells : renewable energy from biomass fermentation*, 2005, pp. 377–399.

[126] Y. Fan, E. Sharbrough, and H. Liu, "Quantification of the internal resistance distribution of microbial fuel cells," *Environ. Sci. Technol.*, vol. 42, no. 21, pp. 8101–8107, 2008.

[127] Y. Hong, D. F. Call, C. M. Werner, and B. E. Logan, "Adaptation to high current using low external resistances eliminates power overshoot in microbial fuel cells," *Biosens. Bioelectron.*, vol. 28, no. 1, pp. 71–76, 2011.

[128] A. K. Manohar, O. Bretschger, K. H. Nealson, and F. Mansfeld, "The use of electrochemical impedance spectroscopy (EIS) in the evaluation of the electrochemical properties of a microbial fuel cell," *Bioelectrochemistry*, vol. 72, no. 2, pp. 149–154, 2008.

[129] D. P. B. T. B. Strik, A. Ter Heijne, H. V. M. Hamelers, S. M, and C. J. N. Buisman, "Feasibility Study on Electrochemical Impedance Spectroscopy for Microbial Fuel Cells: Measurement Modes & Data Validation," *ECS Trans.*, vol. 13, no. 21, pp. 27–41, 2008.

[130] S. Pandit, S. Khilari, S. Roy, M. M. Ghangrekar, D. Pradhan, and D. Das, "Reduction of start-up time through bioaugmentation process in microbial fuel cells using an isolate from dark fermentative spent media fed anode," *Water Sci. Technol.*, vol. 72, no. 1, pp. 106–115, 2015.

[131] Y. Yi, B. Xie, T. Zhao, and H. Liu, "Comparative analysis of microbial fuel cell based biosensors developed with a mixed culture and Shewanella loihica

PV-4 and underlying biological mechanism," *Bioresour. Technol.*, vol. 265, pp. 415–421, 2018.

[132] B.-Y. Chang and S.-M. Park, "Electrochemical Impedance Spectroscopy," *Annu. Rev. Anal. Chem.*, vol. 3, no. 1, pp. 207–229, 2010.

[133] K. Guo, A. Prévoteau, S. A. Patil, and K. Rabaey, "Engineering electrodes for microbial electrocatalysis," *Curr. Opin. Biotechnol.*, vol. 33, pp. 149–156, 2015.

[134] D. Ye *et al.*, "Performance of a microfluidic microbial fuel cell based on graphite electrodes," *Int. J. Hydrogen Energy*, vol. 38, no. 35, pp. 15710–15715, 2013.

[135] X. Wang *et al.*, "Accelerated OH- transport in activated carbon air cathode by modification of quaternary ammonium for microbial fuel cells," *Environ. Sci. Technol.*, vol. 48, no. 7, pp. 4191–4198, 2014.

[136] L. C. Hsu, J. Fang, D. A. Borca-Tasciuc, R. W. Worobo, and C. I. Moraru, "Effect of micro- and nanoscale topography on the adhesion of bacterial cells to solid surfaces," *Appl. Environ. Microbiol.*, vol. 79, no. 8, pp. 2703–2712, 2013.

[137] C. Li and S. Cheng, "Functional group surface modifications for enhancing the formation and performance of exoelectrogenic biofilms on the anode of a bioelectrochemical system," *Crit. Rev. Biotechnol.*, vol. 39, no. 8, pp. 1015–1030, 2019.

[138] F. A. Z. a. Alatraktchi, Y. Zhang, and I. Angelidaki, "Nanomodification of the electrodes in microbial fuel cell: Impact of nanoparticle density on electricity production and microbial community," *Appl. Energy*, vol. 116, pp. 216–222, 2014.

[139] R. Kumar, L. Singh, Z. A.Wahid, and M. F. M. Din, "Exoelectrogens in microbial fuel cells toward bioelectricity generation: a review," *Int. J. energy*

Res., vol. 39, pp. 1048–1067, 2015.

[140] R. Kumar, L. Singh, and A. W. Zularisam, "Exoelectrogens: Recent advances in molecular drivers involved in extracellular electron transfer and strategies used to improve it for microbial fuel cell applications," *Renew. Sustain. Energy Rev.*, vol. 56, pp. 1322–1336, 2016.

[141] M. J. Angelaalincy, R. Navanietha Krishnaraj, G. Shakambari, B. Ashokkumar, S. Kathiresan, and P. Varalakshmi, "Biofilm Engineering Approaches for Improving the Performance of Microbial Fuel Cells and Bioelectrochemical Systems," *Front. Energy Res.*, vol. 6, no. July, pp. 1–12, 2018.

[142] H. Friman, A. Schechter, Y. Ioffe, Y. Nitzan, and R. Cahan, "Current production in a microbial fuel cell using a pure culture of Cupriavidus basilensis growing in acetate or phenol as a carbon source," *Microb. Biotechnol.*, vol. 6, no. 4, pp. 425–434, 2013.

[143] A. J. Slate, K. A. Whitehead, D. A. C. Brownson, and C. E. Banks, "Microbial fuel cells: An overview of current technology," *Renew. Sustain. Energy Rev.*, vol. 101, no. March 2018, pp. 60–81, 2019.

[144] A. Baudler, I. Schmidt, M. Langner, A. Greiner, and U. Schröder, "Does it have to be carbon? Metal anodes in microbial fuel cells and related bioelectrochemical systems," *Energy Environ. Sci.*, vol. 8, no. 7, pp. 2048–2055, 2015.

[145] C. Santoro *et al.*, "Influence of anode surface chemistry on microbial fuel cell operation," *Bioelectrochemistry*, vol. 106, pp. 141–149, 2015.

[146] K. Artyushkova *et al.*, "Relationship between surface chemistry, biofilm structure, and electron transfer in Shewanella anodes," *Biointerphases*, vol. 10, no. 1, p. 019013, 2015.

[147] Y. Xue, X. Li, H. Li, and W. Zhang, "Quantifying thiol-gold interactions

towards the efficient strength control," *Nat. Commun.*, vol. 5, 2014.

[148] S. R. Crittenden, C. J. Sund, and J. J. Sumner, "Mediating Electron Transfer from Bacteria to a Gold Electrode via a Self-Assembled Monolayer," *Langmuir*, vol. 17, no. 22, pp. 9473–9476, 2006.

[149] K. Guo *et al.*, "Effects of surface charge and hydrophobicity on anodic biofilm formation, community composition, and current generation in bioelectrochemical systems," *Environ. Sci. Technol.*, vol. 47, no. 13, pp. 7563–7570, 2013.

[150] M. Füeg *et al.*, "Interfacial electron transfer between Geobacter sulfurreducens and gold electrodes via carboxylate-alkanethiol linkers: Effects of the linker length," *Bioelectrochemistry*, vol. 126, pp. 130–136, 2019.

[151] J. A. La, J. M. Jeon, B. I. Sang, Y. H. Yang, and E. C. Cho, "A Hierarchically Modified Graphite Cathode with Au Nanoislands, Cysteamine, and Au Nanocolloids for Increased Electricity-Assisted Production of Isobutanol by Engineered Shewanella oneidensis MR-1," *ACS Appl. Mater. Interfaces*, vol. 9, no. 50, pp. 43563–43574, 2017.

[152] D. A. Lowy, L. M. Tender, J. G. Zeikus, D. Hyun, and D. R. Lovley, "Harvesting energy from the marine sediment – water interface II Kinetic activity of anode materials ℶ," vol. 21, pp. 2058–2063, 2006.

[153] Sigma Aldrich, "Molecular Self-Assembly," *Material Matters*, vol. 1, no. 2, pp. 1–20, 2006.

[154] R. Belaabed, S. Elabed, A. Addaou, A. Laajab, M. A. Rodríguez, and A. Lahsini, "Synthesis of LTA zeolite for bacterial adhesion," *Boletín la Soc. Española Cerámica y Vidr.*, vol. 55, no. 4, pp. 152–158, 2016.

[155] T. González, M. S. Ureta-Zañartu, J. F. Marco, and G. Vidal, "Effect of Zeolite-Fe on graphite anode in electroactive biofilm development for

application in microbial fuel cells," *Appl. Surf. Sci.*, vol. 467–468, no. March 2018, pp. 851–859, 2019.

[156] X. yuan Wu *et al.*, "Effect of zeolite-coated anode on the performance of microbial fuel cells," *J. Chem. Technol. Biotechnol.*, vol. 90, no. 1, pp. 87–92, 2015.

[157] L. Foglar and M. KljajiĆ, "The interaction of zeolite and bacterial cells for denitrification of the cetina surface water," *12th Int. Conf. Environ. Sci. Technol.*, no. 3, pp. 554–561, 2011.

[158] M. T. Noori, D. Paul, M. M. Ghangrekar, and C. K. Mukherjee, "Enhancing the Performance of Sediment Microbial Fuel Cell using Graphene Oxide – Zeolite Modified Anode and V2O5 Catalyzed Cathode," *J. Clean Energy Technol.*, vol. 6, no. 2, pp. 150–154, 2018.

[159] D. Paul, M. T. Noori, P. P. Rajesh, M. M. Ghangrekar, and A. Mitra, "Modification of carbon felt anode with graphene oxide-zeolite composite for enhancing the performance of microbial fuel cell," *Sustain. Energy Technol. Assessments*, vol. 26, no. July 2017, pp. 77–82, 2018.

[160] A. Angelov, S. Bratkova, and A. Loukanov, "Microbial fuel cell based on electroactive sulfate-reducing biofilm," *Energy Convers. Manag.*, vol. 67, pp. 283–286, 2013.

[161] M. Kubota *et al.*, "Selective adsorption of bacterial cells onto zeolites," *Colloids Surfaces B Biointerfaces*, vol. 64, no. 1, pp. 88–97, 2008.

[162] J. Haavisto *et al.*, "Effects of anode materials on electricity production from xylose and treatability of TMP wastewater in an up-flow microbial fuel cell," *Chem. Eng. J.*, vol. 372, no. April, pp. 141–150, 2019.

[163] C. Santoro, C. Arbizzani, B. Erable, and I. Ieropoulos, "Microbial fuel cells: From fundamentals to applications. A review," *J. Power Sources*, vol. 356, pp. 225–244, 2017.

[164] J. Luo *et al.*, "A new electrochemically active bacterium phylogenetically related to Tolumonas osonensis and power performance in MFCs," *Bioresour. Technol.*, vol. 139, pp. 141–148, 2013.

[165] K. Rabaey, N. Boon, S. D. Siciliano, M. Verhaege, and W. Verstraete, "Biofuel Cells Select for Microbial Consortia That Self-Mediate Electron Transfer," *Appl. Environ. Microbiol.*, vol. 70, no. 9, pp. 5373–5382, 2004.

[166] J. B. Rollefson, C. S. Stephen, M. Tien, and D. R. Bond, "Identification of an extracellular polysaccharide network essential for cytochrome anchoring and biofilm formation in Geobacter sulfurreducens," *J. Bacteriol.*, vol. 193, no. 5, pp. 1023–1033, 2011.

[167] P. L. Tremblay, M. Aklujkar, C. Leang, K. P. Nevin, and D. Lovley, "A genetic system for Geobacter metallireducens: Role of the flagellin and pilin in the reduction of Fe(III) oxide," *Environ. Microbiol. Rep.*, vol. 4, no. 1, pp. 82–88, 2012.

[168] T. Y. Chou, C. G. Whiteley, and D. J. Lee, "Anodic potential on dual-chambered microbial fuel cell with sulphate reducing bacteria biofilm," *Int. J. Hydrogen Energy*, vol. 39, no. 33, pp. 1–7, 2014.

[169] Y. Jiang *et al.*, "Enhancing the response of microbial fuel cell based toxicity sensors to Cu(II) with the applying of flow-through electrodes and controlled anode potentials," *Bioresour. Technol.*, vol. 190, pp. 367–372, 2015.

[170] P. Aelterman, S. Freguia, J. Keller, W. Verstraete, and K. Rabaey, "The anode potential regulates bacterial activity in microbial fuel cells," *Appl. Microbiol. Biotechnol.*, vol. 78, no. 3, pp. 409–418, 2008.

[171] A. Kumar *et al.*, "Catalytic response of microbial biofilms grown under fixed anode potentials depends on electrochemical cell configuration," *Chem. Eng. J.*, vol. 230, pp. 532–536, 2013.

[172] A. Han, H. Hou, L. Li, H. S. Kim, and P. de Figueiredo, "Microfabricated

devices in microbial bioenergy sciences," *Trends Biotechnol.*, vol. 31, no. 4, pp. 225–232, 2013.

[173] L. Peixoto *et al.*, "In situ microbial fuel cell-based biosensor for organic carbon," *Bioelectrochemistry*, vol. 81, no. 2, pp. 99–103, 2011.

[174] B. Liu, Y. Lei, and B. Li, "A batch-mode cube microbial fuel cell based 'shock' biosensor for wastewater quality monitoring," *Biosens. Bioelectron.*, vol. 62, pp. 308–314, 2014.

[175] X. C. Abrevaya, N. J. Sacco, M. C. Bonetto, A. Hilding-Ohlsson, and E. Cortón, "Analytical applications of microbial fuel cells. Part I: Biochemical oxygen demand," *Biosens. Bioelectron.*, vol. 63, pp. 580–590, 2015.

[176] X. C. Abrevaya, N. J. Sacco, M. C. Bonetto, A. Hilding-Ohlsson, and E. Cortón, "Analytical applications of microbial fuel cells. Part II: Toxicity, microbial activity and quantification, single analyte detection and other uses," *Biosens. Bioelectron.*, vol. 63, pp. 591–601, 2015.

[177] H. Yang, M. Zhou, M. Liu, W. Yang, and T. Gu, "Microbial fuel cells for biosensor applications," *Biotechnol. Lett.*, 2015.

[178] L. Su, W. Jia, C. Hou, and Y. Lei, "Microbial biosensors: A review," *Biosens. Bioelectron.*, vol. 26, no. 5, pp. 1788–1799, 2011.

[179] O. O. Soldatkin, B. Ozansoykasap, B. Akatakurc, A. P. Soldatkin, S. V. Dzyadevych, and A. V. El???Skaya, "Elaboration of new method of enzyme adsorption on silicalite and nano beta zeolite for amperometric biosensor creation," *Biopolym. Cell*, vol. 30, no. 4, pp. 291–298, 2014.

[180] B. Ozansoy Kasap, S. V. Marchenko, O. O. Soldatkin, S. V. Dzyadevych, and B. Akata Kurc, "Biosensors Based on Nano-Gold/Zeolite-Modified Ion Selective Field-Effect Transistors for Creatinine Detection," *Nanoscale Res. Lett.*, vol. 12, no. 1, p. 162, 2017.

[181] Sigma Aldrich, "Preparing Self-Assembled Monolayers (SAMs) A Step-by-

Step Guide for Solution-Based Self-Assembly," 2006.

[182] N. Afara, S. Omanovic, and M. Asghari-Khiavi, "Functionalization of a gold surface with fibronectin (FN) covalently bound to mixed alkanethiol self-assembled monolayers (SAMs): the influence of SAM composition on its physicochemical properties and FN surface secondary structure," *Thin Solid Films*, vol. 522, pp. 381–389, 2012.

[183] M. Veiseh, M. H. Zareie, and M. Zhang, "Highly selective protein patterning on gold-silicon substrates for biosensor applications," *Langmuir*, vol. 14, pp. 6671–6678, 2002.

[184] G. Dharanivasan, T. Rajamuthuramalingam, D. M. I. Jesse, N. Rajendiran, and K. Kathiravan, "Gold nanoparticles assisted characterization of amine functionalized polystyrene multiwell plate and glass slide surfaces," *Appl. Nanosci.*, vol. 5, no. 39, 2015.

CURRICULUM VITAE

PERSONAL INFORMATION

Surname, Name: Şen Doğan, Begüm
Nationality: Turkish (TC)
Date and Place of Birth: 5 June 1984, Fatih
Marital Status: Married
Phone: +90 506 256 46 71
email: begum.sen@metu.edu.tr, senbegum@gmail.com

EDUCATION

Degree	Institution	Year of Graduation
MS	METU Chemical Engineering	2011
BS	METU Chemical Engineering	2008
High School	Galatasaray High School, İstanbul	2003

WORK EXPERIENCE

Year	Place	Enrollment
2020 - Present	Mikro Biyosistemler	Senior R&D Engineer
2017 - 2019	Mikro Biyosistemler	R&D Engineer
2013 - 2014	SC Endüstri	Project Engineer
2012-2012	Nanomagnetics Instruments	Test Engineer
2010 - 2011	SC Endüstri	Technical Sales and Business Development Engineer
2002 August	Italcementi Set Group Ankara Cement Plant	Intern Eng. Student
2001 August	Şişecam Anadolu Cam Topkapı Plant	Intern Eng. Student

FOREIGN LANGUAGES

Advanced English, Advanced French, Elementary Spanish, Elementary Italian, Beginner German

PUBLICATIONS

1.   B. Sen Dogan, M. Okan, N. Afsar Erkal, E. Ozgur, O. Zorlu, H. Kulah, "Enhancement of the Start-Up Time for Microliter-Scale Microbial Fuel Cells (µMFCs) via the Surface Modification of Gold Electrodes", Micromachines 2020, 11, 703.

2.   B. Sen Dogan, N. Afsar Erkal, E. Ozgur, O. Zorlu, H. Kulah, "Effect of gold anode thiolation on the performance of microliter scale microbial fuel cell (µMFC)" presented at 28th World Congress on Biosensors, Miami, FL, USA, 2018.

3.   B. Sen Dogan, N. Afsar Erkal, E. Ozgur, O. Zorlu, H. Kulah, "Performance enhancement of MEMS-based microbial fuel cells (µMFC) for microscale power generation", Journal of Physics: Conference Series, Volume 773, 16th International Conference on Micro and Nanotechnology for Power Generation and Energy Conversion Applications (PowerMEMS 2016) 6–9 December 2016, Paris, France.

4.   B. Sen Dogan, N. Afsar Erkal, E. Ozgur, O. Zorlu, H. Kulah, "Performance enhancement of micro-scale microbial fuel cells (µMFC) for nanoscale power generation", presented at 3rd International Congress on Biosensors, Ankara, Turkey, 2016.

5.   B. Sen Dogan, N. Afsar Erkal, E. Ozgur, O. Zorlu, H. Kulah, "Performance enhancement of micro-scale microbial fuel cells (µMFC) for nanoscale power generation", presented at Regenerative Nano-Medicine: From Advanced Delivery Systems to Electronic-Based Devices, Tel Aviv, Israel, 2016.

6.   B. Sen Dogan, "Experimental investigation of agitation hydrodynamics and mixing-time of non-Newtonian solutions", MS Thesis, METU, 2011.

HOBBIES

Sewing, Snowboarding, Puzzle solving.

AWARDS

2015-2016 Academic Year METU Graduate Courses Performance Award